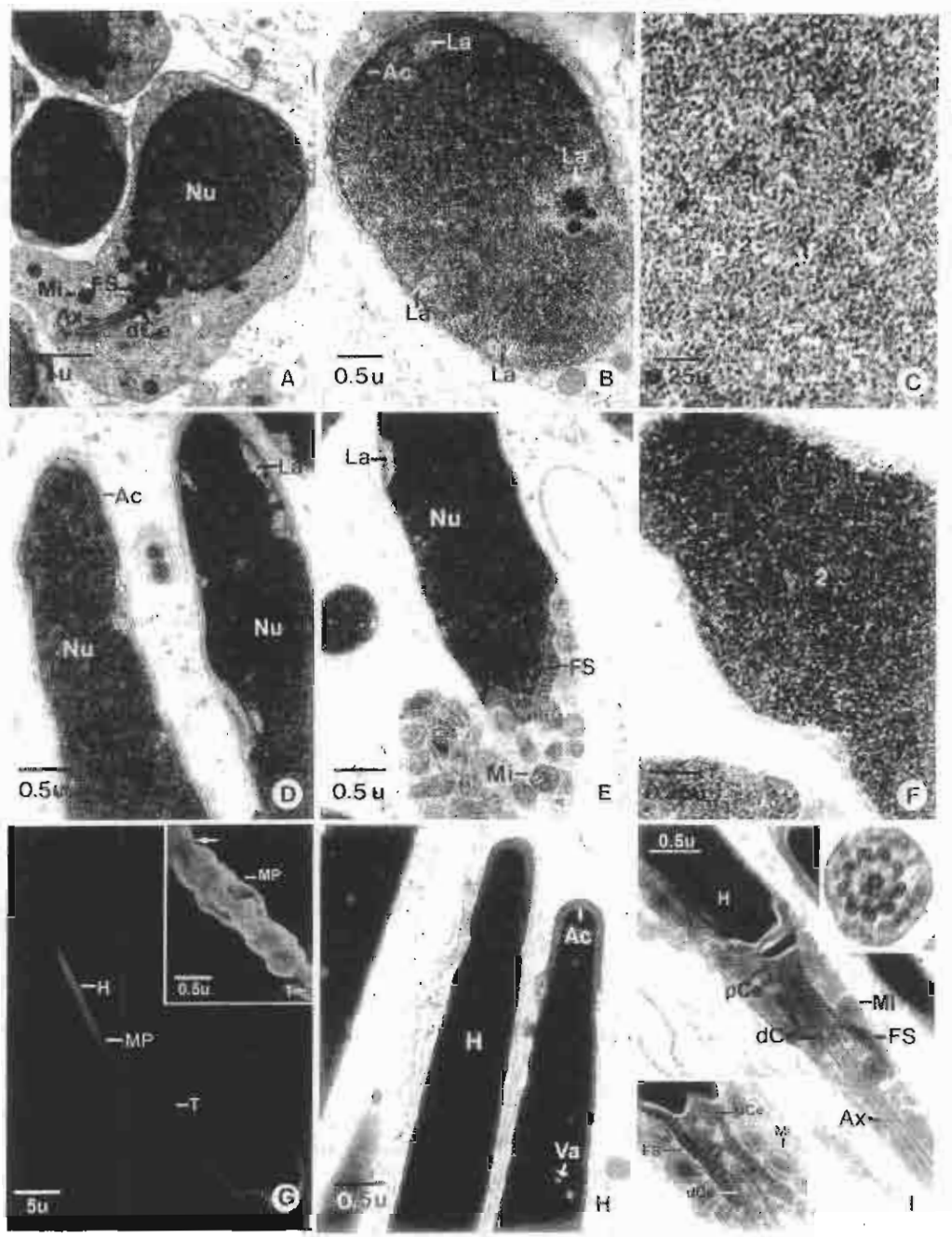


Fig 5.

A-C Spermatid III (St3): the nucleus (Nu) becomes elongated and 30 nm fibers (2) are closely packed together. Due to the increased condensation of chromatin in most part some lightly stained areas (La) within the nucleus that contain fewer chromatin fibers appear. Fibers at 10 nm disappear completely, the flat acrosome (Ac) and proximal end of the tail consisting of striated cylindrical fibrous sheath (FS), distal centriole (dCe) and axoneme (Ax) are present.

D-F Spermatid IV (St4): the nuclear elongation is more pronounced while 30 nm fibers (2) become tightly packed, but the outlines of individual fibers are still visible (in F). Lightly stained area (La) are also observed. The caudal end of nucleus contains a striated cylindrical fibrous sheath (FS) and numerous mitochondria (Mi).

G-I G is the scanning electron micrograph of a spermatozoon: the head (H) has a long cylindrical shape, the tail is very long and flimsy (T) and the middle piece (MP) connects the head and the tail. In TEM micrographs (H, I) the head (H) contains completely condensed and electron opaque chromatin. Only a few vacuoles (Va) are present. A small U-shaped acrosome (Ac) can be observed over the anterior end of the nucleus (in H). The proximal end of the tail consists of a pair of perpendicularly orientated centrioles (pCe, dCe) surrounded by the striated cylindrical fibrous sheath (FS) walls, inside the axoneme (Ax) growing out from the distal centriole. Mitochondria (Mi) surround the fibrous sheath.

have lower transcriptional activity and lower ribosomal synthesis. In other words they may serve primarily as the means to increase the number of early germ cells, as well as the transient steps to primary spermatocytes. The latter then pass through six steps of the first meiotic division, as observed in vertebrate primary spermatocytes.[19] The nuclear volume of LSc starts to increase again compared to Sg2, due to the need to accommodate the increased amount of duplicated chromosomic DNA. When this process is accomplished, the chromatin fibers appear to wind around the dense axes which make their first appearance in late LSc. These dense axes may be the initial site of chromosome condensation or they could later turn into the synap-tonemal complexes which are responsible for the pairings of homologous chromosomes in ZSc. From then on, chromatin fibers are packed more tightly into heterochromatin blocks that transform into larger cords that are increasingly thickened and lengthened in PSc and DSc. Apparently, due to the chromatin condensation transcriptional activity could cease and ribosomal synthesis is lessened, as reflected the disappearance of the nucleoli in PSc. Furthermore, the cytoplasmic organelles, especially ribosomes and mitochondria are drastically decreased, resulting in a much paler stained cytoplasm. Finally, in the DiSc and MSc steps, the chromatin appears as large pieces of condensed chromosomes that are translocated to the equatorial region. The SSc is the cell after the first meiosis in which the haploid chromosomes start to decondense. Four steps of derived spermatids could be identified based on the nuclear size, shape, and chromatin condensation. The first step exhibits loosely packed 30 nm chromatin fibers, which may become unwound from the SSc step. The chromatin fibers are recondensed into a more even mass in St2 as the nuclear volume decreases. St3 have elongated nuclei, which reflects a beginning of morphogenetic changes of the nuclear shape by a force that is yet to be identified. St4 are characterized by highly elongated, almost cylindrical nuclei, having a higher degree of chromatin condensation, even though each fiber still maintains its individuality and width of 30 nm. Subsequently, the cylindrical-shaped heads together with completely condensed chromatin are observed in spermatozoa. Since the manchette is not observed as in mammalian spermatids, and cells in these steps also show a paucity of cytoskeletal elements, the force that modulates the nuclear shape could be mostly due to chromatin condensation.

The acrosome of *R. tigerina* spermatozoa appears in St 2. It is derived from the Golgi complex, and finally assumes an inverted U-shape of a flattened sheet that adheres tightly to the proximal end of the sperm head. Acrosome formation in *R. tigerina* is different from that in mammals in that very few acrosomal granules and vesicles are formed. This perhaps explains the rather thin and relatively small size of this acrosome as compared to that in mammalian sperm.[20] The large mammalian acrosomes are needed for storage of hydrolytic enzymes, largely hyaluronidase, that are responsible for dispersing the multi-layered cumulus cells. In birds, reptiles and amphibians the ova are not surrounded by this group of cells, hence there is no need for large acrosomes in the sperm of these species.[21]

The cytoplasmic volume and cellular organelles also change during spermatogenesis. Initially in Sg1, there are abundant polyribosomes, flat profiles of rough endoplasmic reticulum, sizable Golgi complexes and numerous small mitochondria. During primary spermatocytes, the numbers of various organelles are reduced, except the Golgi complex, which is quite stable in size and is still observed in spermatids. Much of the cytoplasm is gradually relocated toward the posterior pole, and becomes highly vacuolated in late spermatids, and is mostly cast off in spermatozoa. Some cytoplasm still remains at the midpiece, and this is still quite substantial when compared to that observed in mammalian spermatozoa.[22] The midpiece of *R. tigerina* is of the primitive type, which contains a pair of perpendicular centrioles surrounded by the striated cylindrical fibrous sheath with constant periodicity and rootlet-like structures, as observed in other *Rana* and *Xenopus* species.[23] This fibrous sheath may help to stabilize and anchor the midpiece to the caudal end of the nucleus. It probably is not involved in the movement (bending) of the tail like the outer fibrous sheath of mammalian sperm.[24] The principal piece is similar to the endpiece of the mammalian spermatozoa, consisting of only an axoneme surrounded by the plasma membrane.[22]

## Chromatin Organization in the Male Germ Cells of Rana tigerina

During spermatogenesis and spermiogenesis of *R. tigerina*, the chromatin fibers are organized into two fundamental levels, i.e., 10 nm and 30 nm fibers, which are randomly coiled. In LSc, 30 nm fibers appear to wind around a single dense line, which may be the initial part of a chromosome condensation, which becomes enlarged in ZSc (Fig 2G-Fig 2I) and PSc (Fig 3A-Fig 3C). After undergoing the extreme condensation into chromosomes to expedite the process of DNA separation in MSc, the 30 nm fibers become loosened again in SSc (Fig 4A-Fig 4C), so that they could eventually be unfolded and become evenly distributed throughout the nucleus in early spermatids (St1, St2) (Fig 4D-Fig 4I); while 10 nm fibers reappear briefly and disappear again in St3 (Fig 5A-Fig 5C). The 30 nm

chromatin fibers, are re-aggregated and packed tightly into a uniformly dense mass in St4, but still remain as individual units (Fig 5D-5F). It is only in the completely opaque mass in spermatozoa that the individuality of 30 nm fibers disappears (Fig 5H). This observation indicates that the 30 nm fibers do not increase in size nor change in conformation during spermatid differentiation. In contrast, in mammals such as rat,[12] primate,[10] human,[7] or even invertebrates such as mollusk,[25] changes in the degree of chromatin condensation occur during the advanced steps of spermiogenesis due to the replacement of histones by the more basic proteins, including protamines or protamine-liked proteins. From the data in this study, it is believed that 30 nm fibers in *R. tigerina* sperm are simply brought close together and coalesced into the complete electron opaque mass. Many studies of mammalian spermiogenesis such as in mouse, rat[12] and human[7] have indicated that the coiled 30 nm fibers occur in the nuclei of early spermatids, and then these fibers transform into larger straight fibers (rodents) or knobby fibers (primates including humans) during the middle and late spermatid steps.[9,10,26] These fibers eventually become tightly packed or fused in spermatozoa. It is believed that the replacement of histones by TP proteins or protamines, the other more basic testis specific proteins, is instrumental in increasing the size of chromatin fibers and their final condensation.[1,3,12] The latter process could be reinforced by the increase of disulfide bond formation among sperm protamines.[7] In contrast, somatic-type histones are found to be present in the mature spermatozoal nuclei of *R. pipiens*[27] and *R. catesbeiana*.[28] It has also been shown in the latter that there is no protamine in the spermatozoa, but instead there are H1 variants (H1V) existing together with the full set of core histones. Thus, it was suggested that H1V may play a role in chromatin condensation in the spermatozoa of *Rana* species, instead of protamine-like proteins, as observed in mammalian spermatozoa. H1V may help to aggregate the 30 nm fibers into tight packing, while still maintaining the nucleosomal organization. This type of condensation probably uses the same mechanism that occurs during heterochromatization in fully differentiated cells, such as chick erythrocytes, which use another H1 variant (H5) for initiating the condensation of 30 nm nucleosomal fibers.[29]

## Acknowledgements

This study was supported by grants from The Thailand Research Fund (Senior Research Scholar Fellowship to P.S.) and National Science and Technology Development Agency (Ph.D. Scholarship to S.M.).

## References

1. Burgos MH and Fawcett DW (1956) An electron microscope study of spermatid differentiation in the toad, *Bufo arenarum* Hensel. *J Biophysic Biochem Cytol* **2**, 223-240.
2. Reed SC and Stanley HP (1972) Fine structure of spermatogenesis in the South African clawed toad *Xenopus laevis* Daudin. *Ultrastruct Res* **41**, 277-295.
3. Bedford JM and Calvin HI (1974) The occurrence and possible functional significant of -S-S- crosslinks in the sperm, with particular reference to eutherian mammals. *J Exp Zool* **188**, 137-158.
4. Kierszenbaum AL and Tres LL (1978) The packaging unit: A basic structural feature for the condensation of late cricket spermatid nuclei. *J Cell Sci* **33**, 265-283.
5. Oko RJ, Jando V, Wagner CL, Kistler WS and Hermo LS (1996) Chromatin reorganization in rat spermatids during the disappearance of testis-specific histone, H1t, and the appearance of transition proteins TP1 and TP2. *Biol Repro* **54**, 1141-1157.
6. Balhorn R (1982) A model for the structure of chromatin in mammalian sperm. *J Cell Biol* **93**, 298-305.
7. Balhorn R, Cosman M, Thornton K, Krishnan VV, Corzett M, Bench G, Kramer C, *et al* (1999) Protamine mediated condensation of DNA in mammalian sperm. In: *The Male Gamete: From Basic Science to Clinical Applications* (Edited by Gagnon C), pp 55-70. Cache River Press, Vienna, IL.
8. Ward WS, Partin AW and Coffey DS (1989) DNA loop domains in mammalian spermatozoa. *Chromosoma* **98**, 153-159.
9. Holstein AF and Roosen-Runge EC (1981) Atlas of human spermatogenesis. pp 1-224. Berlin Grosse Verlag.
10. Suphamungmee W (2001) Chromatin organization and packaging in the male germ cells of the common tree shew, *Tupaia glis*. M.Sc. Thesis in Anatomy, Faculty of Graduate Studies, Mahidol University.
11. Allen MJ, Bradbury EM and Balhorn R (1997) AFM analysis of DNA-protamine complexes bound to mica. *Nucleic Acids Res* **25**, 2221-2226.
12. Wanichanon C, Weerachatyanukul W, Suphamungmee W, Meepool A, Apisawetakan S, Linthong V, Sretarugsa P, *et al* (2001) Chromatin condensation during spermiogenesis in rats. *Science Asia* **27**, 211-220.
13. Meistrich ML, Trostle-Weige PK and Van Beek ME (1994) Separation of specific stages of spermatids from vitamin A-synchronized rat testes for assessment of nucleoprotein changes during spermiogenesis. *Biol Reprod* **51**, 334-344.
14. Sretarugsa P, Nakiem V, Sobhon P, Chavadej J, Kruatrachue M and Upatham ES (1997) Structure of the testis of *Rana tigerina* and its changes during development and seasonal variation. *J Sci Soc Thailand* **23**, 75-86.
15. Zhao GQ and Garbers DL (2002) Male germ cell specification and differentiation. *Devel Cell* **2**, 537-547.
16. Kali MR (1976) Morphology and kinetics of spermatogenesis in *Xenopus laevis*. *J Exp Zool* **195**, 393-408.
17. Rastogi RK, Iela L, Di Meglio M, Di Matteo L, Minucci S and Izzo-Vitiello I (1983) Initiation and kinetic profiles of spermatogenesis in the frog *Rana esculenta* (Amphibian). *Zool Lond* **201**, 515-525.
18. Lofts B (1990) Amphibia. In: *Marshall's physiology of reproduction: Reproductive cycles in vertebrates* (Edited by

Laming GE), pp127-205. Churchill-Livingstone, Edinburgh.
19. Clermont Y and Leblond CP (1953) Renewal of spermatogonia in the rat. *Amer J Anat* **93**, 475-502.
20. Clermont Y and Leblond CP (1955) Spermiogenesis of man, monkey, ram and other mammals as shown by the "periodic acid-Schiff" technique. *Amer J Anat* **96**, 229-50.
21. Cavazos LA and Melampy RM (1954) A comparative study of periodic acid-reactive carbohydrates in vertebrate testes. *Amer J Anat* **95**, 467-90.
22. Jamieson BGM (1999) Spermatozoal phylogeny of the vertebrata. In: *The Male Gamete: From Basic Science to Clinical Applications* (Edited by Gagnon C), pp304-28. Cache River Press, Vienna, IL.
23. Poirier GR and Spink GC (1971) The ultrastructure of testicular spermatozoa in two species of *Rana*. *J Ultrastruct Res* **36**, 455-65.
24. Fawcett DW and Phillips DM (1969) The fine structure and development of the neck region of the mammalian spermatozoon. *Anat Rec* **165**, 153-84.
25. Sobhon P, Apisawetakan S, Linthong V, Pankao V, Wanichanon C, Weerachatyanukul W, Meepool A, *et al* (2001) Ultrastructure of the differentiating male germ cells in *Haliotis asinina* Linnaeus. *Inv Repro Dev* **39**, 55-66.
26. Sobhon P, Tanphaichitr N and Patilamakarnkool M (1984) Transmission and scanning electron microscopic studies of the human sperm heads extracted with 8M urea, 1% mercaptoethanol and different concentrations of salt. *Acta Anat* **120**, 220-7.
27. Zirkin BR (1970) The protein composition and structure of nuclei during spermiogenesis in the leopard frog, *Rana pipiens*. *Chromosoma* **31**, 231-40.
28. Itoh T, Ausio J and Katagiri C (1997) Histone H1 variants as sperm-specific nuclear proteins of *Rana catesbeiana*, and their role in maintaining a unique condensed state of sperm chromatin. *Mol Repro Dev* **47**, 181-90.
29. Briand G, Kmiecik D, Sautiere P, Wouters D, Benic-Lay O, Bisette G, Mazen A, *et al* (1980) Chicken erythrocyte histone H5. *FEBS Lett.* **112**, 147-51.

BIOLOGY OF REPRODUCTION 69, 1183–1192 (2003)
Published online before print 28 May 2003.
DOI 10.1095/biolreprod.102.010231

# Acquisition of Arylsulfatase A onto the Mouse Sperm Surface During Epididymal Transit[1]

**Wattana Weerachatyanukul,[3,8] Hongbin Xu,[3,5] Araya Anupriwan,[3,8] Euridice Carmona,[3] Michael Wade,[6] Louis Hermo,[7] Solange Maria da Silva,[3] Peter Rippstein,[9] Prasert Sobhon,[8] Prapee Sretarugsa,[8] and Nongnuj Tanphaichitr[2,3,4,5]**

*Hormones/Growth/Development Research Group,[1] Ottawa Health Research Institute, Ottawa, Ontario K1Y 4E9, Canada*
*Departments of Obstetrics and Gynecology,[4] and Biochemistry/Microbiology/Immunology,[5] University of Ottawa, Ottawa, Ontario K1Y 4E9, Canada*
*Environmental and Occupational Toxicology Division,[6] Health Canada, Ottawa, Ontario K1A 0L2, Canada*
*Department of Anatomy and Cell Biology,[7] McGill University, Montreal, Quebec H3A 2B2, Canada*
*Department of Anatomy, Faculty of Science,[8] Mahidol University, Bangkok, Thailand*
*Laboratory Medicine,[9] Anatomical Pathology, Ottawa Hospital, Civic Campus, Ottawa, Ontario K1Y 4E9, Canada*

## ABSTRACT

**Arylsulfatase A (AS-A) is localized to the sperm surface and participates in sperm-zona pellucida binding. We investigated how AS-A, usually known as an acrosomal enzyme, trafficked to the sperm surface. Immunocytochemistry of the mouse testis confirmed the existence of AS-A in the acrosomal region of round and elongating spermatids. However, immunofluorescence and flow cytometry indicated the absence of AS-A on the surface of live testicular sperm. In contrast, positive AS-A staining was observed in the heads of live caudal epididymal and vas deferens sperm. The results suggested that acquisition of AS-A on the sperm surface occurred during epididymal transit. Immunocytochemistry of the epididymis revealed AS-A in narrow and apical cells in the initial segment and in clear cells in all epididymal regions. However, these epithelial cells are in the minority and are not involved in secretory activity. In the caudal epididymis and vas deferens, AS-A was also localized to principal cells, the major epithelial cells. Because principal cells have secretory activity, they may secrete AS-A into the epididymal fluid. This hypothesis was supported by our results revealing the presence of AS-A in the epididymal and vas deferens fluid (determined by immunoblotting and ELISA) and an AS-A transcript in the epididymis (by reverse transcription polymerase chain reaction). Alexa-430 AS-A bound to epididymal sperm with high affinity ($K_d$ = 46 nM). This binding was inhibited by treatment of sperm with an antibody against sperm surface sulfogalactosylglycerolipid. This finding suggests that AS-A in the epididymal fluid may deposit onto sperm via its affinity to sulfogalactosylglycerolipid.**

*epididymis, fertilization, gamete biology, male reproductive tract, sperm*

[1]This work was funded by CIHR (grant no. 10366 to N.T.). W.W. and A.A. are awardees of a scholarship from the National Science and Technology Development Agency of Thailand and the Thailand Research Fund, respectively. W.W., H.X., and A.A. contributed equally to this work.
[2]Correspondence: Nongnuj Tanphaichitr, Ottawa Health Research Institute, 725 Parkdale Ave., Ottawa, ON K1Y 4E9, Canada.
FAX: 613 761-5365; e-mail: ntanphaichitr@ohri.ca

Received: 13 August 2002.
First decision: 12 September 2002.
Accepted: 21 May 2003.

ISSN: 0006-3363. http://www.biolreprod.org

## INTRODUCTION

Arylsulfatase A (AS-A, E.C. 3.1.6.8) is known as a lysosomal/acrosomal enzyme with a molecular mass of 65–68 kDa. The mannose residues on the saccharide moieties of AS-A are phosphorylated, which is the basis of how AS-A is targeted to the lysosomes via its binding to mannose-6-phosphate receptors [1]. AS-A desulfates small artificial substrates (e.g., *p*-nitrocatecholsulfate) and detergent- or saposin B-solubilized natural sulfoglycolipids, i.e., sulfogalactosylceramide (SGC) and sulfogalactosylglycerolipid (SGG) [1–3]. The role of AS-A in keeping the balance of SGC in the neurological system has been well recognized. Individuals genetically deficient in AS-A show SGC accumulation in the nervous tissues, resulting in dementia and paralysis in a syndrome known as metachromatic leukodystrophy [4]. However, the physiological role of acrosomal AS-A is still unclear despite the available information on its enzymatic properties [5–7].

Recently, we demonstrated that AS-A also exists on the surface of mature mouse sperm retrieved from the cauda epididymis and the vas deferens, uterine mouse sperm that have undergone in vivo capacitation [8], and ejaculated pig sperm [9]. Masking sperm surface AS-A by treating live sperm with anti-AS-A immunoglobulin (Ig)G or Fab results in inhibition of sperm-zona pellucida (ZP) binding, indicating that sperm surface AS-A participates in this binding process. Purified AS-A can bind directly to the ZP [8, 9]. AS-A binds to SGG with high affinity ($K_d$ = 8.9 nM) in the absence of a detergent or saposin B, although this binding does not result in SGG desulfation [10]. The high affinity between the two molecules may also explain their colocalization in the sperm head [8, 11]. Because SGG is also engaged in ZP binding, AS-A and SGG may act together as complexes in this binding process. Accumulated evidence suggests that SGG is synthesized in spermatogenic cells and then targeted to their plasma membranes. The level of SGG remains stable during spermiogenesis, sperm maturation, and the initial phase of sperm capacitation [12–14]. However, despite the existence of AS-A transcripts in spermatogenic cells [15] and AS-A glycoprotein in the sperm acrosome [6], it has been unclear whether acrosomal AS-A trafficks to the plasma membrane of spermatogenic cells and testicular sperm or whether AS-A is present in

the epididymal fluid and adsorbed onto the sperm surface during epididymal transit. Here, we present evidence favoring the latter hypothesis, which suggests that acquisition of AS-A onto the sperm plasma membrane may be part of the sperm maturation process.

## MATERIALS AND METHODS

### *Anti-AS-A IgG and Anti-SGG IgG Antibodies*

Anti-AS-A IgG antiserum was produced in our laboratory against human liver AS-A purified as described previously [16] (a gift from Dr. A. Fluharty, University of California, Los Angeles, CA). Details of this antibody production, and purification of its IgG fraction, and preparation of preimmune rabbit serum (PRS) IgG were published previously [8]. Affinity-purified anti-AS-A IgG was then prepared as previously described [17].

Polyclonal rabbit anti-SGG IgG antiserum monospecific to SGG and its analog SGC was produced in our laboratory. Anti-SGG IgG/Fab and its affinity-purified fractions and the corresponding PRS IgG/Fab were prepared as described previously [11].

### *Light Microscopic Immunocytochemistry of AS-A on Mouse Testis, Epididymis, and Vas Deferens Sections*

CD-1 male mice (~10 wk old) were used for all studies. Mice (n = 5) were perfused with Bouin solution in situ through the left ventricle. The testis, epididymis, and vas deferens were removed in one piece and further fixed in Bouin solution for an additional 2 h. Tissues were then embedded in paraffin for sectioning according to standard procedures. Sections (4 μm thick) were deparaffinized and rehydrated through decreasing concentrations of ethanol (100% to 70%). The tissues were treated with 1% hydrogen peroxide in 70% ethanol and subsequently with 1% lithium carbonate in 70% ethanol to quench endogenous peroxidase and to remove residual picric acid, respectively. The tissues were then treated with 300 mM glycine to neutralize residual formaldehyde. The antigen was retrieved by microwaving the tissues (which were immersed in 0.01 M citrate buffer, pH 6.0) for 3 min at the highest power and an additional 7 min at low power. To block nonspecific binding, the tissues were incubated for 15 min at room temperature with 10% normal goat serum in Tris-buffered saline (TBS). The tissues were then reacted (90 min, 25°C) with affinity-purified anti-AS-A IgG. Following successive washing with 0.1% Tween in TBS, the slide was examined for antigen-antibody interaction using the Vectastain ABC Elite kit (Vector Laboratories, Burlingame, CA). This process involved treatment of the slide with biotinylated secondary antibody (goat anti-rabbit IgG, 30 min, room temperature), followed by incubation with avidin-biotin-horseradish peroxidase complex and detection by a reaction with a peroxidase substrate, diaminobenzidine. Concentrations of chemicals and conditions for these treatments were as described by their manufacturers. The brown product of the peroxidase reaction signified AS-A localization. Tissues treated with 10 μg/ml PRS IgG served as negative controls.

### *Collection of Sperm from the Testis, Caput and Corpus Epididymis, and Cauda Epididymis and Vas Deferens and of Fluid from the Cauda Epididymis and Vas Deferens*

To collect testicular sperm, decapsulated testes were first minced into 1- to 2-mm pieces in Kreb Ringer bicarbonate medium buffered with Hepes (KRB-Hepes: 119.4 mM NaCl, 4.8 mM KCl, 1.7 mM $CaCl_2$, 1.2 mM $KH_2PO_4$, 1.2 mM $MgSO_4$, 25 mM sodium lactate, 1 mM sodium pyruvate, 5.6 mM glucose, 28 μM phenol red, 4 mM $NaHCO_3$, and 21 mM Hepes, pH 7.4), supplemented with 0.3% BSA (KRB-Hepes-BSA), and containing 1 mg/ml DNaseI (Sigma, St. Louis, MO). Protease inhibitor cocktail (PIC; Roche Diagnostics, Mannheim, Germany) was also added to the medium at a dose recommended by the manufacturer (i.e., 1 tablet per 10 ml of the medium). Large fragments and clumps of Leydig and Sertoli cells were pelleted (30 × *g*, 25°C, 5 min). The supernatant (2 ml), containing loose testicular cells, testicular sperm, and red blood cells, was layered on top of a 2-ml 45% Percoll solution in KRB-Hepes. The tube was centrifuged (600 × *g*, 25°C, 5 min) to pellet red blood cells, which were then carefully removed using a Pro/Elec Pipet Tip (BioRad Laboratories, Hercules, CA) without disturbing the testicular cells and testicular sperm that were sedimented at the interface between the loaded medium and the 45% Percoll solution. The tube was further centrifuged (1000 × *g*, 25°C, 30 min) to selectively pellet testicular sperm. After removing the top fluid layers, the pelleted testicular sperm were washed (350 × *g*, 25°C, 10 min) once in KRB-Hepes and directly used for immunoblotting or resuspended in KRB-Hepes-BSA for indirect immunofluorescence (IIF) or for Alexa-430 AS-A binding experiments.

To collect caput and corpus epididymal sperm, the caput and corpus epididymis was cut once longitudinally and then immersed in KRB-BSA. Caput and corpus epididymal sperm were allowed to swim out into the medium by incubating the tissue at 37°C with gentle shaking for 15 min. At the end of the incubation, the tissue was removed from the tube, and the cell suspension was centrifuged at 45 × *g* to pellet red blood cells, tissue debris, and cell aggregates. The supernatant containing mainly caput and corpus epididymal sperm was transferred into a new tube and centrifuged at 284 × *g* for 10 min. The pelleted caput and corpus epididymal sperm were washed once in KRB-BSA by centrifugation (284 × *g*, 10 min) and subject to IIF and flow cytometry.

Sperm and fluid were also collected from the vas deferens and cauda epididymis. Collection was first made at the vas deferens by inserting PE10 polyethylene tubing sleeved over a 25-ga needle, which was attached to a 1-ml tuberculin syringe, into the tubule. Following fluid aspiration, the vas deferens tubule was washed twice with PIC-supplemented KRB-Hepes, and all washes were combined with the original fluid. To collect fluid from the cauda epididymis, the organ was longitudinally cut once with a sharp razor blade and gently squeezed with flat-end tweezers. The thick fluid that oozed from the organ was collected and mixed with KRB-Hepes-PIC. Fluid from both the vas deferens and cauda epididymis was combined and centrifuged (500 × *g*, 25°C, 10 min) to pellet sperm. Caudal epididymal and vas deferens sperm were washed once in KRB-Hepes-PIC and resuspended in KRB-Hepes-BSA for IIF. A peripheral plasma membrane protein extract was also prepared from washed caudal epididymal and vas deferens sperm by treatment with a sucrose solution (320 mM) containing 1 mM EDTA and 1 mM ATP (AES) [8] and used for immunoblotting. The collected supernatant was further centrifuged in a Microfuge 18 (Beckman Coulter, Palo Alto, CA) (18 000 × *g*, 4°C, 10 min) to remove all sperm and particulates. The sperm-free fluid was then used for immunoblotting.

### *IIF for AS-A and SGG and Flow Cytometry of AS-A on Live Testicular Sperm, Caput and Corpus Epididymal Sperm, and Caudal Epididymal and Vas Deferens Sperm*

Live testicular sperm, caput and corpus epididymal sperm, and caudal epididymal and vas deferens sperm were separately incubated (5% $CO_2$, 37°C, 30 min) with 10 μg/ml anti-AS-A IgG or affinity-purified anti-AS-A IgG (see [8, 17] for purification and use in immunofluorescence) or with 10 μg/ml affinity-purified anti-SGG IgG [11], all in KRB-Hepes-BSA. Sperm were then washed in the same medium and incubated with 25 μg/ml goat anti-rabbit IgG conjugated with the Alexa 488 fluorochrome (Molecular Probes, Eugene, OR). Caudal epididymal and vas deferens sperm treated with PRS IgG in place of primary antibody served as controls. To assess cell viability during the staining process, propidium iodide (Clontech, Palo Alto, CA) was added to the cell suspension at a final concentration of 0.5 μg/ml 5 min before the the secondary antibody incubation period ended. Sperm were then washed twice in KRB-Hepes-BSA, resuspended in the same medium, mounted onto a slide in PBS/glycerol (1:1, v/v), topped with a cover slip, and viewed under a Zeiss IM35 epifluorescence microscope (Carl Zeiss Canada Ltd., Toronto, ON, Canada).

Live testicular sperm, caput and corpus epididymal sperm, and caudal epididymal and vas deferens sperm that were subjected to immunofluorescent staining (but without propidium iodide incubation) were analyzed by flow cytometry to assess individual fluorescence intensity. After extensive washes to remove unbound fluorescent secondary antibody, the sperm were filtered through a 70-μm mesh (Tube-top Filicon; DAKO Diagnostics Canada, Mississauga, ON, Canada) immediately before analysis on a Coulter Epics Profile II Flow Cytometer (Beckman Coulter, Fullerton, CA). Samples were excited by an argon ion laser at 488 nm, and the emission fluorescence was monitored at 525 ± 20 nm band pass. Sperm cells were gated from debris using their unique properties of forward and side light scattering. Data from at least 5000 events were collected, and relative AS-A staining intensity was determined using FCS Express Software (De Novo Software, Orangeville, ON, Canada).

### *Reverse Transcription Polymerase Chain Reaction of AS-A from Cauda Epididymis and Vas Deferens and from Testes and Nucleotide Sequencing of the Product*

Total RNAs from cauda epididymis and vas deferens and from testes were separately extracted using Trizol reagent (Gibco BRL, Burlington,

ON, Canada), following the manufacturer's protocol. Using RETROscript First-Strand Synthesis Kit for reverse transcription polymerase chain reaction (RT-PCR) (Ambion, Austin, TX), total RNAs (1 μg, determined from $A_{260}$) were reverse-transcribed into first-strand cDNAs in a 20-μl reaction mixture. Subsequently, 2 μl of this reaction mixture containing the first-strand cDNA was used as a template for PCR. The primers for amplification of *AS-A* were as follows: F-ASA: 5′-atggggtctttgctgttcgg-3′ (nucleotides 566–587; numbering as described for human AS-A sequence [18]); R-ASA: 5′-ttctggtaaggtggcateggac-3′ (complementary to nucleotides 2412–2434). Amplification reactions were carried out in a Mastercycler (Brinkmann Instruments, Mississauga, ON, Canada). These reactions were initiated with 10-min denaturation at 94°C, followed by 30 cycles of denaturation at 94°C for 30 sec, annealing at 56°C for 45 sec, and extension at 72°C for 45 sec, and ending with further extension at 72°C for 10 min. RT-PCR products were then resolved by electrophoresis in a 2% agarose gel containing ethidium bromide (0.5 μg/ml) followed by visualization under an ultraviolet lamp (UV Transilluminator, Gel Doc 1000; BioRad). RT-PCR experiments were repeated three times using RNA samples prepared on different days from three different animals. Negative controls were performed in all experiments by omitting the RT step.

The RT-PCR product of AS-A from cauda epididymis and vas deferens was purified by agarose gel electrophoresis. The product band was excised and purified using a Concert Rapid Gel Extraction System (Gibco BRL, Gaithersberg, MD). Approximately 100 ng of the purified PCR product of AS-A was used for nucleotide sequencing, which was performed by the chain termination method using an automated capillary electrophoresis and fluorometric detection system (ABI Prism 3100 Genetic Analyzer, Applied Biosystems, Foster City, CA).

### *Immunoblotting of Sperm and Fluid Collected from Cauda Epididymis and Vas Deferens with Anti-AS-A*

Epididymal fluid collected from the cauda epididymis and vas deferens and the peripheral plasma membrane protein extract of caudal epididymal and vas deferens sperm were subjected to SDS-PAGE (gel: 12% acrylamide, 0.75 mm thick) [19], followed by electroblotting onto nitrocellulose membrane [20]. The blot was incubated with anti-AS-A antiserum followed by horseradish peroxidase (HRP)-conjugated secondary antibody (Bio-Rad). Conditions of the incubation for antibody-antigen interaction were as described previously [8]. The AS-A signals on the nitrocellulose blot were captured by a Typhoon 8600 Variable Mode Imager (Molecular Dynamics, Sunnyvale, CA) in the chemiluminescence mode, using Typhoon Scanner Control 1.0.

### *Quantification of AS-A in the Caudal Epididymal and Vas Deferens Fluid*

AS-A purified from the pig sperm surface extract to a single band on SDS-polyacrylamide gels [9] was used as a standard. Caudal epididymal and vas deferens fluid containing 6 μg of total proteins or AS-A standard (1–15 ng, as quantified using Protein Assay Solution; Bio-Rad) in 100 μl of 100 mM sodium carbonate, pH 9.6, was allowed to attach to the bottom surface of the wells of a Limbro/Titerteck 96-well polystyrene plate (ICN Biomedical, Aurora, OH) overnight at 4°C. The attached proteins were blocked with 1% BSA in TBS at 25°C for 1 h followed by three washes in TBS and 0.05% Tween 20. The protein wells were then incubated with 100 μl of anti-AS-A antiserum (1:1600 dilution in TBS) at 25°C for 1 h. Following successive washing in TBS and 0.05% Tween 20, 100 μl of HRP-goat anti-rabbit IgG (1:3000 dilution in TBS) was added to the wells for incubation at 25°C for 30 min. After washing thoroughly with TBS and 0.05% Tween 20, 100 μl of an HRP substrate, *o*-phenylenediamine dihydrochloride (0.05% in 100 mM sodium citrate, pH 5.0), and $H_2O_2$ (1.5 μl/ml of the substrate solution) were added to the wells, which were then incubated at 25°C until the yellow color developed. The reaction was then stopped with 50 μl of 30% $H_2SO_4$, and the color intensity was measured at $A_{490}$.

### *Binding of Alexa-430 AS-A onto the Caudal Epididymal Sperm*

Alexa-430 AS-A and Alexa-430 ovalbumin were prepared by conjugating AS-A and ovalbumin, respectively, with the Alexa 430 fluorochrome (Molecular Probes) as instructed by the manufacturer. Caudal epididymal sperm ($1.2 \times 10^6$) were incubated (37°C, 5% $CO_2$, 1 h) with various concentrations (0–60 nM) of Alexa-430 AS-A or with 60 nM Alexa-430 ovalbumin in 600 μl of KRB-BSA. At the end of the incubation, sperm were washed free from the unbound protein by centrifugation (600 × *g*, 25°C, 10 min) in KRB-BSA. The washed sperm pellet was resuspended in 600 μl of KRB-Hepes, and 100-μl aliquots (200 000 sperm) were placed in each well of a Costar black 96-well microtiter plate (Corning, Corning, NY) for measurement of fluorescence intensity using a Spectramax GeminiXS spectrofluorometer (Molecular Devices) at the excitation and emission wavelengths of 425 and 520 nm, respectively. The amount of AS-A bound per sperm was then calculated from the Alexa-430 AS-A standard curve. The data obtained were analyzed for the $K_d$ value of AS-A-ZP binding by Scatchard plotting using Grafit 4.0 software for Windows (Erithacus Software, Surrey, U.K.). In an alternative experiment, 600 nM AS-A was included with 60 nM Alexa-430 AS-A for sperm incubation. Measurement of Alexa-430 AS-A binding to sperm was then performed as described above.

To investigate the roles of SGG and mannose phosphate receptors on the sperm surface in AS-A binding, 200 000 caudal epididymal sperm in 150 μl KRB-Hepes were pretreated (37°C, 5% $CO_2$, 30 min) with various concentrations of anti-SGG Fab (0–10 μM), PRS-Fab (0–10 μM), or mannose 6-phosphate (0–5 mM) before incubation with 63 nM Alexa-430 AS-A following the procedure described above. Data were expressed as percentages of the control fluorescence intensity values (i.e., from incubations of Alexa-430 AS-A with sperm without any competitors) for each of the competitor concentrations. Differences in the levels of AS-A binding to sperm in the control incubations (no competitors added) and in those with competitors included were analyzed by ANOVA.

## RESULTS

### *Localization of AS-A in the Testis and Epididymis and Vas Deferens and on Live Testicular Sperm, Caput and Corpus Epididymal Sperm, and Cauda Epididymal and Vas Deferens Sperm*

To elucidate how AS-A, generally known as a lysosomal enzyme, targets to the surface of mature sperm [8, 9], immunocytochemistry of mouse testis and epididymis sections and IIF of live mouse sperm were performed using affinity-purified anti-AS-A IgG antibody. All experiments, performed with tissues and sperm collected from five different mice, gave consistent results. In testes, AS-A immunocytochemical staining was observed in the Sertoli cell cytoplasm, appearing from the base of the seminiferous epithelium toward the supranuclear region, which was stained with higher intensity and showed globular patterns. This finding suggests that the enzyme compartmentalized into cytoplasmic organelles, presumably lysosomes (Fig. 1a). Early residual bodies did not show any reaction, in contrast to late residual bodies, which were intensely stained (Fig. 1b).

Immunocytochemical reaction for AS-A was also observed in spermatids. Staining was intense at the acrosomal cap of round spermatids and at the mature expanded acrosome of elongating spermatids (Fig. 1, a and b). In contrast, AS-A staining was not observed in primary spermatocytes or spermatogonia or in the lumen (Fig. 1, a and b). Tissue sections that were exposed to PRS IgG in place of anti-AS-A IgG showed no staining (Fig. 1c). All of these results indicated that the immunocytochemical staining observed in Sertoli cell organelles, presumably lysosomes, and spermatid acrosomal machinery was specific to AS-A.

IIF of live sperm revealed that the majority of testicular spermatozoa (~80%) showed no staining on the cell surface (Fig. 2A). These sperm also did not stain for propidium iodide, indicating that their plasma membrane was intact. A histogram frequency of AS-A staining intensity, based on flow cytometry analysis, showed a major peak of testicular sperm (~80%), with background fluorescence intensity similar to that of the negative control cells, i.e., mature sperm (caudal epididymal and vas deferens sperm) that were subjected to PRS IgG and Alexa-488-conjugated sec-

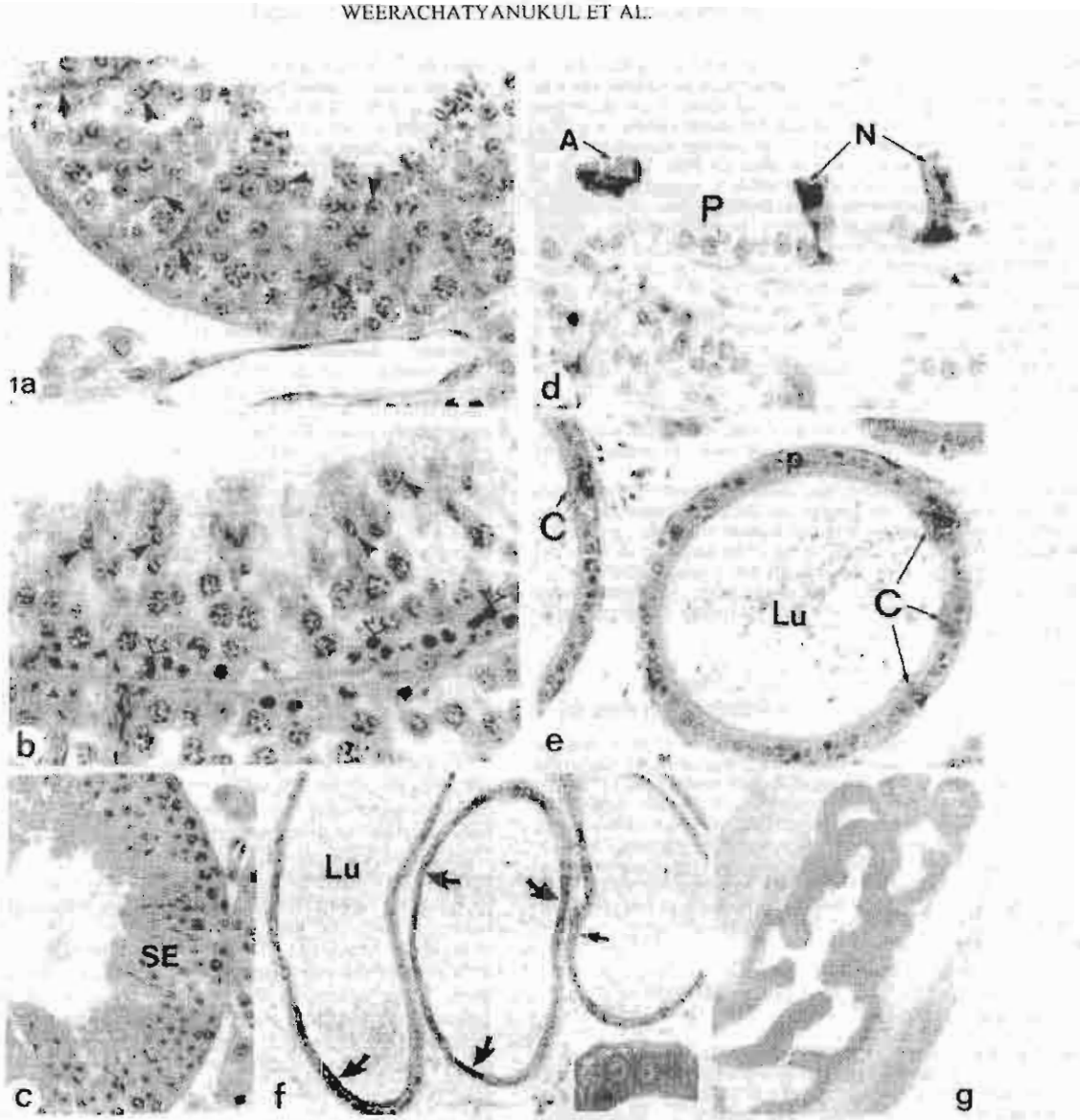


FIG. 1. Light microscopic immunocytochemistry for AS-A in testis (a–c) and epididymis (d–f) sections of adult mice. Sections in a, b, and d–f were exposed to anti-AS-A IgG, whereas the section shown c was incubated with PBS IgG. a) The seminiferous epithelium of the testis is at stage VII of the cycle. At this stage, the immunoperoxidase reaction product is intense in Sertoli cells and appears as columns extending from the base of the seminiferous epithelium to the lumen, revealing densely stained globular masses along their length (arrows). Also reactive are the acrosomic systems of early round (large arrowheads) and late elongating (small arrowheads) spermatids. ×358. b) The seminiferous epithelium is at stage X of the cycle. The Sertoli cells are not intensely reactive at this stage of the cycle; however, the acrosomic systems of the step 10 elongating spermatids are intensely reactive (arrowheads). Also intensely reactive at the base of the epithelium are the late residual bodies (open arrows). ×358. c) Adjacent seminiferous tubules show no reaction product over the entire seminiferous epithelium (SE) when immunostained with PBS IgG. ×235. d) In the initial segment of the epididymis, narrow (N) and apical (A) cells are the only cells to show intense reaction; principal cells (P) are unreactive. ×358. e) In the corpus epididymis, clear cells (C) are intensely reactive, and principal cells (P) are unreactive. ×358. f) In the cauda epididymis, strips of principal cells show intense reaction (coarse arrows), alongside adjacent strips of unreactive principal cells. ×235. Inset: Higher magnification reveals network patterns of staining within the cytoplasm. Among the principal cells, a few clear cells also show intense reaction (straight, small arrow). ×1092. g) In the vas deferens, all principal cells react with the antibody, although the intensity of the staining is weaker than that observed in the cauda epididymis. The lumen (Lu) of the epididymis and its contents do not show any significant reaction. ×352.

ondary antibody (Fig. 3A). The results therefore suggest that live intact testicular sperm are devoid of AS-A on the surface. In contrast, the remaining 20% of testicular sperm were stained with propidium iodide, indicating that their surface membranes were damaged (Fig. 3A). These propidium iodide-positive sperm also showed Alexa-488 staining, although without any consistent patterns. Because these sperm presumably were no longer viable, this fluorescein isothiocyanate staining with inconsistent patterns may reflect nonspecific binding of the primary and/or secondary antibodies to sperm.

The absence of AS-A staining on testicular mouse spermatozoa might be due to the masking of the surface of these sperm. To test this possibility, IIF of SGG, a male

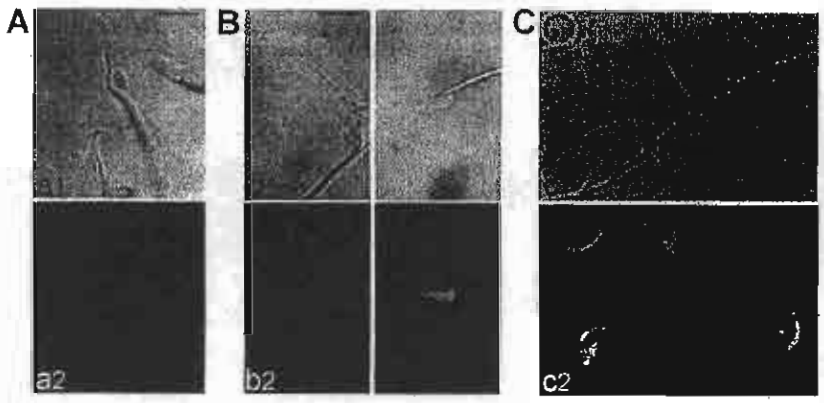


FIG. 2. Indirect immunofluorescence for AS-A on live mouse testicular (A), caput and corpus epididymal (B), and caudal epididymal and vas deferens (C) sperm. Top panels (a1, b1, and c1) are phase contrast micrographs, and bottom panels (a2, b2, and c2) are immunofluorescent micrographs. Note the absence of AS-A staining in testicular sperm and positive AS-A staining in the head (convex ridge and postacrosome) of caudal epididymal and vas deferens sperm. The majority of caput and corpus epididymal sperm did not show AS-A staining, whereas the remainder revealed staining in the postacrosome of the sperm head. Bar = 10 μm.

germ cell surface sulfoglycolipid [11–14], was performed with live testicular sperm and mature sperm from cauda epididymis and vas deferens. Results shown in Figure 4 (A and B) indicated that both testicular and mature sperm exposed to affinity purified anti-SGG IgG possessed specific fluorescent staining patterns, i.e., at the convex ridge of the sperm head and the posterior head region. In contrast, when PRS IgG was used in place of affinity purified anti-SGG IgG for sperm incubation, no fluorescent staining was observed on both sperm types (Fig. 4C). Therefore, it was apparent that SGG could be detected by IIF on the surface of both testicular sperm and mature sperm, this argued against the possibility that the testicular sperm surface was masked.

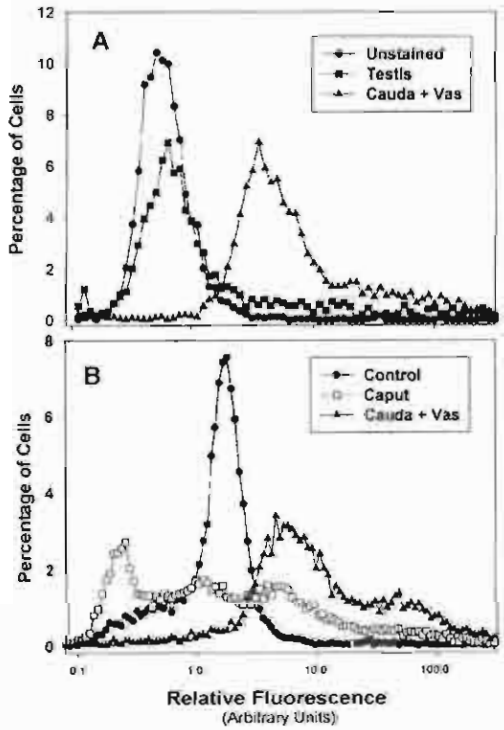


FIG. 3. Frequency histogram of AS-A staining intensity of testicular (—■—), caput epididymal (—□—), and caudal epididymal and vas deferens (—▲—) mouse sperm analyzed by flow cytometry. Sperm exposed to PRS IgG served as a negative control (—●—). A) Comparison between testicular sperm and caudal epididymal and vas deferens sperm. B) Comparison between caput epididymal sperm and caudal epididymal and vas deferens sperm.

Immunocytochemical results revealed the presence of AS-A in the epididymis. In the initial segment, reaction was restricted to narrow and apical cells (as identified by their shape and location [21]) (Fig. 1d). In the caput, corpus and cauda regions, clear cells (as identified by their possession of numerous vacuoles [21]) were reactive (see an example in the corpus, Fig. 1e). In the caudal region, a much greater number of cells reacted with anti-AS-A. The majority of reactive cells often were grouped together, appearing as positively stained strips (Fig. 1f). These cells spanned from the basal membrane to the apical membrane, showed a brush border at a high magnification and were the majority of the epididymal epithelial cells, and therefore they were identified as principal cells [21]. The AS-A immunoreaction in principal cells was over the entire cytoplasm, appearing as network patterns (Fig. 1f, inset). In the vas deferens, most principal cells surrounding the lumen were reactive for AS-A, although the intensity of the staining was not as high as for principal cells in the cauda epididymis (Fig. 1g). However, the staining of AS-A in the lumen in both the cauda epididymis and vas deferens was not readily apparent (see example in Fig. 1, f and g). It is possible that the amount of AS-A secreted into lumen may be small and was therefore washed out from the sections during the processing of the tissue sections.

To further demonstrate that the cauda epididymis and vas deferens were involved in AS-A biosynthesis, RT-PCR was performed on these tissues using AS-A primers synthesized

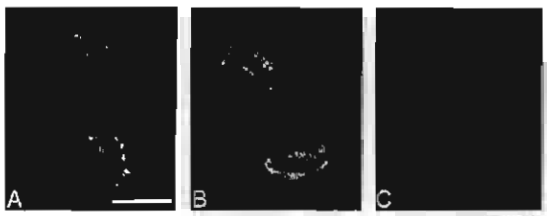


FIG. 4. IIF for SGG on live mouse testicular (A) and caudal epididymal and vas deferens (B) sperm. A and B) Sperm were incubated with affinity-purified anti-SGG IgG. C) Caudal epididymal and vas deferens sperm were exposed to PRS IgG. Note the presence of SGG staining in the convex ridge and postacrosomal region of both testicular sperm and mature sperm. Bar = 10 μm.

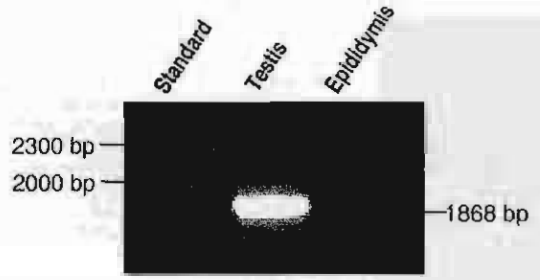


FIG. 5. Long-range RT-PCR products of AS-A from mouse testis, cauda epididymis, and vas deferens. Total RNA fractions extracted from the testis and from the cauda epididymis and vas deferens were subjected to RT-PCR using AS-A primers synthesized based on nucleotides 566–587 and nucleotides 2412–2434 of human testis AS-A cDNA sequence. RT-PCR products were then characterized by agarose gel electrophoresis. RNAs from both the testis and the cauda epididymis and vas deferens gave RT-PCR products of the same size (1868 base pairs). DNA size markers are shown in the left lane.

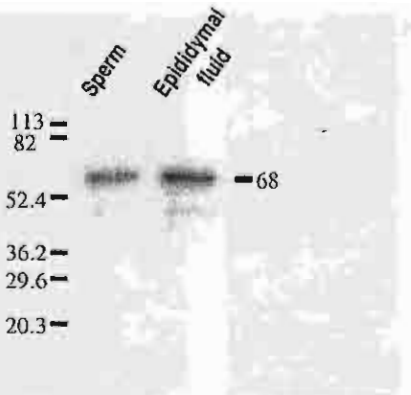


FIG. 6. Immunoblotting of AS-A from an AES extract of caudal epididymal and vas deferens sperm (left lane) and caudal epididymal and vas deferens fluid (right lane). The AES extract (prepared from $20 \times 10^6$ sperm) and epididymal and vas deferens fluid (containing 15 μg of total proteins) were loaded on SDS-polyacrylamide gels for immunoblotting.

based on sequences in the 5′ and 3′ regions of testis AS-A cDNA sequence. RT-PCR products of the same size (1868 base pairs) were obtained from both testis and cauda epididymis and vas deferens RNA (Fig. 5). Nucleotide sequencing revealed 100% identity between these two RT-PCR products, with 100% match to the mouse testis AS-A sequence previously described [22]. These results indicate that the sequence of the AS-A transcript synthesized in the epididymal epithelial cells is identical to that from testis.

Although AS-A reaction was not evident in the lumen of the cauda epididymis and vas deferens, possibly because of the small amount, 95% of live sperm retrieved from these tissues showed positive immunofluorescent staining in the head region (Fig. 2C). Caudal epididymal and vas deferens sperm were collected without any tissue mincing, and >95% of these sperm were viable, as indicated by their ability to exclude propidium iodide. Therefore, AS-A staining observed on these sperm heads, which consistently demonstrated two distinct patterns, should represent AS-A existence on intact sperm in the cauda epididymis and vas deferens. The major staining pattern (80% of total sperm) showed AS-A signals at both the acrosomal ridge and the head posterior region (Fig. 2C), the same sites where SGG is localized (Fig. 4) [11]. In the remaining sperm (20%), AS-A immunofluorescent staining was found only at the acrosomal ridge. The intensity of the AS-A fluorescent signal was variable in the population of caudal epididymal and vas deferens sperm. Flow cytometry, performed on two different experimental days, showed one major peak (histogram frequency) of AS-A staining intensity, encompassing ~70%–80% of caudal epididymal and vas deferens sperm. AS-A staining intensity of the major population of these sperm was ~8–10 times higher than the corresponding background fluorescence observed in sperm collected also from the cauda epididymis and vas deferens and subjected to PRS IgG. Approximately 20%–30% of caudal epididymal and vas deferens sperm showed higher intensity of AS-A staining than did the major peak population (Fig. 3, A and B). Because the majority of caudal epididymal and vas deferens sperm were viable, the trailing of the sperm population showing higher AS-A staining intensity indicated inherent heterogeneity of sperm quality. Corroborating the immunocytochemistry results, which revealed AS-A expression only in endocytotic clear cells in the corpus (Fig. 1e) and caput (data not shown) epididymis, was the absence of AS-A fluorescent staining in the majority (70%) of caput and corpus epididymal sperm (Figs. 2B and 3B). However, another 30% of caput and corpus epidiymal sperm possessed AS-A staining with an intensity similar to that of the major peak of caudal epididymal and vas deferens sperm (Fig. 3B). Fluorescent staining of AS-A in caput and corpus epididymal sperm was localized mainly to the post-acrosomal region of the sperm head (Fig. 2B). This population of caput and corpus epididymal sperm may have come from the epididymis area just above the beginning of the cauda epididymis. AS-A, secreted from principal cells in the cauda region, may diffuse into the lumen of this epididymis area. The transit sperm in this border area may also be more mature than sperm in the proximal region of the caput epididymis and may be capable of capturing AS-A in the epididymal fluid onto their surface. All of these results indicate that AS-A is present on the surfaces of all caudal epididymal and vas deferens sperm and in a minor population of caput epididymal sperm, in addition to its intracellular existence (i.e., in the acrosome; Fig. 1, a and b).

To verify whether AS-A was present in the caudal epididymal and vas deferens lumen, fluid from these reproductive tract regions was collected. Care was taken to cause the least amount of damage to the epithelial cells during collection, which could have resulted in the release of intracellular AS-A into the fluid. Immunoblotting revealed the presence of AS-A in the caudal epididymal and vas deferens fluid (Fig. 6). A single band of AS-A was observed, possessing the same molecular mass (68 kDa) as that of the AS-A present in the mouse sperm surface extract [8]. AS-A present in the fluid retrieved from the cauda epididymis and vas deferens was quantified by ELISA at 1.28 ng/μg of total fluid proteins (an average of two analyses with <4% difference).

### *Binding of Alexa-430 AS-A onto Caudal Epididymal Sperm*

AS-A has high affinity ($K_d$ = 8.9 nM) for SGG monolayers [10], which may explain how AS-A in the caudal epididymal fluid is deposited onto the epididymal sperm surface, provided that SGG on intact sperm has similar affinity to AS-A. Figure 7 shows that Alexa-430 AS-A bound

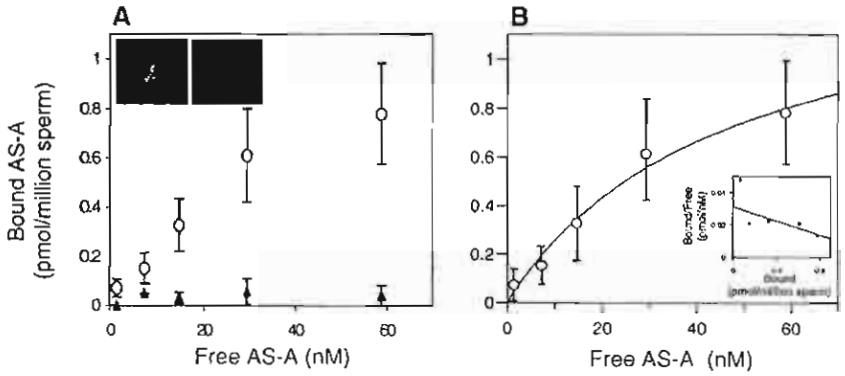


FIG. 7. Binding of Alexa-430 AS-A to caudal epididymal sperm. Alexa-430 AS-A (0–60 nM) was incubated with caudal epididymal sperm ($1.2 \times 10^6$). After washing the unbound protein from sperm, the level of Alexa-430 AS-A binding to sperm (○) was measured spectrofluorometrically. Sperm incubated with 60 nM Alexa-430 ovalbumin (▲) show minimal fluorescence. The amount of Alexa-430 AS-A and Alexa-430 ovalbumin bound to sperm was determined from the standard curve of Alexa-430 AS-A and Alexa-430 ovalbumin, respectively. A) Raw data show the fluorescent pattern of Alexa-430 AS-A binding to caudal epididymal sperm included in the left panel of the inset. In contrast, minimal fluorescence observed in sperm incubated with Alexa-430 ovalbumin is shown in the inset right panel. B) To eliminate the level of nonspecific binding of Alexa-430 AS-A binding to sperm, the fluorescence background of Alexa-430 ovalbumin adhered to sperm was used to subtract the fluorescence reading of sperm-bound Alexa-430 AS-A. Inset: Linear Scatchard plot revealed a $K_d$ of 46 nM. Data at each Alexa-430 AS-A concentration are expressed as mean ± SD from at least three experimental days. Six replicates of sperm samples were used for Alexa-430 AS-A binding for each experimental day.

to caudal epididymal sperm in a concentration-dependent manner (Fig. 7A, open circles). At 60 nM, the binding of Alexa-430 AS-A to sperm was approaching saturation (Fig. 7A). However, binding of Alexa-430 ovalbumin to caudal epididymal sperm was at a very low level (~2% of that observed for Alexa-430 AS-A throughout all concentrations used; Fig. 7A, closed triangles, inset right). The binding of sperm to Alexa-430 ovalbumin was then considered nonspecific, and the values obtained were used for subtraction from the fluorescence values of Alexa-430 AS-A binding to sperm prior to kinetic analysis (Fig. 7B). Fluorescence microscopy revealed that Alexa-430 AS-A bound to the sperm head at the convex ridge and the postacrosomal region (Fig. 7A, insert left). Both of these sites contain SGG (Fig. 4) [11]. When 600 nM unlabeled AS-A was included with 60 nM Alexa-430 AS-A for sperm incubation, binding of Alexa-430 AS-A to sperm was abolished to the background level, implicating specificity of the binding. Analysis of the Alexa-430 AS-A-sperm binding curve revealed $K_d$ of 46.0 ± 15.0 nM AS-A (Fig. 7B), a value within the same range as that of AS-A binding to SGG monolayers [10]. The high SD of this $K_d$ value may reflect inherent heterogeneity of sperm quality. When testicular sperm were used in place of caudal epididymal sperm for incubation with Alexa-430 AS-A, binding of the enzyme to the sperm surface was not observed (data not shown). Possibly, the sperm surface needed to be modified as part of the continuing sperm maturation process during migration through the epididymis to gain the AS-A binding ability. This Alexa-430 AS-A binding to sperm was dependent on surface SGG molecules. Sperm treated with anti-SGG Fab showed a dramatic decrease in Alexa-430 AS-A binding, compared with untreated sperm (Table 1). In contrast, sperm treated with PRS Fab did not show any decrease in Alexa-430 AS-A binding (Table 1). The results strongly suggest that deposition of AS-A onto the sperm surface was via its affinity to SGG on the sperm plasma membrane. Because α-mannosidase, an acidic glycohydrolase present in the epididymal fluid, deposits onto sperm via interaction with mannose-6-phosphate receptor on the sperm surface [23] and because phosphorylation has been identified on the mannose residues of testis AS-A *N*-linked oligosaccharides [24], AS-A deposition onto the sperm surface may also be through its interaction with mannose-6-phosphate receptor. To test this hypothesis, mannose-6-phosphate (having affinity for mannose-6-phosphate receptor) was included in Alexa-430 AS-A-sperm coincubates. Mannose-6-phosphate, even at 1 mM, did not inhibit Alexa-430 AS-A binding to sperm, indicating that deposition of Alexa-430 AS-A onto sperm was not through the mannose-6-phosphate receptor mechanism.

## DISCUSSION

The presence of AS-A in the sperm acrosome has been proposed, based on biochemical characterization [5–7]. Recently, we localized AS-A to the head surface of mouse and pig sperm; this sperm surface AS-A participates in ZP binding [8, 9]. Therefore, information regarding the source of this sperm surface AS-A may be used to develop a

TABLE 1. Binding of Alexa-430 AS-A to mouse sperm is inhibited by anti-SGG Fab but not by mannose-6-phosphate.[a]

| Treatment | Concentration (nmol/treatment) | % Control | % Inhibition |
|---|---|---|---|
| None | | 100 | 0 |
| Anti-SGG Fab[b] | 0.15 | 44.7 ± 11.5[c] | 55 |
| | 0.7 | 38.9 ± 15.1[c] | 61 |
| | 1.5 | 32.7 ± 8.1[c] | 67 |
| PRS Fab | 0.15 | 109.2 ± 6.3 | 0 |
| | 0.7 | 119.1 ± 2.2 | 0 |
| | 1.5 | 116.5 ± 9.8 | 0 |
| Mannose-6-phosphate | 7 | 98.6 ± 3.6 | 0 |
| | 70 | 97.5 ± 4.8 | 0 |
| | 350 | 95.9 ± 6.3 | 0 |

[a] Mouse sperm (200 000) in 150 μl KRB-Hepes were used for each treatment. Because the level of SGG is ~600 pmol per $10^6$ sperm, the 200 000 sperm used for each treatment contained 0.12 nmols of SGG.
[b] The molar ratios of anti-SGG Fab to SGG in treated sperm were 1.25, 5.83, and 12.5 times that of SGG in the treated sperm.
[c] $P < 0.005$, compared with controls (no treatment).

means to regulate sperm fertilizing ability. Immunocytochemistry results of mouse testis sections confirmed the presence of AS-A in the acrosome and acrosomal processes of round and elongating spermatids, respectively (Fig. 1). However, AS-A was absent on the testicular sperm surface, as revealed by IIF of live sperm (Fig. 2). In contrast, SGG was present on the surface of testicular sperm (Fig. 4). Because the galactosyl sulfate moiety, the antigenic epitope of SGG, rises only a short distance from the sperm plasma membrane bilayer, the positive staining of SGG suggests that the testicular sperm surface was not masked, and peripheral plasma membrane proteins, such as AS-A [8, 9], should be even more exposed. Therefore, the negative IIF staining of AS-A on live testicular sperm strongly suggests its absence on the surface of these sperm and argues against the possibility that acrosomal AS-A is mobilized to the sperm surface during spermiogenesis.

Immunocytochemical staining also revealed the presence of AS-A in Sertoli cells. In the majority of these cells, the globular body-like staining patterns of AS-A, regionalized mainly in the supranuclear region, might reflect lysosomal localization of the enzyme. This postulation is supported by previous reports of the presence of AS-A in lysosomes of Sertoli cells [25] and other somatic cells [18, 26–30] (Fig. 1a). Late residual bodies present in Sertoli cells of certain stages of the spermatogenic cycle were also stained intensely with anti-AS-A (Fig. 1b), although early residual bodies showed negative staining. Because the late residual bodies eventually fuse with the Sertoli cell lysosomes [31], the results suggest that AS-A present in the late residual bodies is derived from Sertoli cell lysosomes following the fusion of one with the other. This result for AS-A is similar to that described for β-hexosaminidase A [32]. AS-A in Sertoli cells does not appear to be secreted, because the enzyme was not found in the medium of primary culture of mouse Sertoli cells (N. Tanphaichitr, unpublished results).

Results from IIF and flow cytometry analyses for AS-A on live testicular sperm, caput and corpus epididymal sperm, and caudal epididymal and vas deferens sperm (Figs. 2 and 3) indicate that AS-A is acquired by the sperm surface during sperm transit through the epididymis. A few lines of evidence indicate that principal cells from the cauda epididymis and vas deferens are the source of this sperm surface AS-A. Immunocytochemistry results revealed AS-A staining in strips of principal cells in the cauda epididymis (Fig. 1f) and most of the principal cells in the vas deferens (Fig. 1g). Principal cells are recognized for their secretory activities [21, 33]. The network patterns of AS-A staining in principal cells (Fig. 1f, inset), resembling the endoplasmic reticulum and Golgi apparatus [34], suggest that AS-A is synthesized in principal cells. Similar staining patterns have been noted in principal cells for SGP-2, immobilin, and other known secreted proteins of the epididymis [35]. The presence of the AS-A transcript in the epididymis as shown by RT-PCR (Fig. 5) also supports this interpretation. Immunoblotting confirmed the presence of AS-A in the epididymal fluid (Fig. 6). These results strongly suggest that AS-A is secreted by epididymal epithelial cells into the lumen.

Although immunocytochemistry also revealed the presence of AS-A in the initial segment, caput, and corpus and cauda epididymis, the enzyme was restricted to apical cells, narrow cells, and clear cells (Fig. 1, d–f). As demonstrated for other lysosomal enzymes, immunocytochemical reaction and electron microscopic immunogold labeling in these cell types appear to represent the targeting of these enzymes from the Golgi apparatus via small vesicles directly to their lysosomes, which were abundant in these cells [21, 31, 36, 37]. This may also be the case for AS-A. Alternatively, because narrow cells, apical cells, and clear cells are known for their endocytotic activities [21, 33], AS-A present in these cells may have originated from transit sperm with damaged acrosomes through the endocytosis mechanism. AS-A in these cells may function in desulfation of SGG, endocytosed from remnant membrane vesicles in the epididymal fluid. These vesicles could originate from the shedding of excess plasma membranes of round spermatids during their differentiation to testicular spermatozoa and/or from plasma membranes of damaged sperm in transit through the initial segment and the proximal region of the caput epididymis.

Once secreted in the fluid, AS-A may readily be deposited onto the caudal epididymal and vas deferens sperm surface. This proposal is supported by the observation that AS-A in the epididymal fluid and that on the sperm surface have the same molecular mass (68 kDa) (Fig. 6). Deposition of AS-A onto the mature sperm surface occurred through its high affinity for surface SGG ($K_d$ = 46 nM) (Fig. 7 and Table 1). However, deposition was not dependent on mannose-6-phosphate receptor, which is present on the sperm surface [38]; millimolar concentrations of mannose-6-phosphate did not inhibit Alexa-430 AS-A binding to intact caudal epididymal sperm (Table 1). The interaction between AS-A and mannose-6-phosphate receptor on the sperm surface may be of a low affinity, making it impossible for mannose-6-phosphate to compete with AS-A binding to sperm surface SGG, which occurred with high affinity.

ELISA results indicated that AS-A is a minor protein in the caudal epididymal fluid (i.e., 0.13% by weight of total proteins in the caudal epididymal and vas deferens fluid). This result and the strong implication, presented herein, that sperm surface AS-A originates from the epididymal fluid explain why AS-A exists in very small amounts on the surface of mature mouse sperm (1 pmole/$10^6$ sperm [8]). The physiological significance of sperm surface AS-A, however, has been demonstrated. AS-A remains on the anterior head surface of uterine mouse sperm and ejaculated pig sperm and is involved in sperm-egg interaction both in vitro and in vivo [8, 9]. The very small amount of AS-A in the epididymal fluid explains why immunocytochemistry could not detect AS-A in this entity. The molar ratio of AS-A to SGG is very low in mature sperm (SGG is about 600 pmoles/$10^6$ sperm [39], and AS-A is 1 pmole/$10^6$ sperm). This low molar ratio may be essential in maintaining the integrity of the sperm plasma membrane. When purified AS-A at a nonphysiological high concentration was added to capacitated sperm, the sperm developed a premature acrosome reaction [10]. The wide distribution of free SGG molecules (AS-A unbound) may be beneficial for interaction between AS-A-SGG complexes and the ZP glycans. AS-A, being a peripheral plasma membrane protein [8], may first bind to the ZP glycans and anchor them next to the sperm surface for additional interaction with the galactosylsulfate head groups of SGG molecules, which are extended only a short distance from the sperm plasma membrane bilayers. Carbohydrate-carbohydrate interaction between the sugar head groups of glycolipids with other glycans has been well documented and may also be the basis of SGG-ZP glycan interaction [40, 41]. Although this type of interaction is not as strong as protein-

carbohydrate or protein-protein interactions, it can be compensated by availability of multiple glycolipid molecules within the glycan-binding domain. Restricted secretion of AS-A by the epididymis may thus regulate the low molar ratio of AS-A to SGG with a beneficial consequence of better binding of mature sperm to the ZP. As observed with other molecules involved in egg interaction (e.g., P26H [42], α-mannosidase [43], and DE protein [44, 45]), acquisition of AS-A by the sperm surface constitutes part of sperm maturation by providing sperm with increasing ZP-binding ability.

## ACKNOWLEDGMENT

The authors thank Ms. Terri van Gulik for manuscript preparation.

## REFERENCES


1. Rahi H, Srivastava PN. Isolation and characterization of the pig endometrial arylsulphatase A. Biochem J 1983; 211:649–659.
2. Mehl E, Jatzkewitz H. Cerebroside 3-sulfate as a physiological substrate of arylsulfatase A. Biochim Biophys Acta 1968; 151:619–627.
3. Fluharty AL, Edmond J. Arylsulfatase A and B from human liver. Methods Enzymol 1978; 50:537–547.
4. Kolodny EH, Fluharty AL. Lysosomal disorders. In: Scriver CR, Beaudet LL, Sly WS, Valle D (eds.). The Metabolic and Molecular Bases of Inherited Disease. New York: McGraw-Hill; 1995:2693–2741.
5. Brandon CI, Srivastava PN, Heusner GL, Payrer-Hosken RA. Extraction and quantification of acrosin, β-N-acetylglucosaminidase, and arylsulfatase-A from equine ejaculated spermatozoa. J Exp Zool 1997; 279:301–308.
6. Dudkiewicz AB. Purification of boar acrosomal arylsulfatase A and possible role in the penetration of cumulus cells. Biol Reprod 1984; 30:1005–1014.
7. Gadella BM, Colenbrander B, van Golde LMG, Lopes-Cardozo M. Characterization of three arylsulfatases in semen: seminolipid sulfohydrolase activity is present in seminal plasma. Biochim Biophys Acta 1992; 1128:155–162.
8. Tantibhedhyangkul J, Weerachatyanukul W, Carmona E, Xu H, Anupriwan A, Michaud D, Tanphaichitr N. Role of sperm surface arylsulfatase A in mouse sperm-zona pellucida binding. Biol Reprod 2002; 67:212–219.
9. Carmona E, Weerachatyanukul W, Soboloff T, Fluhary AL, White D, Promdee L, Ekker M, Berger T, Buhr M, Tanphaichitr N. Arylsulfatase A is present on the pig sperm surface and is involved in sperm-zona pellucida binding. Dev Biol 2002; 247:182–196.
10. Carmona E, Weerachatyanukul W, Xu H, Fluharty AL, Anupriwan A, Shoushtarian A, Chakrabandhu K, Tanphaichitr N. Binding of arylsulfatase A to mouse sperm inhibits gamete interaction and induces the acrosome reaction. Biol Reprod 2002; 66:1820–1827.
11. White D, Weerachatyanukul W, Gadella B, Kamolvarin N, Attar M, Tanphaichitr N. Role of sperm sulfogalactosylglycerolipid in mouse sperm-zona pellucida binding. Biol Reprod 2000; 63:147–155.
12. Lingwood CA. Colocalization of sulfogalactosylacylalkylglycerol (SGG) and its binding protein during spermatogenesis and sperm maturation. Topology of SGG defines a new testicular germ cell membrane domain. Biochem Cell Biol 1986; 64:984–992.
13. Kornblatt MJ. Synthesis and turnover of sulfogalactoglycerolipid, a membrane lipid, during spermatogenesis. Can J Biochem 1979; 57:255–258.
14. Tanphaichitr N, Smith J, Kates M. Levels of sulfogalactosylglycerolipid in capacitated motile and immotile mouse sperm. Biochem Cell Biol 1990; 68:528–535.
15. Kreysing J, Polten A, Lukatela G, Matzner U, von Figura K, Gieselmann V. Translational control of arylsulfatase A expression in mouse testis. J Biol Chem 1994; 269:23235–23261.
16. Sarafian TA, Fluharty AL, Kihara H, Helfand G, Edmond J. Large-scale purification of pyrogen-free human arylsulfatase A. J Appl Biochem 1982; 4:126–132.
17. Ahmankitpanit V, White D, Suwajanakorn S, Kan F, Nanking M, Wells G, Tanphaichitr N. Role of egg sulfolipidimmobilizing protein I (SLIP1) on sperm-egg plasma membrane binding. Biol Reprod 1999; 61:749–756.
18. Stein C, Gieselmann V, Kreysing J, Schmidt B, Pohlmann R, Waheed A, Meyer HE, O'Brien JS, von Figura K. Cloning and expression of human arylsulfatase A. J Biol Chem 1989; 264:1252–1259.
19. Laemmli UK. Cleavage of structural proteins during the assembly of the head of bacteriophage T4. Nature 1970; 227:680–685.
20. Towbin H, Gordon J. Immunoblotting and dot immunobinding—current status and outlook. J Immunol Methods 1984; 72:313–340.
21. Hermo L, Robaire B. Epididymal cell types and functions. In: Robaire B, Hinton BT (eds.). The Epididymis: From Molecules to Clinical Practice. New York: Kluwer/Plenum; 2002:81–102.
22. Kreysing J, Polten A, Hess B, von Figura K, Menz K, Steiner F, Gieselmann V. Structure of the mouse arylsulfatase A gene and cDNA. Genomics 1994; 19:249–256.
23. Belmonte SA, Challa A, Gutierrez LS, Bertini F, Sosa MA. α-Mannosidase from rat epididymal fluid is a ligand for phosphomannosyl receptors on the sperm surface. Int J Androl 1998; 21:277–288.
24. Sommerlade HJ, Selmer T, Ingendoh A, Gieselmann V, von Figura K, Neifer K, Schmidt B. Glycosylation and phosphorylation of arylsulfatase A. J Biol Chem 1994; 269:20977–20981.
25. Moviglia GA, Cavicchia JC, Bertini F. Lysosomal enzymes in cells separated from rat testis. J Reprod Fertil 1982; 66:123–127.
26. Fujii T, Kobayashi T, Honke K, Gasa S, Ishikawa M, Shimizu T, Makita A. Proteolytic processing of human lysosomal arylsulfatase A. Biochim Biophys Acta 1992; 1122:93–98.
27. Leznicki AJ, Rozanska M. Localizaiton of arylsulphatase A and B activities in rat kidney. Acta Biochim Pol 1991; 38:151–156.
28. Kelly BM, Yu CZ, Chang PL. Presence of a lysosomal enzyme, arylsulfatase-A, in the prelysosome-endosome compartments of human cultured fibroblasts. Eur J Cell Biol 1989; 48:71–78.
29. Leznicki A, Bleszynski W. Histochemical localization of the soluble arylsulphatase activities in rat brain. Histochemie 1970; 24:251–265.
30. Clendenon NR, Allen N. Assay and subcellular localization of the arylsulphatases in rat brain. J Neurochem 1970; 17:865–879.
31. Morales C, Clermont Y, Nadler NJ. Cyclic endocytic activity and kinetics of lysosomes in Sertoli cells of the rat: a morphometric analysis. Biol Reprod 1986; 34:207–218.
32. Hermo L, Adamali HI, Maharan D, Gravel RA, Trasler JM. β-Hexosaminidase immunolocalization and α- and β-subunit gene expression in the rat testis and epididymis. Mol Reprod Dev 1997; 46:227–242.
33. Hermo L, Badran H, Andonian S. The structural organization and functions of the epithelium of the vas deferens. In: Robaire B, Hinton BT (eds.). The Epididymis: From Molecules to Clinical Practice. New York: Kluwer/Plenum; 2002:233–250.
34. Robaire R, Hermo L. Efferent ducts, epididymis, and vas deferens: structure, functions and their regulation. In: Knobil E, Neill J (eds.). The Physiology of Reproduction, 1st ed. New York: Raven Press; 1988:999–1080.
35. Hermo L, Barin K, Oko R. Developmental expression of sulfated glycoprotein-2 in the epididymis of the rat. Anat Rec 1994; 240:327–344.
36. Hermo L, Oko R, Robaire B. Epithelial cells of the epididymis show regional variations with respect to the secretion of endocytosis of immobilin as revealed by light and electron microscope immunocytochemistry. Anat Rec 1992; 232:202–220.
37. Igdoura SA, Hermo L, Morales CR. Sulfated glycoprotein-2 synthesized by nonciliated cells of the efferent ducts is targeted to the lysosomal compartment. Microsc Res Tech 1994; 29:468–480.
38. Barbieri AM, Sosa MA, Grimalt P, Mayorga LS, Bertini F. Phosphomannosyl receptors on the surface of spermatozoa from the cauda epididymis of the rat. Int J Androl 1995; 18:113–119.
39. Furimsky A, Kates M, Tanphaichitr N. Cholesterol and phospholipid contents and molar distribution of phospholipid saturated/monounsaturated and polyunsaturated fatty acyl chains of non-capacitated and capacitated mouse sperm. Biol Reprod 2001; 64(suppl 1):300 (abstract 493).
40. Hakomori S. Cell adhesion/recognition and signal transduction through glycosphingolipid microdomain. Glycoconj J 2000; 17:143–151.
41. Zheng M, Hakomori S. Soluble fibronectin interaction with cell surface and extracellular matrix is mediated by carbohydrate-to-carbohydrate interaction. Arch Biochem Biophys 2000; 374:93–99.
42. Legare C, Berube B, Boue F, Lefievre L, Morales CR, El-Alfy M, Sullivan R. Hamster sperm antigen P26h is a phosphatidylinositol-anchored protein. Mol Reprod Dev 1999; 52:225–233.
43. Tulsiani DRP, NagDas SK, Skudlarek MD, Orgebin-Crist MC. Rat sperm plasma membrane mannosidase: localization and evidence for

proteolytic processing during epididymal maturation. Dev Biol 1995; 167:584–595.
44. Ellerman DA, Brantua VS, Martinez SP, Cohen DJ, Conesa D, Cuasnicu PS. Potential contraceptive use of epididymal proteins: immunization of male rats with epididymal protein DE inhibits sperm fusion ability. Biol Reprod 1998; 59:1029–1036.
45. Moore A, Ensrud KM, White TW, Frethem CD, Hamilton DW. Rat epididymis-specific sperm maturation antigens. I. Evidence that the 26 kD 4E9 antigen found on rat caudal epididymal sperm tail is derived from a protein secreted by the epididymis. Mol Reprod Dev 1994; 37: 181–194.

*Journal of Shellfish Research*, Vol. 23, No. 4, 1087–1095, 2004.

# SEROTONERGIC AND FMRF-AMIDERGIC NEURONS IN THE NERVE GANGLIA OF *HALIOTIS ASININA* LINNAEUS

SASIPORN PANASOPHONKUL,[1] PRAPEE SRETARUGSA,[1]* NARUMOL ANUNRUANG,[1] SOMJAI APISAWETAKAN,[1] PORNCHARN SAITONGDEE,[1] SUCHART E. UPATHUM,[2] TANES POOMTONG,[3] PETER J. HANNA,[4] AND PRASERT SOBHON[1]

[1]*Department of Anatomy, Faculty of Science, Mahidol University, Rama VI Road, Bangkok 10400, Thailand;* [2]*Department of Medical Science, Faculty of Science, Burapha University, Chonburi 20130, Thailand;* [3]*The Coastal Aquaculture Development Center, Department of Fisheries, Klongwan, Prachaubkirikhun Province 77000, Thailand;* [4]*The School of Biological and Chemical Sciences, Deakin University, Geelong, Victoria 3174, Australia*

***ABSTRACT*** The neurons containing serotonin and FMRF-amide were immunohistochemically localized in the cerebral, pleuropedal and visceral ganglia of *Haliotis asinina*. The large (~10 × 20 μm in diameter) and medium size (~7 × 10 μm in diameter) neurons of these three ganglia contained immunoreactivities to both antibodies against serotonin and FMRF-amide, whereas the more numerous small size neurons (<6 × 8 μm in diameter) did not show these immunoreactivities. The large neurons had oval-shaped nuclei containing mostly euchromatin and long cytoplasmic processes, whereas the medium size neurons, which could be neurosecretory cells, contained round nuclei with patches of heterochromatin and lack processes. The 5-HT immunoreactive cells were concentrated in the upper half of the medial edge of the cerebral ganglion, the edge of ventral and dorsal horns of the pleuropedal ganglion, and the right latero-ventral edge of the visceral ganglion; whereas the FMRF-amide immunoreactive neurons were concentrated in the dorsal and ventral edges of the cerebral ganglion, the edge of dorsal horn and the dorsal edge of the body of the pleuropedal ganglion, and the left latero-ventral and latero-dorsal edge of the visceral ganglion. The 5-HT cells were most numerous in the cerebral (~70/2,300 cells per section), and the pleuropedal ganglia (~120/2,700 cells per section), whereas they were least numerous in the visceral ganglion (~50/400 cells per section). The FMRF-amide cells were most numerous in the cerebral (~76/2,000 cells per section), and the pleuropedal ganglia (~130/2,500 cells per section), whereas they were least numerous in the visceral ganglion (~60/1,050 cells per section). The present study suggests that serotonin and FMRF-amide are major neurotransmitters in the neural ganglia, with only the large- and medium-sized neurons involved in the production and storage of these two neurotransmitters.

***KEY WORDS:*** *Haliotis asinina*, serotonin, FMRF-amide, immunohistochemistry, nerve ganglia

## INTRODUCTION

Serotonin (5-hydroxytryptamine; 5-HT) and tetrapeptide Phe-Met-Arg-Phe-amide (FMRF-amide) are neurotransmitters that play many important roles in controlling the physiologic and behavioral processes of invertebrates (Kuang et al. 2002, Mercier et al. 2003). In molluscs, 5-HT controls heartbeat (Skelton et al. 1992), locomotion (McClellan et al. 1994, Satterlie & Norekian 1995), feeding (Kupfermann & Weiss 1981), memory and learning (Nelson & Alkon 1997), and reproduction (Ram et al. 1996, Juneja & Koide 1996). FMRF-amide can evoke muscle tension (Schot & Boer 1982, Buckett et al. 1990), modulate cardiac output (Buckett et al. 1990), and reproduction (Lehman & Greenberg 1987). By immunolocalization methods, 5-HT and FMRF-amide have been observed in many ganglia of the central nervous system (CNS) of gastropod molluscs (Audesirk 1985, Elekes 1992, Croll et al. 2001, Fickbohm et al. 2001), especially in the pulmonate snails, *Helix pomatia* and *Helix aspersa* (Griffond et al. 1986, Lehman & Price 1987, Hernadi et al. 1989, Elekes & Nassel 1990, Hernadi 1992). Other gastropods that have also been investigated are a sea hare *Aplysia kurodai*, a land snail *Achatina fulica* (Fujii & Takeda 1988), an aquatic snail *Lymnaea stagnalis* (Audesirk 1985), and an opisthobranch *Phestilla sibogae* (Croll et al. 2001). The 5-HT and FMRF-amide immunoreactive neurons have been identified in the CNS of all these species with specific distribution patterns. For example, in *Aplysia kurodai* and *Achatina fulica*, the 5HT-immunoreactive cells and neuropils were observed in all ganglia except the left pleural ganglia. The sizes of these neurons are generally large, and some reach up to 50–70 μm in diameter. FMRF-amide immunoreactive neurons have been located throughout the central ganglia (cerebro-pleural, parietal, pedal, and visceral ganglia) of *Phestilla sibogae*, and about 65–100 intensely labeled neurons were observed in these ganglia, whereas another 40–45 neurons were weakly or variably stained (Croll et al. 2001). A similar study has been done in an aquatic snail, *Lymnaea stagnalis*, in which FMRF-amide immunoreactive neurons and neuropils were consistently found in the cerebral, pedal, right parietal, and visceral ganglia (Audesirk 1985). Moreover, the colocalization of 5-HT and FMRF-amide has also been performed in a chiton, *Lepidopleurus asellus*, which is a primitive mollusc species (Moroz et al. 1994). Both types of neurons are distributed in characteristic patterns in the CNS (i.e., the 5-HT immunoreactive neurons are concentrated in the ventral cords while FMRF-amide immunoreactive neurons in the lateral cords). In addition, a tight network of 5-HT and FMRF-amide immunoreactive nerve fibers were found in the body wall and the foot muscle (Moroz et al. 1994). The prevalence of serotonergic and FMRF-amidergic neurons in the CNS in gastropods implies that they are important neurotransmitters in these animals.

In contrast to the higher gastropods, very few works along this line have been carried out in the primitive gastropods. Only two studies reported the presence of 5-HT in the cerebral ganglion of developing larvae of red abalone, *Haliotis rufescens* (Kataoka et al. 1987, Barlow & Truman 1992) and 5-HT-immunoreactive fibers in the outer zone of the retinal plexiform layer and the optic nerve trunk (Kataoka et al. 1987). In the present study, we have examined and compared the distribution of 5-HT and FMRF-

*Corresponding author. E-mail: scpsr@mahidol.ac.th

aminergic neurons in the neural ganglia of the CNS of *Haliotis asinina*, a tropical abalone commonly found in Thai coastal waters.

## MATERIALS AND METHODS

### *Tissue Collection*

Adult male *H. asinina* (age >16 mo) were collected from a land-based aqua culture system at Coastal Aquaculture Development Center, Department of Fisheries, Prachaubkirikhun Province, Thailand. They were kept in concrete tanks housed in the shade and well flushed with mechanically circulated sand-filtered seawater and provided with an air delivery system to maintain the stable controlled environment. The optimum level of salinity is about 22.5–32.5 ppt and temperature ~22°C to 26°C (Singhagraiwan & Doi 1999). They were fed with macroalgae (usually *Gracilaria spp.* and *Laminaria spp.*), supplemented with artificial food.

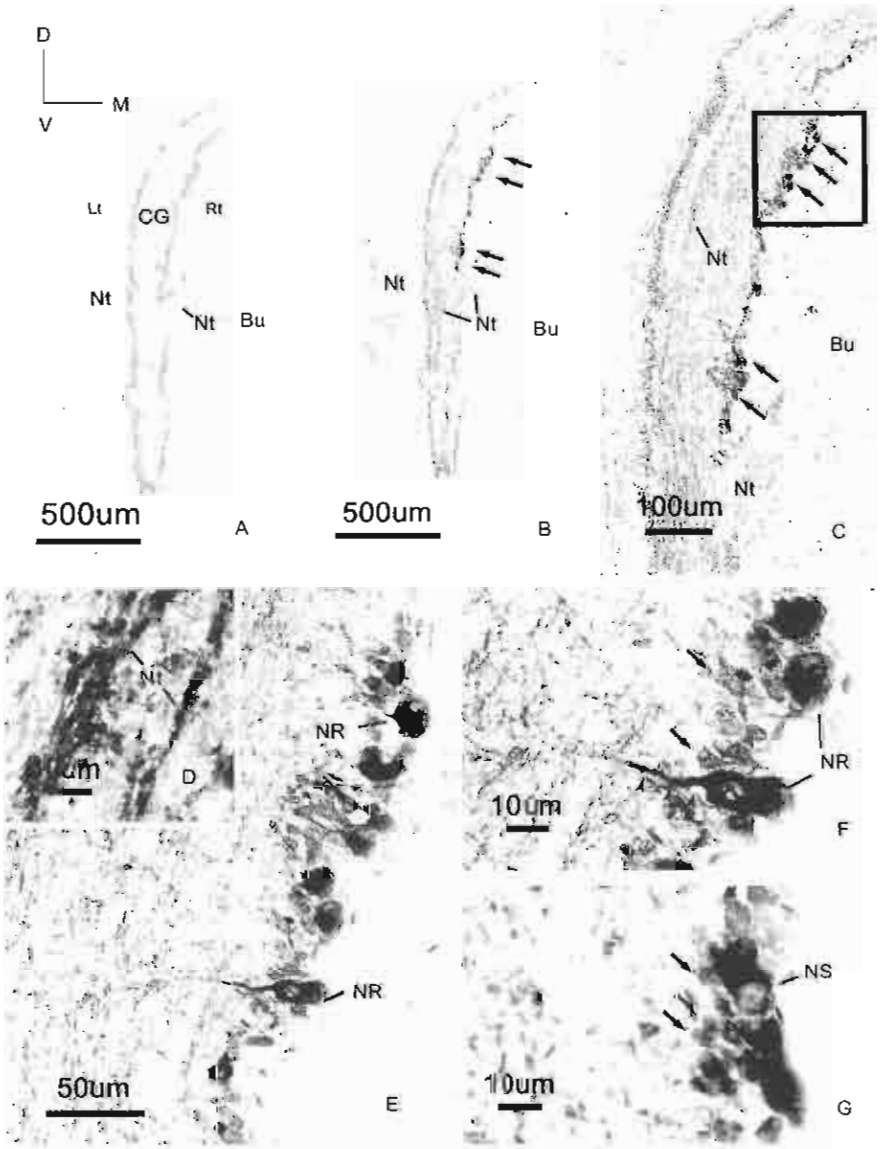


Figure 1. LM micrographs illustrating the location and characteristics of serotonergic neurons and nerve fibers in the cerebral ganglia of *H.asinina*: A. A negative control cross section showing a cerebral ganglion (CG) and nerve bundles (Nt) arising from the ganglion to buccal mass (Bu). D = dorsal, V = ventral, M = medial, Lt = left side, Rt = right side. B & C. 5-HT neurons (black dots- arrows), concentrated in the upper half of the cortex at the medial edge of the ganglion, with the immunoreactive nerve fibers (Nt) distributed throughout the neuropil of the ganglion, and the nerve branch running into the buccal mass (Bu). D. A high-power micrograph of the neuropil of a cerebral ganglion, showing the varicosities of 5-HT immunoreactive nerve fibers (Nt). E. A micrograph from the boxed area in C, showing a row of serotonergic neurons in the cortex of the ganglion. F & G. High-power micrographs of the two types of serotonergic neurons from E, the large neuron (NR) characterized by the presence of long axon (arrowheads), and the medium-size neurosecretory neuron (NS). No immunoreactivity is detected in the small neurons (arrows).

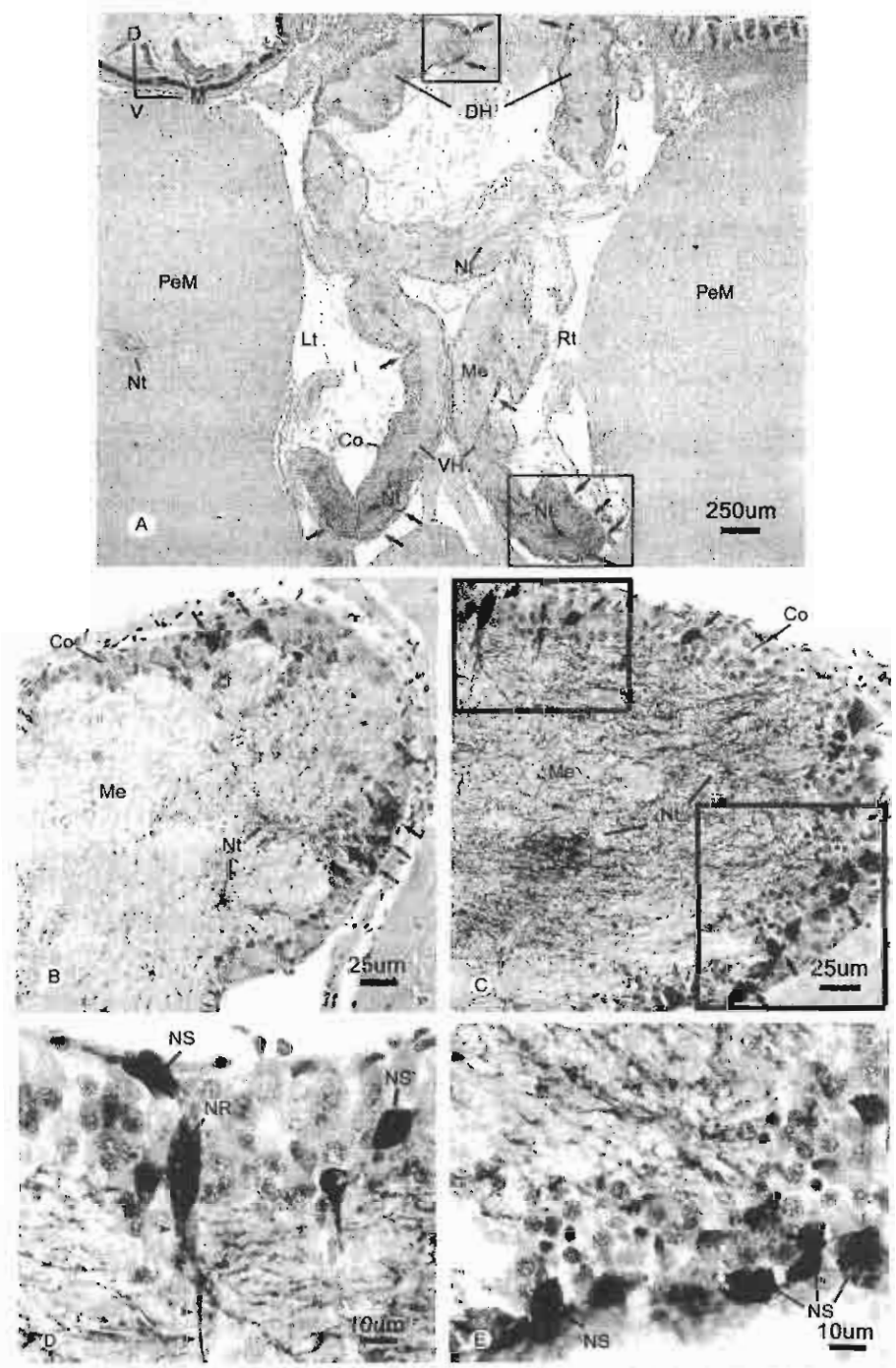


Figure 2. LM micrographs of a mid cross section of the pleuropedal ganglia of *H. asinina*, illustrating the distribution and characteristics of serotonergic neurons and nerve fibers. A. A low-power micrograph, showing the distribution of 5-HT neurons (arrows) concentrated in the upper or lower one-third of the cortex (Co) of the dorsal (DH) or ventral horns (VH). The positively stained nerve fibers (Nt) are also present in the medulla (Me) and pedal muscle (PeM). Lt = left, Rt = right. B & C. Medium-power micrographs of the boxed areas of left dorsal horn (B) and right ventral horn (C) in A, showing groups of serotonergic neurons (arrows) in the cortex (Co) and positively stained nerve fibers (Nt) in the medulla (Me). D & E. High-power micrographs of serotonergic neurons from the boxed area in C, showing the large size neuron (NR) characterized by the long axon (arrowheads), and medium-size neurosecretory cells (NS) without processes.

*Antibodies Against 5-HT and FMRF-Amide*

The rabbit polyclonal antibody against 5-HT was purchased from Zymed Laboratories Inc. For antibody against FMRF-amide, the peptide (Sigma Company) was dissolved in deionized water at 0.5 mg/mL. This solution was mixed with keyhole lympet hemocyanin (KLH) (10 mg/mL) in 1:1 ratio. Then, glutaraldehyde was added up to 0.375% with 1 M glycine-HCl. After that, the solution was mixed with 0.1 M phosphate buffered saline (PBS) containing complete Freund's adjuvant in 1:1 ratio for subcutane-

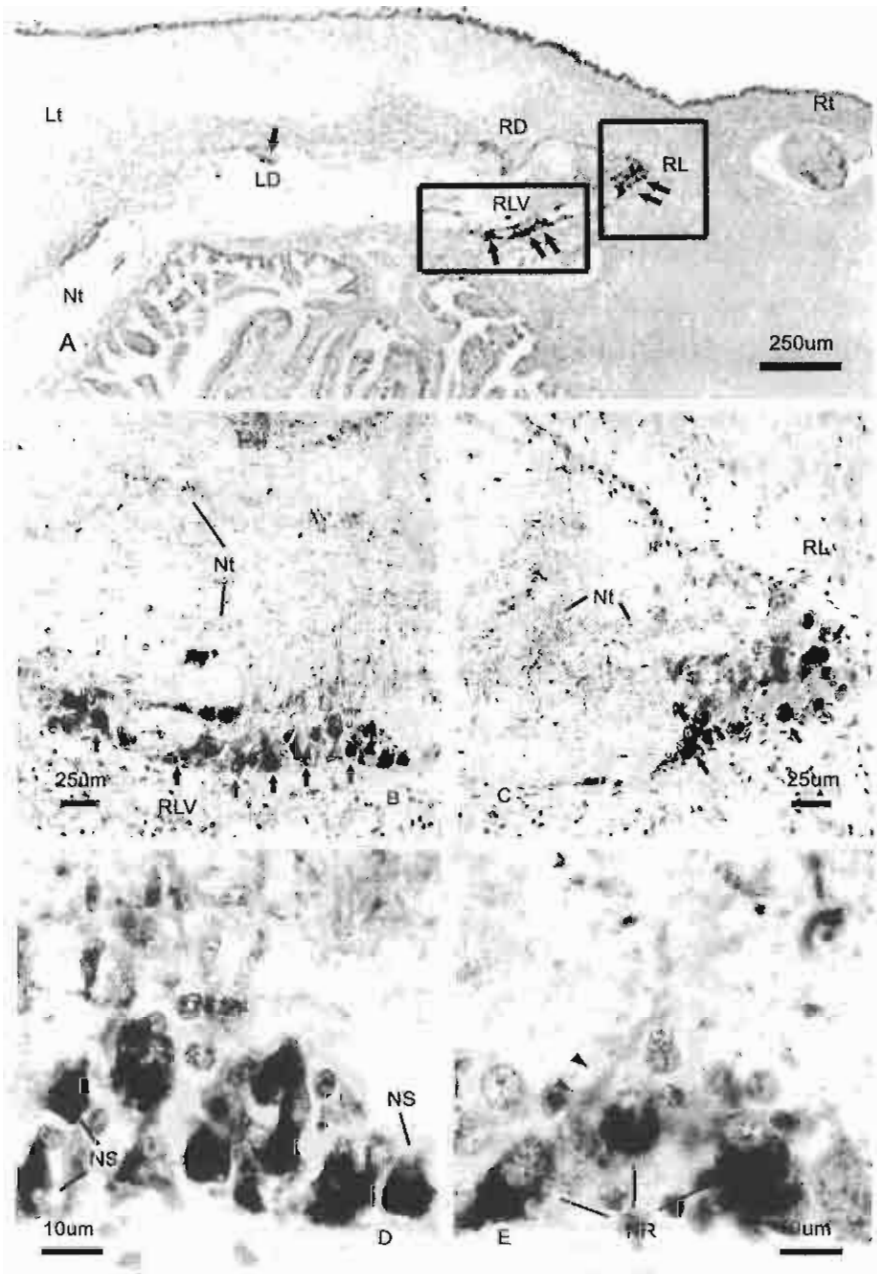


Figure 3. LM micrographs of a cross section of a visceral ganglion, illustrating the location and characteristics of serotonergic neurons and nerve fibers. A. A low-power micrograph, showing two groups of serotonergic neurons (arrows) in the right lateral (RL-arrows) and right latero-ventral (RLV-arrows) edge of the ganglion, whereas only few positive cells are found in the right and left dorsal edge (RD, LD-arrows). A few immunoreactive nerve fibers (Nt) are also present in the ganglion. B & C. Medium-power micrographs, showing groups of 5-HT neurons from the boxed areas in A, and the 5-HT immunoreactive nerve fibers in the medulla region. D & E. High-power micrographs, showing both types of large (NR) and medium (NS) size serotonergic neurons in the boxed areas in A.

ous injection into experimental mice (300 μL/mouse). After 14 days, a similar dose of FMRF-KLH mixed with incomplete Freund's adjuvant was injected to boost the immune response of the animals. On day 49, the blood was collected from the heart bleeding and centrifuged at 5,000*g*, and the serum was collected, mixed with 20 folds in volume of KLH solution to preabsorb antiKLH in the antiserum. Then, the dot blot ELISA was used to detect the specificity of the mouse antiFMRF-amide polyclonal antibody, and make sure that antiKLH was completely absorbed. The preabsorbed antiserum was used to stain the sections of cerebral, pleuropedal and visceral ganglia.

### *Immunoperoxidase Method*

Ten adult male *H. asinina* weighing more than 20 g were anesthesized with 5% $MgCl_2$, then the shells were removed. Cerebral, pleuropedal, and visceral ganglia were dissected out and fixed in Bouin's solution at 4°C for 12–16 h. Specimens were washed in 70% ethanol for removal of the fixative. Then, they were dehydrated through a graded series of ethanol (70% to 100%) for 30–45 min each depending on the size of the specimens, cleared with dioxane, infiltrated and embedded in paraffin wax, and sectioned at 5-μm thick. For immunostaining, the paraffin sections of each ganglion were deparaffinized with xylene, rehydrated through a graded series of ethanol (100% to 80%), and finally in 70% ethanol containing 1% Lithium carbonate ($LiCO_3$). The endogenous peroxidase was blocked by treating the sections with 3% $H_2O_2$ in methanol for 30 min. Then, the sections were covered with 4% bovine serum albumin (BSA) in 100 mM phosphate buffered saline, containing 0.25% triton-X 100, pH 7.4 (PBST), for 30 min. Following the blocking step, the consecutive sections were incubated in either the rabbit anti5-HT or mouse antiFMRF-amide serum as the primary antibodies, for 1 h, at 37°C. After incubation, the sections were washed three times with PBST, then incubated in the HRP-conjugated goat antirabbit or anti mouse IgG as the secondary antibodies, for 30 min, at 37°C. Finally, the sections were immersed in the substrate solution containing 0.03% w/v DAB, 0.3% $NiCl_2$, and 0.1% $H_2O_2$ in 50 mM Tris buffer pH 7.2, washed several times with distilled water, counter-stained with Hematoxylin, and mounted in the permount solution. The sections were observed and photographed by a Nikon microscope equipped with digital camera DXM 1200. In addition, the numbers of serotonergic and FMRF-amidergic neurons in each ganglion of each abalone were counted and estimated as number of positive cells per total number of cells per section, which were taken at the middle of each ganglion.

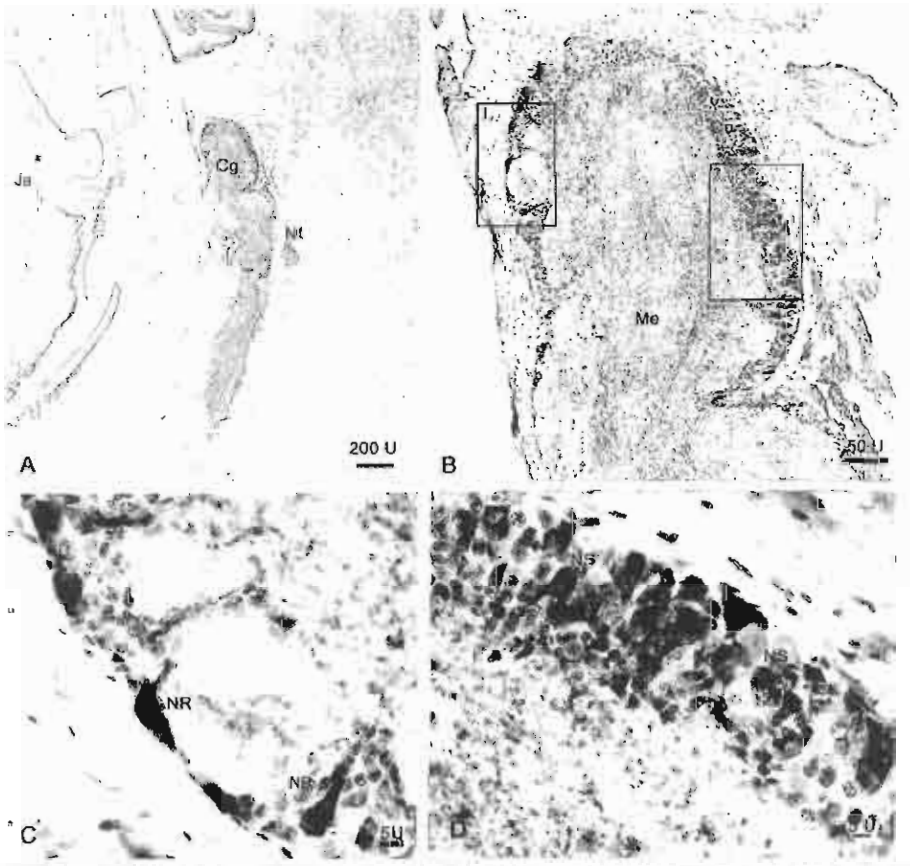


Figure 4. A, Low-power micrograph of a cross section of cerebral ganglia showing the distribution of the FMRF-amide cells (black color) concentrated at the upper and lower parts of lateral and the dorso-medial edges of the ganglion. B, Medium-power micrograph, showing the concentration of immunoreactive FMRF-amide cells in the cortex (Co) of the upper half of the cerebral ganglion, and numerous immunoreactive nerve fibers in the medulla (Me). C & D, High magnification showing the FMRF-amide immunoreactive large neurons (NR) and medium size neurons (NS) in the cortex of the cerebral ganglion. Ja = Jaw.

## RESULTS

### *Immunohistochemical Localization*

By using immunoperoxidase technique enhanced with nickel chloride ($NiCl_2$) we were able to localize two separate sets of neurons containing 5-HT and FMRF-amide in the cerebral, pleuropedal and visceral ganglia. The patterns of distribution of these two types of neurons in each ganglion are described below.

### *Cerebral Ganglion*

The 5-HT cells are concentrated in the upper half of the cortex of medial edge of the ganglion (Figs. 1B, C, Fig. 7A), whereas there are few widely scattered 5-HT cells in the lateral edge of the ganglion. FMRF-amide cells are concentrated in the cortex of the dorsal and ventral edges of the ganglion whereas the lateral edge and the dorso-medial edge have only few widely scattered FMRF-amide cells (see Figs. 3A, B, Fig. 7A). Both 5-HT and FMRF-amide immunoreactive nerve fibers were also observed throughout the neuropils of the ganglia. The 5-HT immunoreactive nerves branching out from the ganglia were also observed around the head

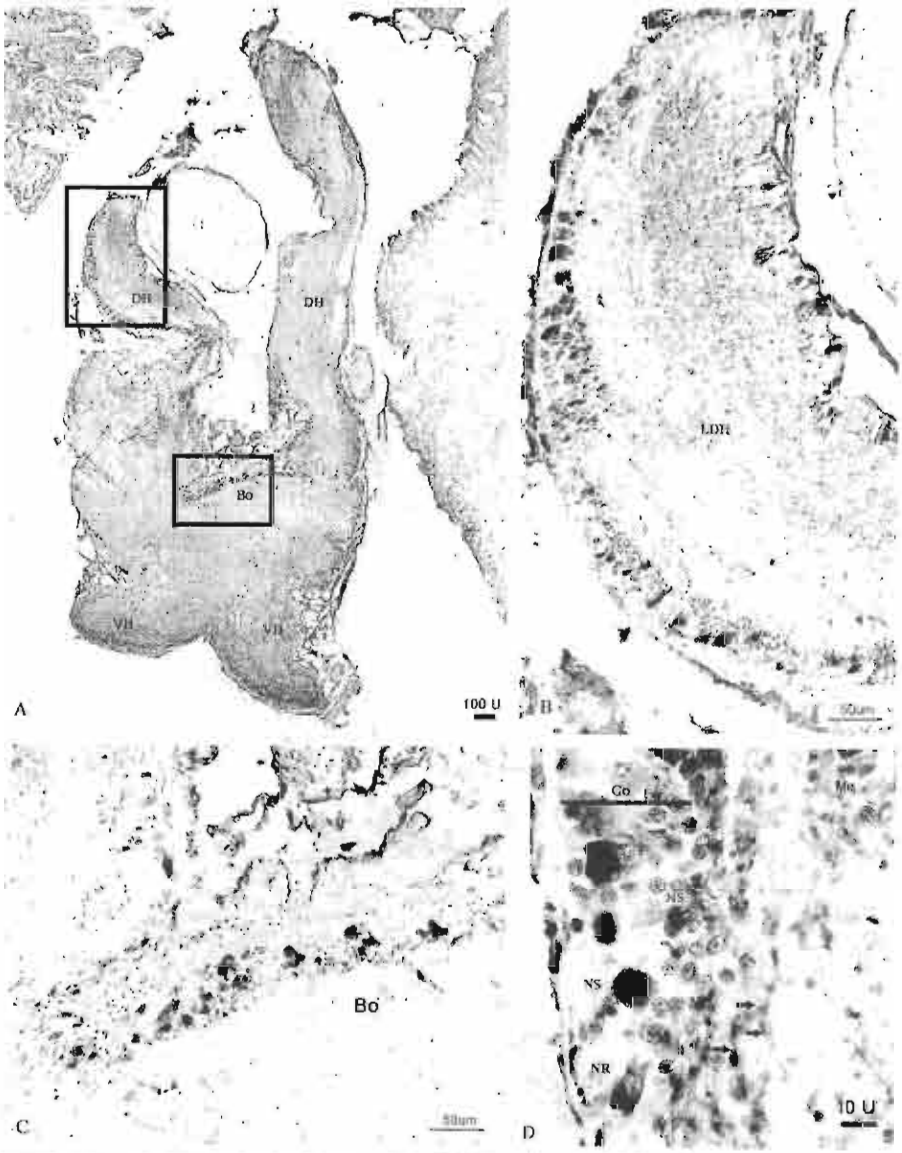


Figure 5. A. Low-power micrograph showing the distribution of the FMRF-amide cells (black color) concentrated in the cortex of the upper one-third of both medial and lateral edges of the dorsal horn (DH), and the dorsal edge of the body part (Bo) of the pleuropedal ganglia. B & C. Medium-power micrographs of FMRF-amide immunoreactive cells in the cortex of left dorsal horn (LDH) and dorsal edge of the body (Bo) of pleuropedal ganglia. D. A high-power micrograph of left dorsal horn (DH) in A, showing immunoreactive large (NR) and medium size neurons (NS) in the cortex (Co), and nerve fibers with varicosities (arrows) in medulla (Me) of the ganglia.

and buccal areas of the abalone, but fewer FMRF-amide immunoreactive fibers were found (Fig. 1B, see Fig. 4A later). Based on the histologic characteristics, the serotonergic neurons could be classified into 2 types (i.e., the large and medium size neurons). The large oval or pyrimidal shape neurons (about 10 × 20 μm) contain the oval-shaped nuclei with complete euchromatin, and usually large nerve processes (Figs. 1E, F), whereas the medium size neurons (about 7 × 10 μm), which could be neurosecretory cells, contain round nuclei with patches of heterochromatin (Upatham et al. 1998, Kruatrachue et al. 1999, Thongkukiatkul et al. 2000) and lacking processes (Fig. 1G). However, there was no immunoreactivity of 5-HT in the cell bodies of small neurons (<6 × 8 μm) (Figs. 1F, G). Similarly, from the histologic characteristics, FMRF-amidergic neurons are also mostly the large size neurons and medium size neurons, with no staining in the small neurons (Figs. 4C, D). The number of 5-HT cells are about 70/2,300 cells per section in comparison to 76/2,000 cells per section for FMRF-amide cells.

### *Pleuropedal Ganglion*

In pleuropedal ganglia, the 5-HT cells were found concentrated in the upper and lower one-third part of the dorsal and ventral horns of the ganglion (Fig. 2A to C, Fig. 7B) with widely scattered 5-HT cells on the lateral edge of the ventral horn (Fig. 2A, Fig. 7B). FMRF-amide cells were found concentrated in the cortex of the upper one-third of the dorsal horn and the dorsal edge cortex of the body, with few widely scattered positive cells in the ventral horn and the ventral edge of the body (Fig. 5A). The immunoreactivity of both types of nerve fibers were also found throughout the neuropils of the ganglia, especially in the dorsal and ventral horn regions, (Fig. 5A, C). Histologically, there are only two types

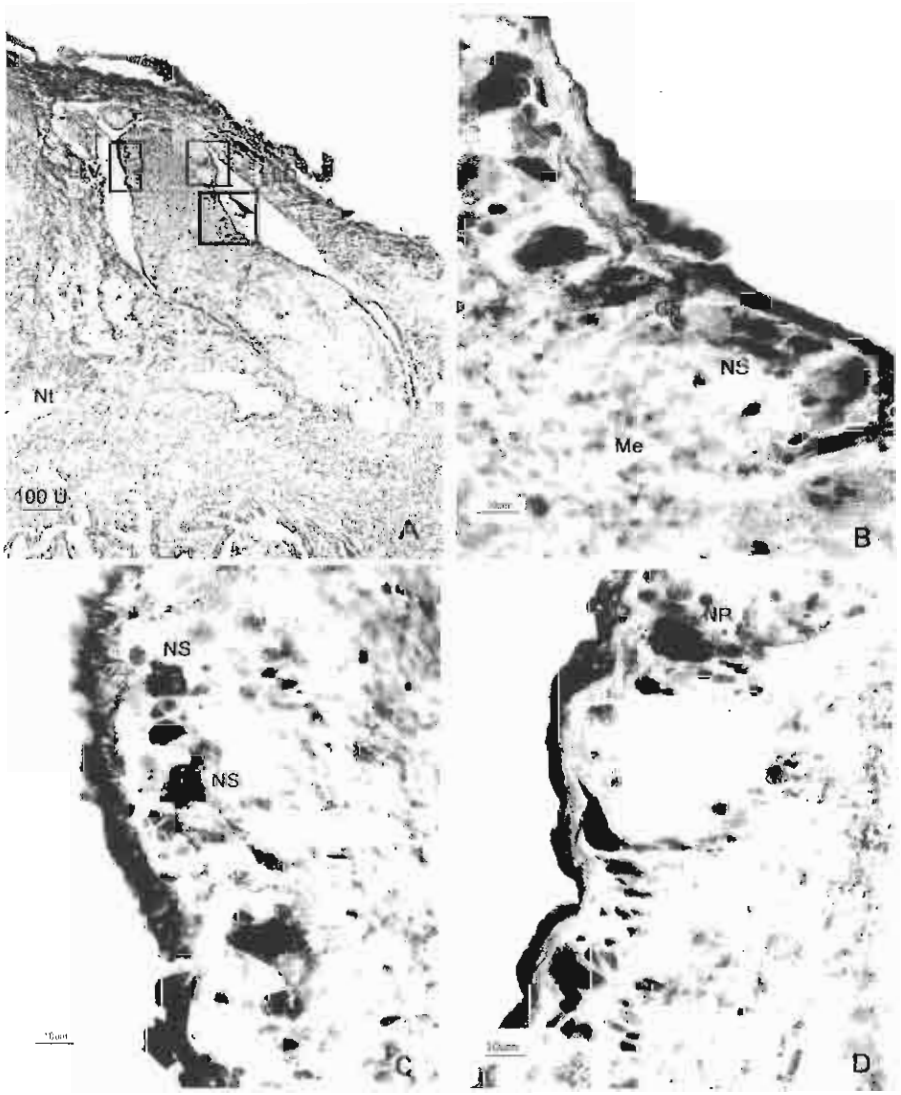


Figure 6. A. A medium-power micrograph and high-power micrographs (B, C, & D) of the visceral ganglion, showing the immunoreactive large (NR) and medium size neurons (NS) in the cortex region (Co) of the left latero-ventral (LLV) and dorsal (LLD) edges of the ganglion.

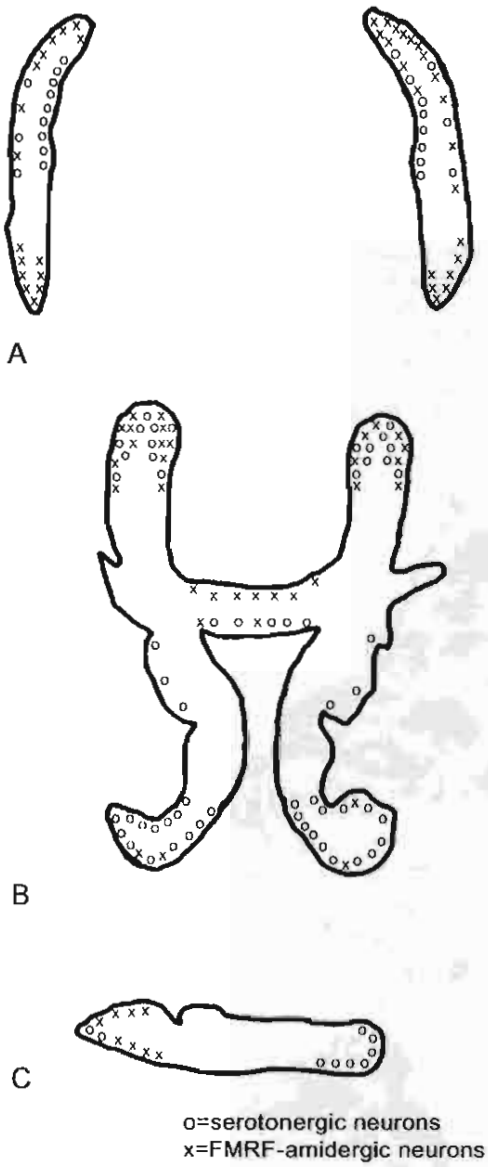


**Figure 7. A schematic diagram summarizing the distinctive distribution patterns of 5-HT and FMRF-amide immunoreactive neurons in the cerebral A, pleuropedal B, and visceral ganglia C of adult *H. asinina*. O = serotonergic neurons, x = FMRF-amidergic neurons.**

of immunoreactive 5-HT and FMRF-amide neurons with similar characteristic as those found in the cerebral ganglia (Figs. 2D, E, Fig. 5D). The numbers of both types of these neurons are approximately equal and they are evenly distributed in specific areas of the ganglia as mentioned. There are about 120/2,700 cells per section for serotonergic neurons in the ganglion, and about 130/2,500 cells per section for FMRF-amide cells.

*Visceral Ganglion*

The 5-HT neurons are concentrated on the right lateral and latero-ventral edge of the ganglion (Figs. 3A to C, Figure 7C), while the FMRF-amidergic neurons are concentrated on the left latero-ventral and latero-dorsal edge (Fig. 6A, Fig. 7C). A few immunoreactive nerve fibers containing 5-HT and FMRF-amide were also observed in the neuropil of the ganglion (Figs. 3A to C). The two types of immunoreactive neurons for both 5-HT and FMRF-amide could also be identified, with similar characteristics as in the cerebral and pleuropedal ganglia (Figs. 3D, E, Fig. 6B to D). The number of serotonergic neurons is about 50/400 cells per section, whereas that of FMRF-amide cells is about 60/1,050 cells per section.

## DISCUSSION

The distribution of 5-HT and FMRF-amide, the major neurotransmitters, have been widely studied in a number of invertebrates (Beltz & Kravitz 1983, Nassel et al. 1985, Fujii & Takeda 1988, Too & Croll 1995, Raikova et al. 2000) including the gastropod molluscs (Audesirk 1985, Elekes 1992, Croll et al. 2001, Fickbohm et al. 2001). However, most previous studies have been done in the opisthobranch and pulmonate species, the higher gastropods. Up to now, there are few works on the prosobranch including abalone, which belong to the most primitive subclass of gastropods (Barlow & Truman 1992).

In the present study, we have studied the distribution patterns of these two types of neurotransmitters in the central ganglia of *H. asinina*. The results showed the presence of immunoreactive 5-HT and FMRF-amide neurons in all three ganglia, with the distinctive distribution patterns in each ganglion as summarized in Figure 7. Both serotonergic and FMRF-amidergic neurons also showed a tendency to be grouped into clusters as in higher gastropods, whereas in species of the lower classes, such as, platyhelminthes, annelida, and arthropoda, serotonergic neurons tend to be more widely scattered (Fujii & Takeda 1988).

*H. asinina* possesses a fairly high number of both serotonergic and FMRF-amidergic neurons in all three ganglia, especially in the pleuropedal ganglia. Fujii and Takeda (1988) found that the number of serotonergic neurons in invertebrates tends to increase in the higher phyla. Furthermore, it was found that one of the main factors that controls the number of 5-HT cells is the physiologic condition. In a snail *Helix pomatia*, it was reported that the number of serotonergic cells in the central ganglia changed with the physiologic conditions of the animals (i.e., they increased during active phase and decreased during hibernation) (Hiripi & Salanki 1973).

While the immunoreactive 5-HT and FMRF-amide neurons were observed in all three ganglia, the immunoreactive nerve fibers containing 5-HT were found concentrated in the neuropils of the ganglia, as well as in musculature of the head, buccal, and foot regions, whereas FMRF-amide fibers were only found in the neuropils and around the hemolymph sacs. These characteristics were similar to the higher gastropod molluscs (Schot & Boer 1982, Fickbohm et al. 2001). Therefore, it is possible that serotonergic neurons may play a primary role in controlling the muscle contraction for head and foot movement and feeding, as in other gastropods, whereas FMRF-amidergic neurons may function mainly as a neuromodulator in the CNS.

The sizes of both serotonergic and FMRF-amidergic neurons are different from those in other gastropods, especially in a pulmonate and opisthobranch molluscs, also in which the positive neurons showed remarkable size range (Fickbohm et al. 2001). In *H. asinina*, both immunoreactive neurons are confined to the large nerve cells with processes and the medium size nerve cells with no processes. The large neurons could be equivalent to the large neu-

rons as classified by Kruatrachue et al. (1999), which seem to be the motor neurons controlling the musculature of head, buccal, and foot region via their long axon. The medium size cells have all characteristics of neurosecretory cells (Kruatrachue et al. 1999). Interestingly all small size nerve cells, which are believed to be association or interneurons, are nonimmunoreactive. Thus, the strong presence of 5-HT and FMRF-amide in the CNS of *H. asinina* suggests that both neurotransmitters have important roles in controlling the physiologic and behavioral responses of this animal as in the other gastropods.

## ACKNOWLEDGMENTS

This research was supported financially by the Thailand Research Fund (Senior Research Scholar Fellowship to Prasert Sobhon, and the Royal Golden Jubilee Ph.D. Scholarship to Sasiporn Panasophonkul).

## LITERATURE CITED

Audesirk, G. 1985. Amine-containing neurons in the brain of *Lymnaea stagnalis*: distribution and effects of precursors. *Comp. Biochem. Physiol.* 81:359–365.

Bailow, L. A. & J. W. Truman. 1992. Patterns of serotonin and SCP immunoreactivity during metamorphosis of the nervous system of the red abalone, *Haliotis rufescens*. *J. Neurobiol.* 23:829–844.

Beltz, B. S. & L. A. Kravitz. 1983. Mapping of serotonin-like immunoreactivity in the lobster nervous system. *J. Neurosci.* 3:585–602.

Buckett, K. J., M. Peters, G. J. Dookray, J. Van Minnen & P. R. Benjamin. 1990. Regulation of heartbeat in *Lymnaea* by motoneurons containing FMRFamide-like peptides. *J. Neurophysiol.* 63:426–435.

Croll, R. P., D. Y. Boudke & M. G. Hodfield. 2001. Histochemical survey of transmitters in the central ganglia of the gastropod mollusc, *Phestilla sibogae*. *Cell Tissue Res.* 305:417–435.

Elekes, K. 1992. Neurotransmitters in the gastropod CNS: comparative immunocytochemistry. *Acta. Biol. Hung.* 43:213–220.

Elekes, K. & D. R. Nassel. 1990. Distribution of FMRFamide-like immunoreactive neurons in the central nervous system of the snail *Helix pomatia*. *Cell Tissue Res.* 262:177–190.

Fickbohm, D. J., P. L. Lynn-Bullock, N. Spitzer, H. K. Caldwell & P. S. Katz. 2001. Localization and quantification of 5-hydroxytryptophan and serotonin in the central nervous systems of *Tritonia* and *Aplysia*. *J. Comp. Neurol.* 437:91–105.

Fujii, K. & N. Takeda. 1988. Phylogenetic detection of serotonin immunoreactive cells in the central nervous system of invertebrates. *Comp. Biochem. Physiol. C.* 89:233–239.

Griffond, B., H. H. Boer & J. Wijdenes. 1986. Localization and function of an FMRFamide-like substance in the aorta of *Helix aspersa*. *Cell Tissue Res.* 246:303–307.

Hernadi, L. 1992. Relationships between the distribution of serotonergic cell bodies and the running of vascular elements in the central nervous system of the snail, *Helix pomatia*. *Comp. Biochem. Physiol. A* 103: 85–92.

Hernadi, L., K. Elekes & K. S. Rozsa. 1989. Distribution of serotonin-containing neurons in the central nervous system of the snail *Helix pomatia*. Comparison of immunocytochemical and 5,6-dihydroxytryptamine labelling. *Cell Tissue Res.* 257:313–323.

Hiripi, L. & J. Salanki. 1973. Seasonal and activity dependent changes of the serotonin level in the CNS and heart of the snail (*Helix pomatia* L.). *Comp. Gen. Pharmac.* 4:285–292.

Juneja, R. & S. S. Koide. 1996. Biochemical pathways involved in serotonin-regulated *Spisula* oocyte maturation and fertilization. *Invert. Reprod. Dev.* 30:47–53.

Katuoka, S., T. Y. Yamamoto & R. Yui. 1987. Serotonergic efferent nerve fibers in the retinal plexiform layer of the abalone. *Tohuku J. Exp. Med.* 153:333–346.

Kruatrachue, M. A., A. Thongkukiatkul, P. Sobhon, E. S. Upatham, C. Wanichanon, P. Sretarugsa, Y. Chitramvong & V. Limthong. 1999. The ultrastructure of neurons and neuroglia in the cerebral and pleuropedal ganglia of *Haliotis asinina* Linnaeus. *Science Asia* 25:137–142.

Kuang, S., S. A. Doran, R. J. Wilson, G. G. Goss & J. I. Goldberg. 2002. Serotonergic sensory-motor neurons mediate a behavioral response to hypoxia in pond snail embryos. *J. Neurobiol.* 52:73–83.

Kupfermann, I. & K. R. Weiss. 1981. The role of serotonin in arousal of feeding behaviour of *Aplysia*. In: B. L. Jacobs & A. Gelperin, editors. Serotonin neurotransmission and behaviour. Cambridge, MA: MIT Press, pp. 255–287.

Lehman, H. K. & D. A. Price. 1987. Localization of FMRFamide-like peptides in the snail *Helix aspersa*. *J. Exp. Biol.* 131:37–53.

Lehman, H. K. & M. J. Greenberg. 1987. The actions of FMRFamide-like peptides on visceral and somatic muscles of the snail *Helix aspersa*. *J. Exp. Biol.* 131:55–68.

McClellan, A. D., G. D. Brown & P. A. Getting. 1994. Modulation of swimming in *Tritonia*: excitatory and inhibitory effects of serotonin. *J. Comp. Physiol. A.* 174:257–266.

Mercier, A. J., R. Friedrich & M. Boldt. 2003. Physiological functions of FMRFamide-like peptides (FLPs) in crustaceans. *Microsc. Res. Tech.* 60:313–324.

Moroz, L. L., L. Nezlin, R. Elofsson & D. Sakharov. 1994. Serotonin and FMRFamide-immunoreactive nerve elements in the chiton *Lepidopleurus asellus* (Mollusca, Polyplacophora). *Cell Tissue Res.* 275:277–282.

Nassel, D. R., E. P. Meyer & N. Klemm. 1985. Mapping and ultrastructure of serotonin-immunoreactive neurons in the optic lobes of three insect species. *J. Comp. Neurol.* 232:190–204.

Nelson, T. J. & D. L. Alkon. 1997. Biochemistry of molluscan learning and memory. *Bioessays.* 19:1045–1053.

Raikova, O. I., M. Reuter, U. Jondelius & M. K. Gustafsson. 2000. The brain of the Nemertodermatida (Platyhelminthes) as revealed by anti-5HT and anti-FMRF amide immunostainings. *Tiss. Cell.* 32:358–365.

Ram, J. L., P. P. Fong & K. Kyozuka. 1996. Serotonergic mechanisms mediating spawning and oocyte maturation in the zebra mussel, *Dreissena polymorpha*. *Invert. Reprod. Dev.* 30:29–37.

Satterlie, R. A. & T. P. Norekian. 1995. Serotonergic modulation of swimming speed in the pteropod mollusc *Clione limacina*. III. Cerebral neurons. *J. Exp. Biol.* 198:917–930.

Schot, L. P. & H. H. Boer. 1982. Immunocytochemical demonstrations of peptidergic cells in the pond snail *Lymnaea stagnalis* with an antiserum to the molluscan cardioactive tetrapeptide FMRF-amide. *Cell Tissue Res.* 225:347–354.

Singhagraiwan, T. & M. Doi. 1999. Seed production and culture of a tropical abalone, *Haliotis asinina* Linne. The Eastern Marine Fisheries Development Center, Thailand: Department of Fisheries, Ministry of Agriculture and Cooperatives.

Skelton, M., A. Alevizos & J. Koester. 1992. Control of the cardiovascular system of *Aplysia* by identified neurons. *Experientia.* 48:809–817.

Thongkukiatkul, A., E. S. Upatham, P. Sobhon, M. Kruatrachue, V. P. Chitramvong, C. Wanichanon, T. Pumthong & J. Negrumal. 2000. Histological studies of the pleuropedal ganglion, visceral ganglion and pedal cord ganglia of *Haliotis asinina*. *J. Med. & Appl. Malacol.* 10: 111–120.

Too, C. K. L. & R. P. Croll. 1995. Detection of FMRFamide-like immunoreactivities in the sea scallop *Placopecten magellanicus* by immunohistochemistry and Western blot analysis. *Cell Tissue Res.* 281:295–304.

Upatham, E. S., A. Thongkukiatkul, M. Kruatrachue, C. Wanichanon, V. P. Chitramvong, S. Sahavacharun & P. Sobhon. 1998. Classification of neurosecretory cells, neurons and neuroglia in the cerebral ganglia of *Haliotis asinina* Linnaeus by light microscope. *J. Shellfish Res.* 17: 737–742.

*Journal of Shellfish Research*, Vol. 23, No. 4, 1097–1106, 2004.

# SENSORY RECEPTORS ON CEPHALIC AND EPIPODIAL TENTACLES OF *HALIOTIS ASININA* LINNAEUS

**CHAITIP WANICHANON,[1]* PRAPHAPORN LAIMEK,[1] NATPILA CHITCHULANON,[1] WORAWIT SUPHAMUNGMEE,[1] SOMJAI APISAWETAKAN,[1] VICHAI LINTHONG,[1] PRAPEE SRETARUGSA,[1] MALEEYA KRUATRACHUE,[2] EDWARD SUCHART UPATHAM,[3] TANES POOMTONG,[4] AND PRASERT SOBHON[1]**

*Departments of [1]Anatomy and [2]Biology, Faculty of Science, Mahidol University, Rama VI Road, Bangkok 10400, Thailand, [3]Department of Medical Science, Faculty of Science, Burapha University, Chonburi 20130, Thailand, [4]The Coastal Aquaculture Development Center, Department of Fisheries, Klongwan, Prachuabkirikun Province 77000, Thailand*

*ABSTRACT* *Haliotis asinina*, a tropical abalone, has a pair each of cephalic, optic, appendage tentacles at the anterior end of the head, and numerous epipodial tentacles distributed on the periphery of its body. The cephalic and epipodial tentacles are essentially sensory organs with similar general structure. In a mature adult (about 16 mo-old), the cephalic tentacle measures about 3.77 cm in length and 0.14 cm in diameter, whereas the epipodial tentacle measures about 9.27 mm in length and 0.59 mm in diameter. In cross sections, each tentacle has a bundle of nerve fiber forming the core structure, surrounded by a thick layer of circular muscle, which also branches into radially oriented fibers. These fibers are interlaced with thick paraxially orientated fibers; together they account for the size and mobility of the tentacles. The surface of both types of tentacles can be divided into three parts: the basal part exhibits slight corrugation consisting of small folds alternated with grooves, the middle part has numerous short hillock-shaped papillae, and the top part has a very high concentration of cone-shaped papillae. Each papilla comprises a group of densely stained ciliated neuroepithelial cells, surrounded by lightly stained supporting epithelial cells bearing microvilli. Gamma amino butyric acid (GABA) was found, by immunohistochemistry, to be highly concentrated in the neuroepithelial cells. The rest of epithelium of both kinds of tentacles is of a columnar type, consisting of clear cells bearing microvilli and goblet cells. The GABA containing neuroepithelial cells are scattered widely among them.

*KEY WORDS:* *H. asinina*, tentacle, histology, sensory receptor, GABA

## INTRODUCTION

Tentacles are important sense organs of gastropods, which contain tactile and chemoreceptor cells in abundance (Chase 1981, Chase & Croll 1981). The cephalic tentacles are among the most important prosobranch sense organs, although little attention has been paid to their histologic structure and function. They are richly endowed with sensory cells, which may be significantly different in each of the major groups of gastropods (Haszprunar 1988, Beesley et al. 1998). Ito et al. (2000) stained the neurons in the tentacles in a terrestrial slug, *Limax marginatus*, by backfilling of the tentacular nerves with Lucifer yellow. Four types of stained neurons comprising sensory neurons, gamma cells, ganglion cells, and lateral cells, were identified in the superior and inferior tentacles. In *Haliotis tuberculata*, a temperate species of abalone, the cephalic tentacle has a mixed sensory and motor nerve, which are centrally located and extends along the length of the tentacle. On the periphery of the nerve, there are sinuses located between muscle fibers, and the latter are arranged longitudinally, obliquely and transversely. Covering the muscle is the surface epithelium that is shown to have folds or papillae (Crofts 1929). The epithelium is of cuboidal type, which consists of 3 cell types: sensory cells, supportive epithelial cells, and widely scattered mucus cells. The sensory cells are spindle-shaped with darkly stained nuclei and supporting cells that are oval and more transparent (Crofts 1929, Bevelander 1988). The epipodium is a series of small tentacles arising from the dorsal part of the foot. They often have the same shape and structure as the cephalic tentacles, although they are much smaller (Crofts 1929, Haszprunar 1988). Crofts (1929) indicated that the epipodial tentacles of *H. tuberculata* had 2 types of epithelial cells: supporting cells and sensory cells.

The present study reports on the structure of both the cephalic and epipodial tentacles of *Haliotis asinina* Linnaeus, a tropical abalone commonly distributed along the Thai coastal water, as observed by light and scanning electron microscopes. In addition, immunohistochemistry showed that GABA, a major neurotransmitter of gastropods, is highly concentrated in the sensory epithelial cells.

## MATERIALS AND METHODS

### *Collection of Abalone Specimens*

Adult abalones over 12-mo-old were obtained from a land-based culture system at Coastal Aquaculture Development Center, Department of Fisheries, Prachaubkirikun Province, Thailand. They were reared in concrete tanks housed in the shade, and well flushed with mechanically circulated sand-filtered seawater, and provided with an air delivery system to maintain a stable controlled environment. The optimum level of salinity used was ~22.5–32.5 ppt, and the temperature about 22 °C to 26 °C (Singhagraiwan & Doi 1993). They were fed with macroalgae (usually *Gracilaria* spp. and *Laminaria* spp.), supplemented with artificial food.

They were anesthetized in 5% $MgCl_2$, after which their shells were removed. The tentacles (cephalic, epipodial and appendage) were measured, dissected out and processed for light microscope (LM) and scanning electron microscope (SEM) studies.

### *Specimen Preparation for SEM*

Tentacles were cut and fixed in a Karnovsky fixative (4% glutaraldehyde 2% paraformaldehyde in 0.1M sodium cacodylate

* Corresponding author. E-mail: scewn@mahidol.ac.th.

buffer), pH 7.8, at 4 °C overnight, and washed in 0.1 M sodium cacodylate buffer. They were postfixed in 1% osmium tetroxide in 0.1 M sodium cacodylate buffer for 1 h, at 4 °C. Then, they were dehydrated in graded series of ethanol, and dried in a Hitachi HCP-2 critical point drying machine, using liquid $CO_2$ as a transitional medium. They were then mounted on aluminum stubs and coated with platinum and palladium in an ion sputtering apparatus, Hitachi E 5000. The specimens were examined in a Hitachi S-2500 scanning electron microscope with an accelerating voltage of 15 kV.

### *Specimen Preparation for LM*

Specimens were fixed in Bouin solution in 0.14 M NaCl for 24 h and washed with 70% ethyl alcohol. They were then dehydrated through a graded series of ethanol, cleared with dioxane, infiltrated and embedded in paraffin. Five-micron-thick sections were cut and stained with Harris hematoxylin and eosin.

For semithin section, specimens were fixed in Karnovsky fixative, pH 7.8, at 4 °C for overnight, and washed with 0.1M sodium cacodylate buffer. They were postfixed in 1% osmium tetroxide in 0.1M sodium cacodylate buffer, at 4 °C, for 1 h. Then, they were dehydrated in a graded series of ethanol and embedded in Araldite 502 resin. Sections were cut at 1-μm thickness with Porter Blum MT-2 μL tramicrotome, and stained with methylene blue or PAS-methylene blue. Examination and photographing of the tissue sections were done under a Nikon eclipse E600 microscope and Nikon digital camera DXM1200.

### *Immunoblotting for GABA*

The neural and tentacular tissues were tested for the presence of GABA by homogenizing the cerebral ganglia, pleuropedal ganglia, tentacular, and epipodial tentacles collected from adult *H. asinina* in 0.1 M sodium phosphate buffer saline (PBS) containing 1 mM phenyl-methyl-sulfunyl-fluoride (PMSF). The homogenate was centrifuged at 12000*g* for minutes, after which the supernatant was collected, and the protein contents determined by Lowry method (Lowry et al. 1951). Proteins were adjusted to be about 1 mg/mL by adding the extraction buffer. A 1-μL of each suspension at the dilutions at 1:1, 1:10, and 1:100 were spotted onto nitocellulose (NC) sheets. The NC sheets were then incubated in 5% skimmed milk for blocking of nonspecific binding before being incubated in the primary antibody (mouse monoclonal antibody against GABA, Sigma Chemical Co, USA). Peroxidase-conjugated goat antimouse IgG (Zymed Laboratories) was used as the secondary antibody. The antigen-antibody complexes were then visualized by enhanced chemiluminescence using a LumiGlo kit (KPL, Gaithersburg, MA), with detection made on X-ray film. For positive control neural tissues, the mouse brain was collected and treated similarly.

### *Immunohistochemistry*

Additional 5-μm sections of paraffin-embedded tentacular and epipodial tentacles, as prepared for LM study, were placed on glass slides, deparaffinized, and rehydrated in ethanol and distilled water. They were then stained by an immunoperoxidase method, by first immersing in 0.1M PBS, pH 7.4, containing 0.3% $H_2O_2$ to block endogenous peroxidase, followed by 0.1% glycine in buffer to block free aldehyde groups from the fixative, then in 10% normal goat serum in the buffer for 1 h, in monoclonal antibody (MoAb) (Sigma Chemical Co, USA) at 1:300 dilution, at 20 °C overnight. The sections were thoroughly washed with PBS, followed by incubation in HRP-conjugated secondary antibody (Goat antimouse IgG-HRP, Zymed Laboratories) at 1:200 dilution, for 2 h, and labeled with an aminoethyl carbazole substrate kit (AEC, Zymed Laboratories) for 30 min. Finally, the sections were counter-stained with Harris hematoxylin before being mounted in buffered glycerol, and photographed in Nikon eclipse E600 microscope and Nikon digital camera DXM1200.

## RESULTS

### *Cephalic Tentacle*

Cephalic tentacles of mature female abalone (age about 16 mo) were 3.77 ± 0.59 cm in length and 0.14 ± 0.03cm in diameter (Table 1), whereas the length of cephalic tentacles and the diameters of mature male abalone of similar age was 3.38 ± 0.57 cm and 0.12 ± 0.02 cm, respectively. Noticeably, at the same age the female shell was longer than that of male, and its weight was also heavier than that of male (Table 1).

A cephalic tentacle is round and tapered from the base to the tip (Figs. 1A to C). Based on the surface features as observed under SEM, the tentacle could be divided into 3 parts (i.e., 1/10 basal, 1/10 middle and 8/10 top). There are gradual changes between adjacent parts. The basal part has a smooth surface. It consists of many folds, alternated with grooves (Fig. 1E). Many sensory papillae are located on the folds. On the middle part of the tentacle, there are more papillae on each fold (see Fig. 3C). These papillae are distributed separately and appear taller than those at the base. Each appears as a hillock covered with microvilli and encircling cilia at the tip (Figs. 2C, E). On the top part of the tentacle, the papillae are longer and more numerous than those on the middle part (Fig. 1F). Each appears as a slender truncated cone, projecting perpendicularly to the tentacle's surface (Figs. 2A, F). On top of each papilla, there is a tuft of long cilia, whereas the rest of its surface is covered with microvilli (Figs. 2D,F).

In paraffin sections, the longitudinal section of a cephalic tentacle also exhibits the three parts, based on the degree of surface folding that show gradual changes between adjacent parts (Fig.

TABLE 1.

Sizes of cephalic tentacles and epipodial tentacles of adult *H. asinina*.

| Sex | Weight (g) | Shell Length (cm) | ±SD | Cephalic Tentacle Length (cm) | ±SD | Diameter of Cephalic Tentacle (cm) | ±SD | Epipodial Tentacle Length (cm) | ±SD | Diameter of Epipodial Tentacle (cm) | ±SD |
|---|---|---|---|---|---|---|---|---|---|---|---|
| Male | 29 | 3.77 | 0.62 | 3.38 | 0.57 | 0.12 | 0.02 | 0.80 | 0.24 | 0.06 | 0.01 |
| Female | 33 | 4.11 | 0.64 | 3.77 | 0.59 | 0.14 | 0.03 | 0.93 | 0.32 | 0.06 | 0.02 |

All data are based on 16-mo old fresh abalone of each sex ($n = 15$). SD, standard deviation.

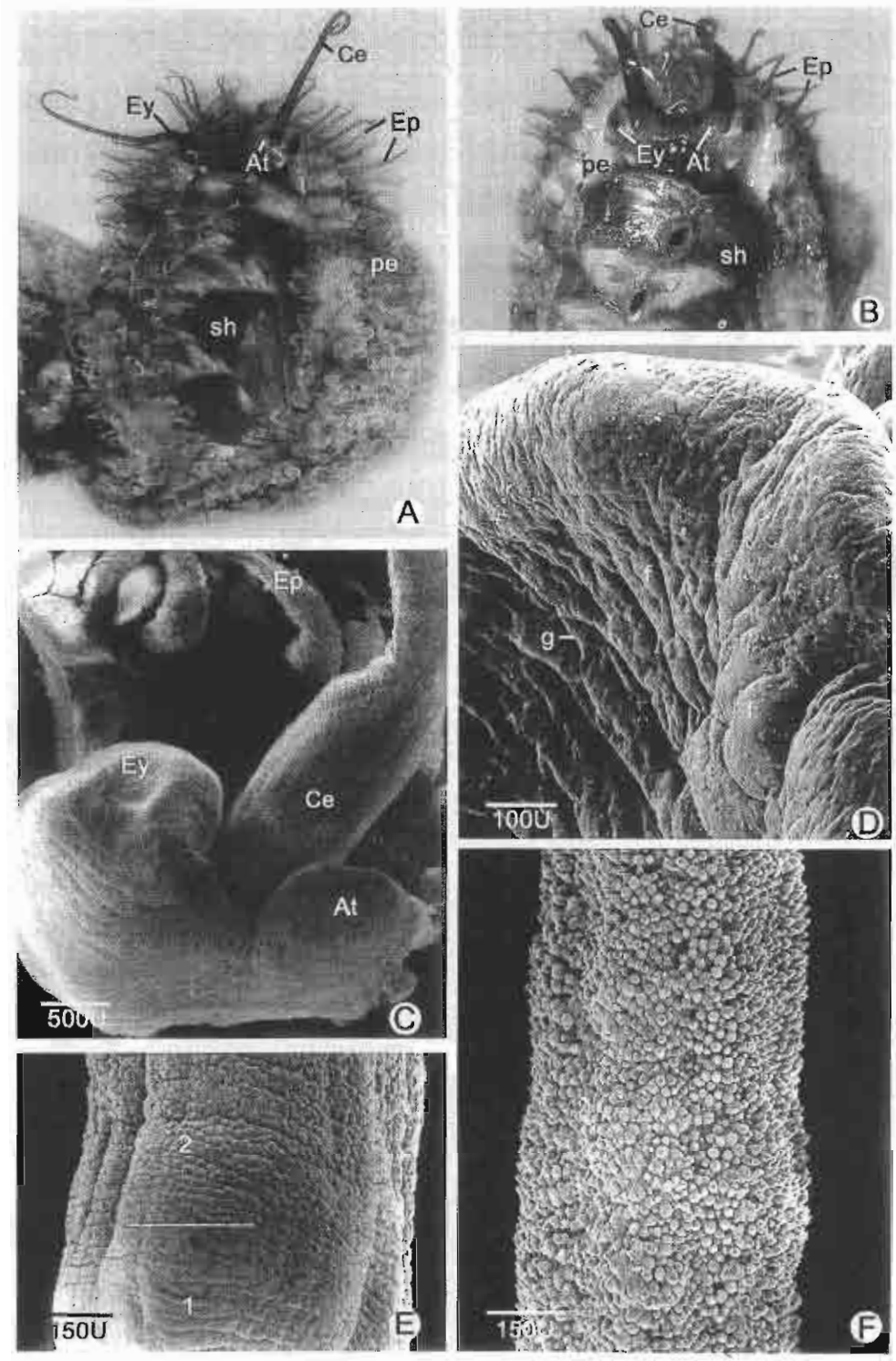


Figure 1. A & B. SEM photographs of the dorsal view showing the external features of an adult (16 mo old) *H. asinina*. At = appendage tentacle, Ep = epipodial tentacle, Ey = eye, pe = pedal muscle, sh = shell, Ce = cephalic tentacle. C. A low-power SEM micrograph showing the location and appearances of the optic (Ey), cephalic (Ce), and appendage (At) tentacles from lateral to medial. D. Higher magnification of the appendage tentacle showing many grooves (g) and folds (f). E. A low-power SEM micrograph of a cephalic tentacle shows the basal (1) and middle (2) parts of the tentacle. F. A low-power SEM micrograph of the cephalic tentacle shows the top part of the tentacle that has numerous sensory papillae.

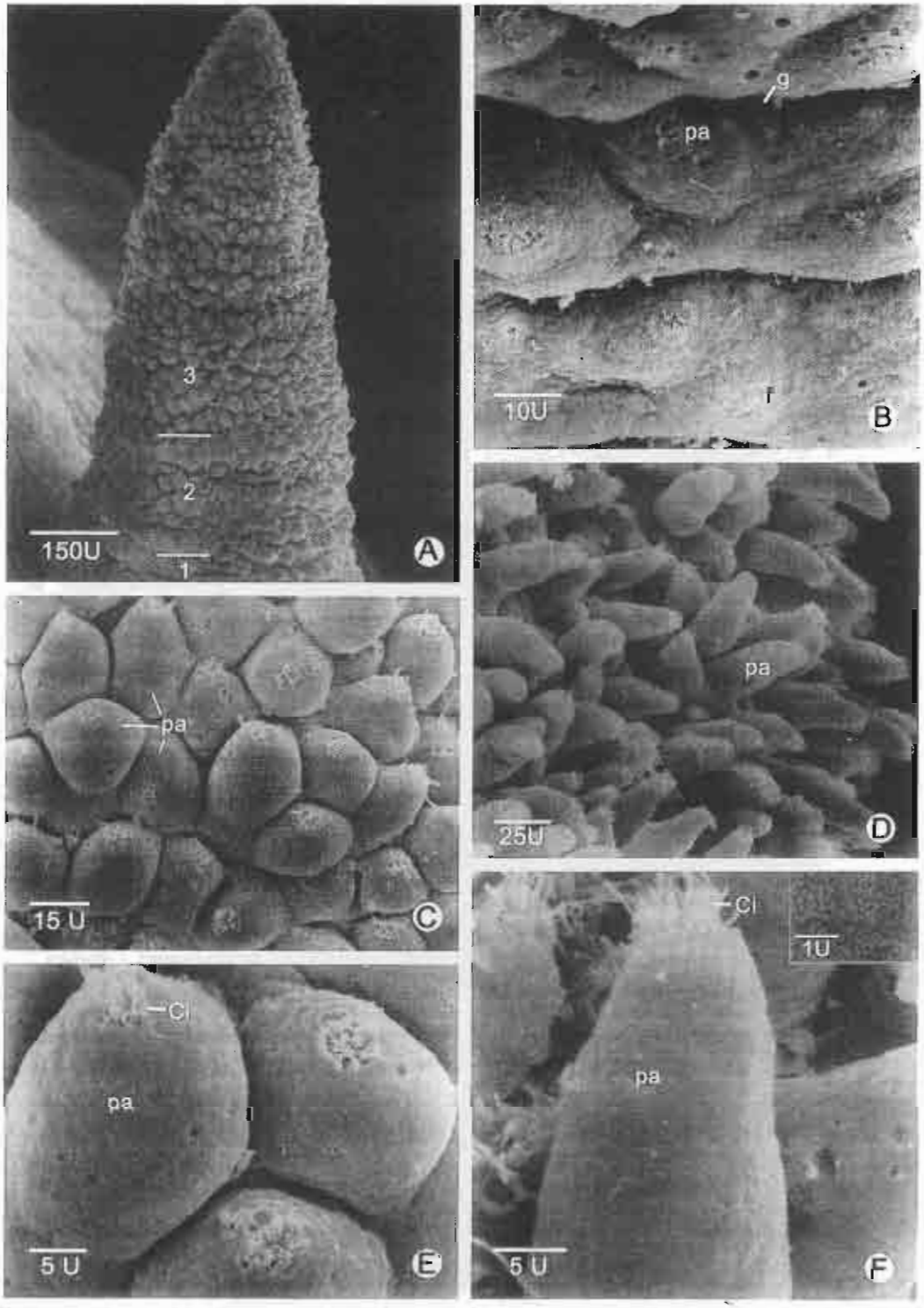


Figure 2. A. A low-power SEM micrograph showing the cone-shaped and knobby surface of an epipodial tentacle that is divided into 3 areas: basal (1), middle (2), top (3) parts. B. A medium-power SEM micrograph of the basal part showing grooves (g) alternated folds (f); the former contain many short papilla (pa). C. A medium-power SEM micrograph of the middle part of cephalic tentacle showing the surface that has short but stout papillae (pa). D. A medium-power SEM micrograph of the papillae (pa) on the top part of a cephalic tentacle, all of which are long and have a cone shape. E. A high-power SEM micrograph of a papilla of the middle part showing a bulbous shape with a tuft of cilia (Ci) on top. F. A high-power SEM micrograph of the top part showing many tall cone-shaped papillae (pa) with numerous long cilia (Ci) on top, whereas the rest of its surface is covered with microvilli (inset).

3A). Along the axis of each tentacle, there is a central tentacular nerve running along its whole length, and gives rise to the radial branches that innervate the surrounding muscle (Figs. 3B, C). Covering the tentacle is a simple columnar epithelium lying on a thick basement membrane (Figs. 3D, E). The cells in the epithelium covering the papilla can be classified into three types, based on their histologic characteristics and staining affinities. They are: (1) a sensory cell that is spindle shaped with a round or oval shape nucleus, and contains darkly-stained chromatin (Figs. 3D, E). The cytoplasm is dense and stained blue with methylene blue and pinkish purple with PAS-methylene blue. There are long cilia at the tip of each sensory cell, which give rise to the ciliary tuft at the top of each papilla as observed under SEM; (2) a supporting cell which has a columnar or pyramidal shape, and it is generally larger than the sensory cells. It has a round or oval nucleus that contains mostly euchromatin with a few blocks of heterochromatin (Figs. 3D, E). The cytoplasm is clearer than sensory cell, and appears light blue after staining with methylene blue, and light pinkish with PAS-methylene blue stain. The supporting cell has a brush border that is made of microvilli; and (3) a goblet cell, which is a type of mucin-producing cell with a small nucleus and oval shape that is mostly euchromatin (Fig. 3D). The cytoplasm is large, clearer, and stained light blue with methylene blue and pinkish with PAS-methylene blue. At the point where sensory cells aggregate to form a papilla, fibers from the tentacular nerve terminate at a group of these cells that have cilia on top (Fig. 3E).

### *Epipodial Tentacle*

The general structure of an epipodial tentacle is similar to that already described for a cephalic tentacle, but each tentacle is about two times narrower and four times shorter than the cephalic tentacle (Fig. 1A, Table 1). Based on the surface features observed under SEM, each tentacle could also be divided into 3 parts (i.e., 1/5 basal, 1/5 middle, and 3/5 top) (Fig. 2A). Each part has characteristic structures (Figs. 2B, C, D), but there are gradual changes between adjacent parts. The surface of the basal part has folds alternated with grooves (Fig. 2B). On the folds are many short bulbous papillae, each has a circle of cilia on the top (Fig. 2B). In contrast, at the middle part the grooves and folds become less obvious, whereas the papillae are wider and longer, and each appears as a hillock with a circle of cilia on top (Figs. 2C, E). On the top part of an epipodial tentacle there are numerous papillae that are more slender than those on the lower parts, and each appears as a truncated cone with a circle of cilia at the top (Figs. 2D, F).

In spite of its much shorter length, the epipodial tentacle histologically resembles the cephalic tentacle. There are a bundle of epipodial tentacle nerves in the central axis (Figs. 4A, B). Most of surface epithelium, particularly at the basal part of the tentacle, is covered by columnar cells bearing a brush border (Figs. 4C, D). The papilla comprises of three types of epithelial cells with the same characteristics and staining affinities as those of papillae located on a cephalic tentacle (Figs. 4C, D).

### *Appendage Tentacle*

In addition to the cephalic, optic, and epipodial tentacles, *H. asinina* has a pair of vestigial appendage tentacles. Each is short with a half circle shape, and is covered by numerous irregular folds, alternated with grooves (Fig. 1D). The folds are covered by epithelial cells bearing numerous microvilli.

Transverse sections of the appendage tentacle reveal similar interior structure (i.e., nerve and muscle) to that of the cephalic and epipodial tentacles. The columnar epithelium, which covers the tentacle, also comprises three types of cells that are evenly spread over the surface without being organized into sensory papillae.

### *Immunoblots of GABA*

The extracts of *H. asinina* neural tissues (i.e., cerebral and pleuropedal ganglion) are strongly stained for GABA almost equal to that of mouse brain extract (Fig. 5). However, both tentacular and epipodial tentacular tissues are only slightly stained for GABA.

### *Sensory Cells Containing GABA*

Both of the cephalic and epipodial tentacles have similar patterns of immunostaining for GABA in the cells of epithlium and in the muscle (Fig. 6B). The most prominent immunoreactive cells were sensory cells aggregated at the center of each papilla, which could be readily identified by the presence of cilia on their apical surface (Fig. 6C). Of the remaining surface epithelial cells, the immunoreactive cells are sensory cells, which are widely scattered among the supporting cells (Figs. 6D to F). The nerve bundle and its radiating nerve fibers in both types of tentacles exhibited GABA immunoreactivity (Fig. 6B). In the control the immunostaining is negative (Fig. 6A).

## DISCUSSION

### *Cephalic and Epipodial Tentacles*

As in other prosobranch mollusks, the cephalic tentacles of *H. asinina* are the major sensory organs for perceiving the environment conditions because they are the outgrowths from the anterior end of the head (Zaitseva 1997, Beesley et al. 1998). In cross sections the basic structure of the cephalic tentacle is similar to that of other species of *Haliotis* because the tentacular nerve is in the middle of longitudinally orientated muscle fibers, and it is covered by a simple columnar epithelium (Croft 1929, Bevelander 1988, Beesley et al. 1998). In this study, it was found that the epithelium of cephalic tentacles of *H. asinina* has 3 types of cells: sensory cells, supporting cells; which are the majority of cell type, and mucus cells. This is in agreement with the study by Croft (1929) who reported similar finding in the cephalic tentacle of *H. tuberculata*. The sensory cells of the tentacles of *Haliotis* are not subepithlial as in pulmonate mollusks (Wright 1974), but are part of the epithelium similar to that in *P. elegans* (Zaitseva 1997). The sensory cells could be easily identified as having oval shaped nucleus with densely stained chromatin and cytoplasm in contrast to the supporting cells that have much clearer nuclei and cytoplasm. In the basal part of the cephalic tentacle, they are widely scattered in the epithelium and are located in the middle and top parts and concentrated in the center of each papilla. Underneath the papilla, there is a nerve branch from the central tentacular nerve bundle that may supply the sensory cells. This situation is similar to the nerve bundles of *P. elegans*, which connect their sensory dendrites to the epithelium of the tentacle tip (Zaitseva 1997). On

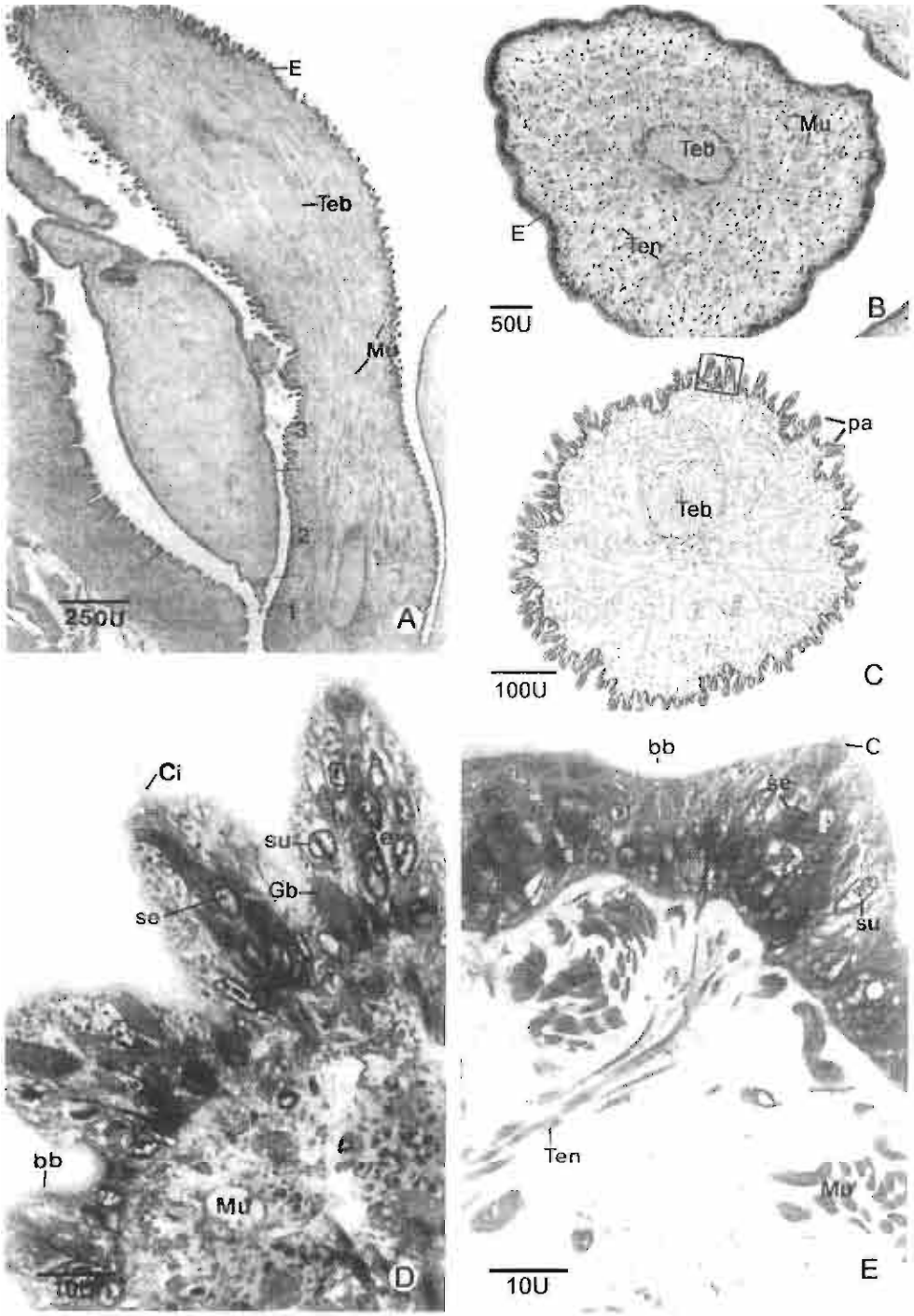


Figure 3. Paraffin sections (A to C) and semithin sections (D & E) of cephalic tentacles. A. A low-power LM micrograph of a longitudinal section of cephalic tentacle showing 3 parts: basal (1), middle (2) and top (3). Note the presence of cephalic tentacular nerve bundle (Teb) in the axis of the tentacle. Mu-muscle fasciculus. B & C. A medium-power LM micrograph of a cross section of the basal and top parts, respectively, showing cephalic tentacular nerve bundles (Teb) in the axis. The tentacle is surrounded by an epithelium. E. Mu-muscle fasciculus, pa-papillae, Ten-tentacular nerve. D. A high-power LM micrograph of a semithin plastic section of the top part stained with methylene blue, showing 3 types of cells in the papillae: sensory cell (se), supporting cell (su) and goblet cell (Gb). A group of cilia (Ci) is present on the top of each papillae and linked with the sensory cells, the papillae are more slender and longer than those on the middle part of the tentacle. E. A high-power LM micrograph of a semithin plastic section of the basal part stained with methylene blue, showing an epithelium with brush border (bb). The epithelium contains sensory cell (se), supporting cell (su). Muscle fasciculi (Mu) are seen in the connective tissue underlying the epithelium.

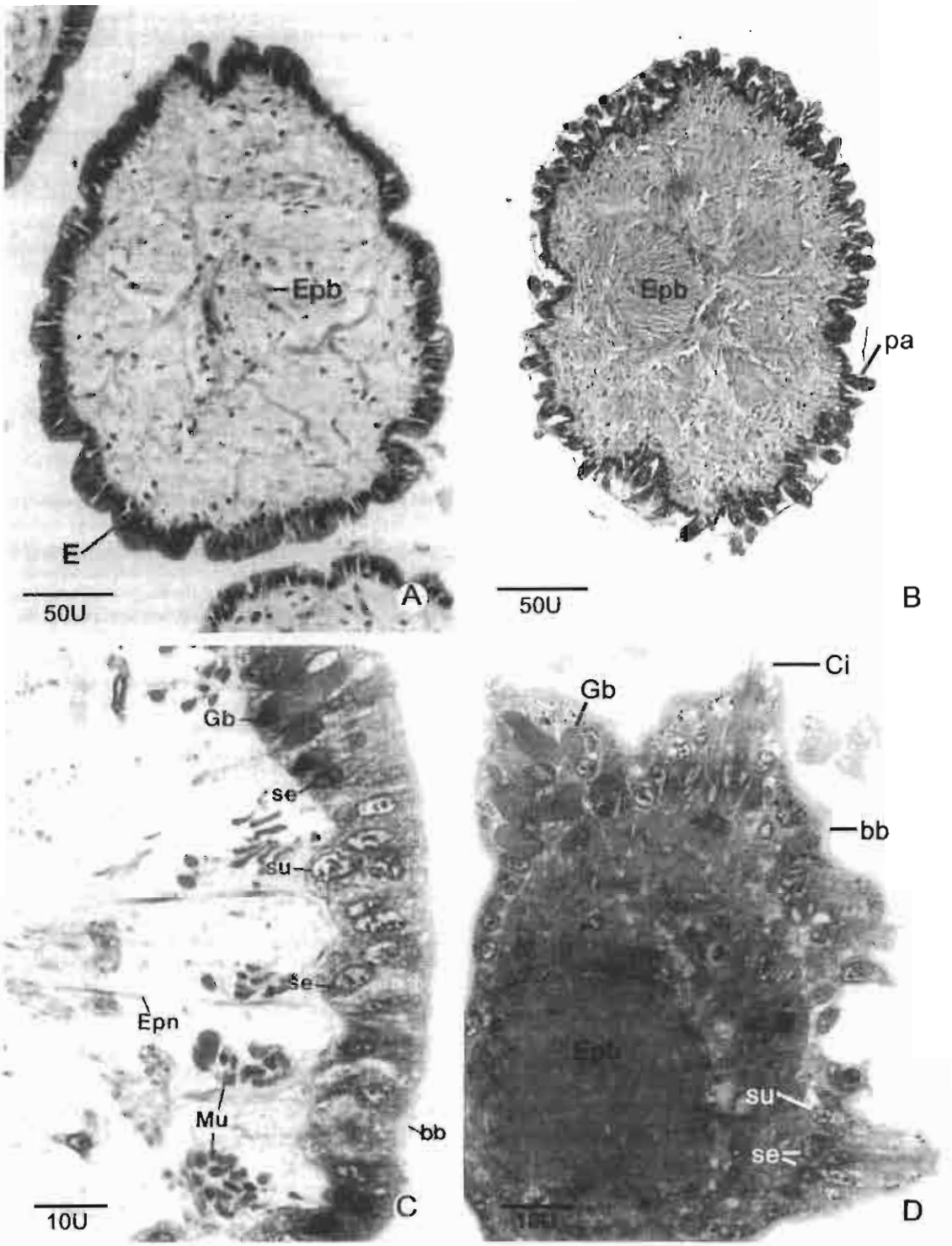


Figure 4. Paraffin sections (A & B) and semithin sections (C & D) of epipodial tentacles. A. A low-power LM micrograph of a cross section of the basal part showing surface epithelium (E) that has few papillae, and a nerve bundle (Epb) in the axis. B. A low-power LM micrograph of a cross section of the top part showing numerous surface papillae (pa) and a nerve bundle (Epb) in the axis. C. A high-power micrograph of interpapillary area of the basal part of an epipodial tentacle stained with methylene blue, showing surface epithelium with brush border (bb), but no papillae. The epithelium consists of goblet cell (Gb), sensory cell (se), and supporting cell (su). The underlying connective tissue contains muscle fasciculus (Mu) and nerve (Epn) to innervate the sensory cells of the epithelium. D. A high-power LM micrograph of the papillae, showing sensory cell (se) with cilia (Ci) at the center of a papilla, supporting cell (su) and goblet cell (Gb). The epithelium is covered with brush border (bb).

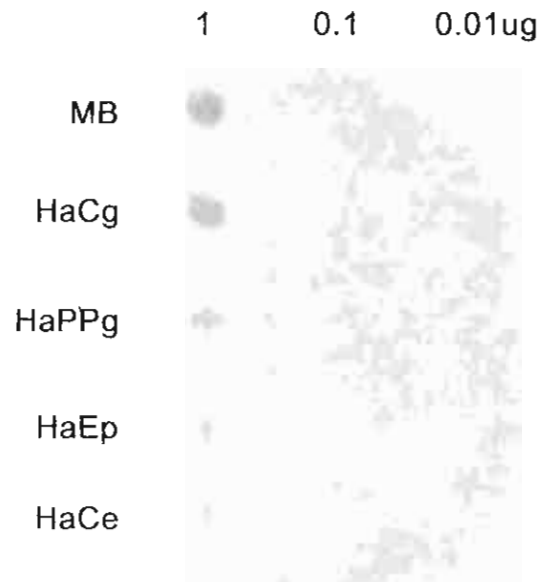


**Figure 5. Chemiluminescent detection of GABA in immunoblots of abalone tissues. Extracts of tissues from cephalic tentacle (HaCe), epipodial tentacle (HaEp), cerebral ganglion (HaCg), and pleuropedal ganglion (HaPPg) were spotted in duplicate onto a nitocellulose membrane at 0.01, 0.1, and 1 µg of protein in the extraction buffer. All extracts were positively stained for GABA as well as mouse brain (MB), used as a positive control.**

the apical surface of each papilla. SEM showed that there was a bundle of long twisted cilia that in cross section were demonstrated to belong to the sensory cells. In contrast, the supporting cells bear only microvilli that appear in LM as a brush border. The goblet cells are also widely scattered in the epithelium, and few are located in the papilla epithelium. Unlike the epithelium lining the mantle and the hypobranchial gland, the tentacular epithelium is probably not the major site for mucin production because it specializes mostly in the sensory perception.

The epipodial tentacles are smaller and shorter than the cephalic tentacles. They are numerous and located around the foot muscle. They have been shown in this study, as well as in the study by Crofts (1929), to have a basic structure similar to that of the cephalic tentacles. However, the muscle bundles in the epipodial tentacles are smaller and do not appear as regularly arranged as those in the cephalic tentacles. The cephalic tentacles are used for exploring the environment and for seeking out food, while avoiding danger; therefore, they need longer and stronger muscle bundles to stretch and retract them over a long distance. Alternatively the epipodial tentacles function more in support of the cephalic tentacles in finding food and receiving chemical stimuli around the abalone's body. Hence, epipodial tentacles are smaller and shorter than the cephalic tentacles and only project out for a short distance around the body, therefore these tentacles do not need as strong a muscle as in the former.

The group of ciliated sensory cells in the papillae of cephalic and epipodial tentacles are structurally very much like those in the olfactory epithelium or taste buds of vertebrates (Kierszenbaum 2002). Thus, the papillae may function mostly as chemoreceptors similar to the olfactory epithelium and taste buds of the vertebrates. This is supported by many investigators who have shown that, in addition to tactile reception, the cephalic tentacles also act as chemical receptors because they can respond to the chemical stimuli, odor, and food (Preston & Lee 1973, Farkas & Shurey 1976, Chase 1981, Bell & Tubin 1982, Voss & Schmidt 2001). Shinozono et al. (2001) reported that the metacerebro-procerebral neuron (MPN) of *Limax marginatus* is an output-neuron from the procerebrum. The MPN receives monosynaptic inputs from the superior and inferior tentacle nerves. The MPN, thus, may receive olfactory information via two pathways (i.e., one directly from the tentacle and the others by way of the procerebrum) and possibly functions by integrating both sources of inputs. Similar sensory inputs may be gathered by epipodial tentacles because their papillae have identical structural organization.

### *Immunohistochemistry*

This study has demonstrated the presence of GABA cells of both cephalic and epipodial tentacles. Identification of the immunostained cells is based on the characteristics and the position of cells. These cells are mostly the sensory cells aggregated at the center of each papilla, or single sensory cells widely scattered in the rest of the tentacular epithelium. GABA is the major inhibitory neurotransmitter in the central nervous system and a neuromodulator in certain peripheral tissues vertebrates (Satteile 1992). In marine invertebrates, GABA is a neurotransmitter that stimulates growth and metamorphosis of the larvae into more mature stage (Aminur & Veharai 2001), and in abalone it specifically stimulates settlement and metamorphosis (Morse et al. 1988) and feeding of larvae (Arshavsky et al. 1993). Therefore, it is highly possible that the GABAergic sensory cells in the papillae of both cephalic and epipodial tentacle play important parts in sensing the availability of food and perhaps also controlling the feeding behavior of the postmetamorphosed abalone up to and during the adult stage.

### *Appendage Tentacle*

The pulmonate mollusks have 2 pairs of tentacles: the superior and inferior tentacles, and the anterior and posterior tentacles, which are called the cephalic tentacle and rhinophore (Beesley et al. 1998). Rhinophores have shapes ranging from simple tapering rods to elaborate lamellae or tubular organs (Beesley et al. 1998). In the prosobranch mollusks, there is one pair of cephalic tentacles, and they do not have a rhinophore (Beesley et al. 1998). In this study, we found a pair of short and small tentacles that had a dome shape and were located dorso-medial to the base of the cephalic tentacle. They were called appendage tentacles. It is possible that these tentacles are homologous to the pulmonates rhinophores, but they remain as vestigial structures. The appendage tentacle has a simple columnar epithelium containing supporting and mucus cells, but much fewer sensory cells, there were no papilla like those on the cephalic and epipodial tentacles, and there are no well organized muscles and nerve fibers. Thus, they may just be rudimentary structures.

## ACKNOWLEDGMENTS

This research was supported financially by the Thailand Research Fund to Prasert Sobhon for a Senior Research Scholar Fellowship.

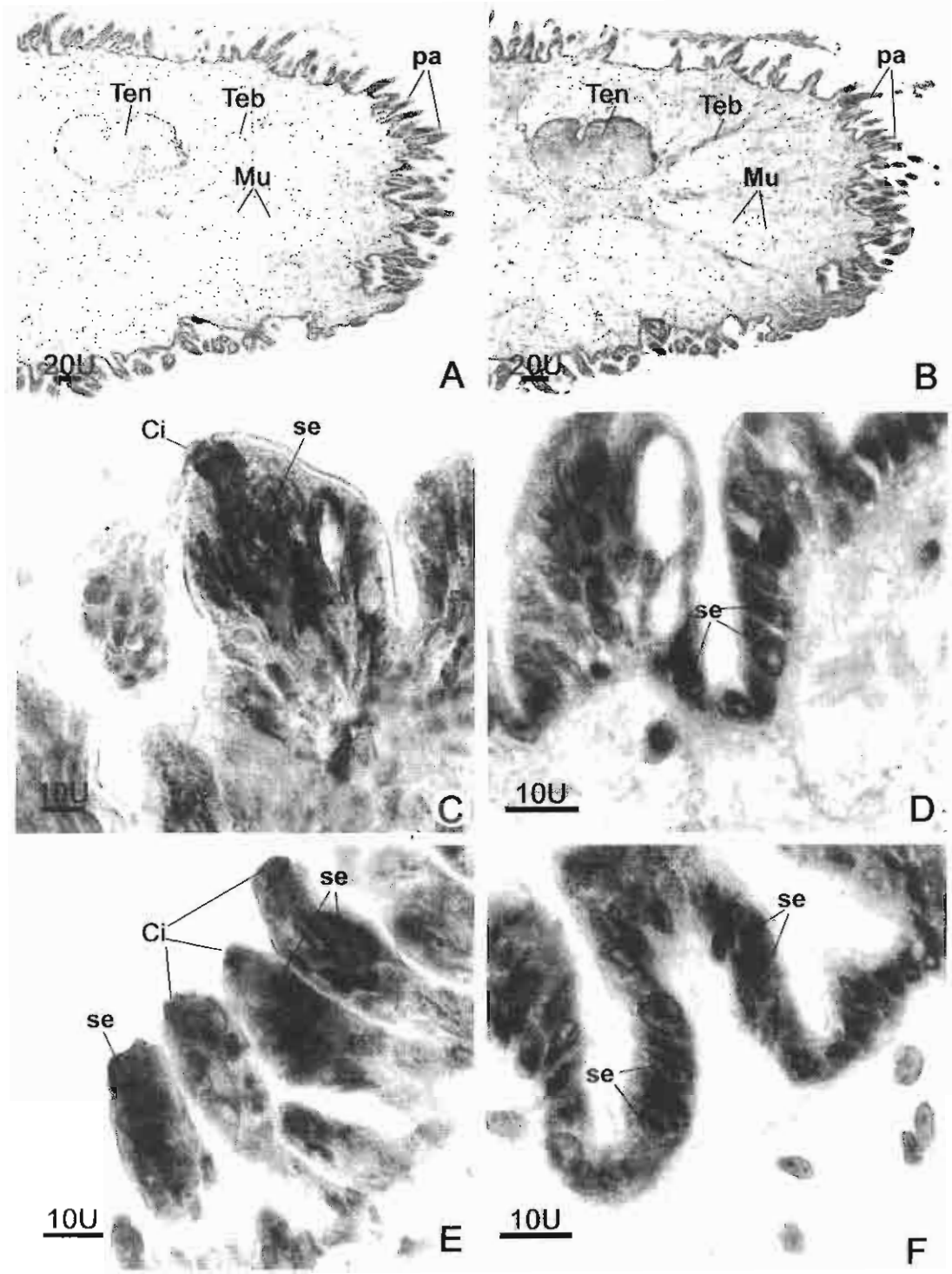


Figure 6. Light micrographs of the cephalic and epipodial tentacle sections stained for GABA by an immunoperoxidase method. A. Control section shows no staining in the cross section of a cephalic tentacle. B. An adjacent paraffin section stain with antiGABA showing positive staining in the epithelium covering papillae (pa) and the nerve bundle (Teb) and its fibers (Ten) traversing the muscle fasciculus (Mu). C & D. Higher magnifications of sections of the epithelium covering cephalic tentacles stained for GABA, and showing intense staining of the sensory cells (se) at the tip and the base of a papilla. E & F. A cross section of the upper part of an epipodial tentacle epithelium stained for GABA, and showing the same pattern of positive staining in the sensory cells (se) at the tip and the base of the papillae.

## LITERATURE CITED


Ammur, R. M. & T. Veharai. 2001. Induction of metamorphosis and substratum preference in four sympatric and closely related species of Sea Urchins (Genus *Echinometra*) in Okinawa. *Zool. Stud.* 40:29–43.

Arshavsky, Y. I., T. G. Deliagina, G. N. Gamkrelidze, G. N. Orlovsky, Y. V. Panchin & L. B. Popova. 1993. Pharmacologically induced elements of the hunting and feeding behavior in the pteropod mollusk *Clione limacina* I. Effects of GABA. *J. Neurophysiol.* 69:512–521.

Beesley, P. L., G. J. B. Ross & A. Wells. 1998. Class gastropoda. In: Mollusca. The southern synthesis, Part B. Fauna of Australia Vol. 5. Victoria, Australia: CSIRO Publishing. pp. 565–604.

Bell, W. J. & T. R. Tubin. 1982. Chemo-orientation. *Biol. Rev.* 57:219–260.

Bevelander, G. 1988. Abalone gross and fine structure. Pacific Grove, California: The Boxwood Press. pp. 40–51.

Chase, R. 1981. Electrical responses of snail tentacle ganglion to stimulation of the epithelium with wind and odors. *Comp. Biochem. Physiol.* 70A:149–155.

Chase, R. & R. P. Croll. 1981. Tentacular function in snail olfactory orientation. *J. Comp. Physiol.* 143:357–362.

Croll, D. R. 1929. Haliotis. *Liverpool Mar. Biol. Comm. Mem.* 29:33–36.

Farkas, S. R. & H. H. Shorey. 1976. Anemotaxis and odour-trial following by the terrestrial snail *Helix aspersa*. *Anim. Behav.* 24:686–689.

Haszprunar, G. 1988. On the origin and evolution of major gastropod groups, with special reference to the streptoneura. *J. Moll. Stud.* 54: 367–441.

Ito, I., H. Nakamura, T. Kimura, H. Suzuki, T. Sekiguchi, K. Kawabata & E. Ito. 2000. Neuronal components of the superior and inferior tentacles in the terrestrial slug, *Limax marginatus*. *Neurosci. Res.* 37:191–200.

Kierszenbaum, A. L. 2002. Histology and cell biology: an introduction to pathology. USA: Mosby, Inc. pp. 341–396.

Lowry, O. H., N. J. Rosebrough, A. L. Farr & R. J. Randall. 1951. Protein measurement with folin phenol reagent. *J. Biochem.* 193:265–275.

Morse, D. E., N. Hooker, A. N. C. Morse & R. A. Jensen. 1988. Control of larval metamorphosis and recruitment in sympathetic agaricild corals. *J. Exp. Biol. Ecol.* 116:193–217.

Preston, R. J. & R. M. Lee. 1973. Feeding behavior in *Aplysia californica*: Role of chemical and tactile stimuli. *J. Comp. Physiol. Psychol.* 82: 368–381.

Sattelle, D. B. 1992. Receptore for L-Glutamate and GABA in the nervous system of an insect (*Periplaneta Americana*). *Comp. Biochem. Physiol.* 103:429–438.

Shimozono, S., S. Watanabe, T. Inoue & Y. Kirino. 2001. Identification and characterization of an output neuron from the oscillatory molluscan olfactory network. *Brain Res.* 921:98–105.

Singhagrarwan, T. & M. Doi. 1993. Seed production and culture of a tropical abalone, *Haliotis asinina* Linne. Thailand: The Eastern Marine Fisheries Development Center, Department of Fisheries, Ministry of Agriculture and Cooperatives.

Voss, M. & H. Schmidt. 2001. Electrophysiological responses to thermal stimuli in peripheral nerves of the African giant snail, *Archachatina marginata* S. *J. Thermal Biol.* 26:21–27.

Wright, B. R. 1974. Sensory structure of the tentacles of the slug, *Arion ater* (Pulmonata,Mollusca) I. Ultrastructure of the distal epithelium, receptor cells and tentacular ganglion. *Cell. Tiss. Res.* 151:229–244.

Zantseva, O. V. 1997. Structural organization of receptor elements and organs of the land mollusk *Pomatias elegans* (Prosobranchia). *Neurosci. Behav. Physiol.* 27:533–540.

*Journal of Shellfish Research*, Vol. 23, No. 4, 1107–1112, 2004.

# HISTOLOGY OF HYPOBRANCHIAL GLAND AND GILL OF *HALIOTIS ASININA* LINNAEUS

CHAITIP WANICHANON,[1,*] PRAPHAPORN LAIMEK,[1] VICHAI LINTHONG,[1] PRAPEE SRETARUGSA,[1] MALEEYA KRUATRACHUE,[2] EDWARD SUCHART UPATHAM,[3] TANES POOMTONG,[4] AND PRASERT SOBHON[1]

[1]*Department of Anatomy, Faculty of Science, Mahidol University, Rama 6 Road, Bangkok 10400, Thailand;* [2]*Department of Biology, Faculty of Science, Mahidol University, Rama 6 Road, Bangkok 10400, Thailand;* [3]*Department of Medical Science, Faculty of Science, Burapha University, Chonburi 20130, Thailand;* [4]*The Coastal Aquaculture Development Center, Department of Fisheries, Klongwan, Prachuabkirikun Province 77000, Thailand*

***ABSTRACT*** The hypobranchial gland of *Haliotis asinina* exhibits major and minor folds that are called leaves and leaflets. When viewed by scanning electron microscope, numerous tufts of rod-shaped cilia, paddle-like cilia, and clusters of granules being exocytosed from the pores were observed on the surface of the leaves and the leaflets. In transverse sections, each of the leaf and the leaflet can be divided into two areas: the basal area consists mainly of two types of large goblet cells, and the apical area that contains a mixture of supporting cells, sensory cells and four types of mucus-secreting cells. *H. asinina* has bipectinate gills. Gills are observed in abalone at the age of 1 mo, and the number and length of their filaments increase with age. In mature abalone, there are about 17 filaments per each gill with equal numbers on both sides. The length of the longest filament is approximately 2.48 mm. Each filament is supported axially by a thin collagenous connective tissue. On the efferent side, there is a V-shaped chitinous skeletal rod. Epithelium lining the filament is composed of tall columnar cells bearing microvilli mixed with ciliated columnar cells and mucus cells.

***KEY WORDS:*** *H. asinina*, gill, hypobranchial gland, histology, SEM

## INTRODUCTION

The hypobranchial gland is a single or paired, highly glandular area of the epidermal lining the roof of the mantle cavity (Hyman 1967). Two such glandular areas, one on each side of the rectum, occur in *Haliotis*, and the left one is larger than the right one (Crofts 1929). The hypobranchial gland consists of regular folds or lamellae oriented at right angles to the mantle wall (Hyman 1967). The histology of the hypobranchial gland has been investigated (Crofts 1929, Bevelander 1988). Crofts (1929) described three types of cells in the hypobranchial gland of *Haliotis tuberculata*: mucus cells with spindle shaped secretion, mucus cells with granules, and ciliated cells. Bevelander (1988) described 3 types of cells in the hypobranchial gland of *H. rufescens*: mucus cells with rod-like elements, mucus cells with granular cytoplasm, and supporting cells.

Gills are the principal organs for respiratory gas exchange in mollusks. They are positioned in the mantle cavity (Crofts 1929, Eertman 1996), so they are affected by many substances that flow through the mantle cavity (Schulte-Oehlmann et al. 2000). The studies on gastropod gill morphology is very limited; a few papers have been published on the structure of gills of pulmonate *Siphonaria capensis* (De Villiers & Hodgson 1987) and of some caenogastropod species. The gill structure of the investigated gastropods shows basic uniformity because the gill filaments are composed of a ridge and an extended sheet of nonciliated cells. However, the gill filaments of these various species of gastropods differ in the shape of the filaments (corrugated, triangular, or rounded). Each gill filament is covered with a single layered epithelium of either cuboidal (Schulte-Oehlmann et al. 2000) or columnar cells (Crofts 1929). However, there seems to be a difference in the thickness of the epithelial cells. A hemocoelic space occupies the center of each filament (Eertman 1996, De Villiers & Hodgson 1987). Crofts (1929) found that in *H. tuberculata*, the V-shaped chitinous skeletal rod, attached to one side of the gill epithelium was similar to that in cephalopoda (Haszprunar 1987). The epithelium of the gill of *S. capensis* and *H. tuberculata* consists of three types of cell: nonciliated cell, ciliated cell, and secretory cell (De Villiers & Hodgson 1987).

To the best of our knowledge, there is still no information on the histology of hypobranchial glands and gills in *H. asinina*, a common abalone species found along the coastal water of Thailand, which is considered to be one of the economic aquatic animals that has been cultured for commercial exploitation. Hence, this study reports on the histology of hypobranchial glands and gills of this species.

## MATERIALS AND METHODS

### *Collection of Abalone Specimens*

Abalones were obtained from a land-based culture system at Coastal Aquaculture Development Center, Department of Fisheries, Prachaubkirikun Province, Thailand. They were reared in concrete tanks housed in the shade, and well flushed with mechanically circulated sand-filtered seawater, and provided with an air delivery system to maintain the stable controlled environment. The optimum level of salinity is ~22.5–32.5 ppt, and the temperature ~22 °C to 26 °C (Singhagraiwan & Doi 1993). They were fed with macroalgae (usually *Gracilaria* spp. and *Laminaria* spp.), supplemented with artificial food.

They were anesthetized in 5% $MgCl_2$, after which their shells were removed. The gills and hypobranchial glands were dissected out and processed for light microscope (LM) and scanning electron microscope (SEM) studies.

### *Specimen Preparation for LM*

Specimens were fixed in Bouin fluid in 0.14 M NaCl for 24 h and washed with 70% ethyl alcohol. Then, they were dehydrated through a graded series of ethanol, cleared in dioxane, infiltrated

*Corresponding author. E-mail: sccwn@mahidol.ac.th

and embedded in paraffin. Five-micron-thick sections were cut and stained with hematoxylin and eosin.

For semithin sections, specimens were fixed in Karnovsky fixative (2% paraformaldehyde and 4% glutaraldehyde in 0.1 M sodium cacodylate buffer, pH 7.8) at 4 °C for overnight, and washed with 0.1 M sodium cacodylate buffer. They were postfixed in 1% osmium tetroxide in 0.1 M sodium cacodylate buffer at 4 °C for 1 h. Then, they were dehydrated in graded series of ethanol and embedded in Araldite 502 resin. Sections were cut at 1-μm thickness with Porter Blum MT-2 μLtramicrotome, and stained with methylene blue or PAS-methylene blue (Hayat 1993). Examination of the tissues sections was done under an Olympus Vanox light microscope.

### *Specimen Preparation for SEM*

Hypobranchial glands were cut and fixed in a Karnovsky fixative (4% glutaraldehyde 2% paraformaldehyde in 0.1 M sodium cacodylate buffer), pH 7.8 at 4 °C, for overnight, and washed in 0.1 M sodium cacodylate buffer. They were postfixed in 1% osmium tetroxide in 0.1 M sodium cacodylate buffer for 1 h at 4 °C. Then, they were dehydrated in graded series of ethanol, and dried in a Hitachi HCP-2 critical point drying machine, using liquid $CO_2$ as a transitional medium. They were then mounted on aluminum stubs and coated with platinum and palladium in an ion sputtering apparatus, Hitachi E 5000. The specimens were examined in a Hitachi S-2500 scanning electron microscope with an accelerating voltage of 15 kV.

## RESULTS

### *Hypobranchial Gland*

The hypobranchial gland of *H. asinina* is located on the dorsal surface of the mantle cavity and runs parallel to the gill. It appears as a large yellow pectinated ridge whose lateral sides are connected to the gills by a thin mantle membrane (Figs. 1A and B, 2A). Each gland consists of many axes, from each of which 8 to 11 leaves arise (Fig. 1B). Under SEM, the major folds or leaves decline from the axis to the lower level and branch into two to three terminals. Many minor folds or leaflets branch off from both sides of each leaf (Fig. 1C). The hypobranchial gland exhibits many tufts of rod-shaped cilia, paddle-liked cilia, and granules that are exocytosed from pores on the surface of leaves and leaflets (Figs. 1E and F). In contrast, the junction between the axis and leaf has fewer ciliary tufts, round granules that are being exocytosed from pores on the fold, and there are deep grooves between the folds (Fig. 1D).

In transverse section, each leaf and leaflet can be divided into 2 areas: the basal area, which consists mainly of large mucus cells and the apical area that contains a mixture of supporting cells, sensory cells, and small mucus-secreting cells having goblet appearance (Figs. 2B and C, 3A). These cells have the following characteristics.

1. Supporting cells. These cells vary in shape; they can be triangular, oval, or spindle (Figs. 3B and C). The nucleus is oval and contains mostly pale-stained euchromatin. The upper part of this cell type is wide and shows many long microvilli.
2. Sensory cells. These cells are elongated in shape, and they contain euchromatic oval nuclei with many nucleoli (Figs. 3B and C). The upper part of this cell type is narrow and reaches the surface of the epithelium where it bears some cilia.
3. Mucus cells. These cells are filled with many mucin granules and have oval shape. Based on the staining characteristics with PAS-methylene blue on semithin sections, there are 4 types of mucus cells (Figs. 3B and C). Type-1 is a mucus cell with a round nucleus and PAS and methylene blue negative granules in the cytoplasm. It is located near the basement membrane (Figs. 3B and C). Type-2 is a mucus cell with flattened euchromatic nucleus and numerous blue granules packed tightly together in the cytoplasm (Figs. 3B and C). Type-3 is a small mucus cell whose cytoplasm is filled with PAS-positive round granules (Figs. 3B and C). Type-4 is the largest mucus cell containing large heterogenous granules with either pinkish or bluish (methylene blue positive) hues (Fig. 3C).

In the basal area, there are 2 types of mucin cells lying in alternation. Type-1 is the mucus cell, which contain homogenous purple (methylene blue positive) material in the cytoplasm (Fig. 3D). Type-2 is the mucus cell containing homogeneous pale pink (PAS positive) material with streaks of deep pink rod-liked materials embedded in the former (Fig. 3D).

### *Gills*

*H. asinina* has two bipectinate gills, positioned slightly to the left of the center in the mantle cavity and pointing anteriorly (Figs. 1A and B). The gills are attached to the mantle by a thin membrane. There are equal numbers of filaments on both sides (i.e., about 17 filaments per each gill). All filaments lie parallel to each other. Each is a delicate pleat with blunt free tip and is corrugated in the middle (Fig. 4A).

Transverse sections through the gill filaments reveal that they are covered with a single layered epithelium (Figs. 4B to E). Each filament is supported axially by a thin collagenous connective tissue, enclosing the hemocoelic space, which contains hemocytes (Fig. 4E). On the efferent side, there is a V-shaped opaque chitinous skeletal rod (Fig. 4B), serving as the attachment site for muscles that could bring about considerable movement of the gill filament. The gill filament is lined by a columnar epithelium that varies much in thickness in different parts (Figs. 4B to E). Most of the epithelial cells on the proximal and distal ends of a filament are tall columnar bearing microvilli, which appears as brush border under LM, with ciliated epithelial cells (Figs. 4B, C, and E). There are numerous cilia on the region of the apical ciliary band (Fig. 4B) and the lateral ciliary band (Fig. 4C). However, in most of the filaments, the cells are cuboidal and have no cilia (Fig. 4D). Four types of cells can be identified in the epithelium covering the efferent side of the filament (Fig. 4B): (1) the cuboidal cells with round nuclei on the lateral side of the skeletal rod; (2) the ciliated tall columnar cells in the distal end of the filament; (3) the small columnar cells with dense granules and microvilli; (4) the mucus cells with large basophilic or small metachromatic granules in the efferent filament.

The afferent epithelium of the gill filament comprises of 4 types of cells (Fig. 4E). These are: (1) the cuboidal cells with round nuclei with euchromatin and distinct nucleoli on the lateral side; (2) the tall columnar cells with round or oval nuclei located in the terminal epithelium; (3) the ciliated columnar cells in the distal end of the filament; (4) the mucus cell with numerous dense granules packed tightly together in the apical cytoplasm (Fig. 4E).

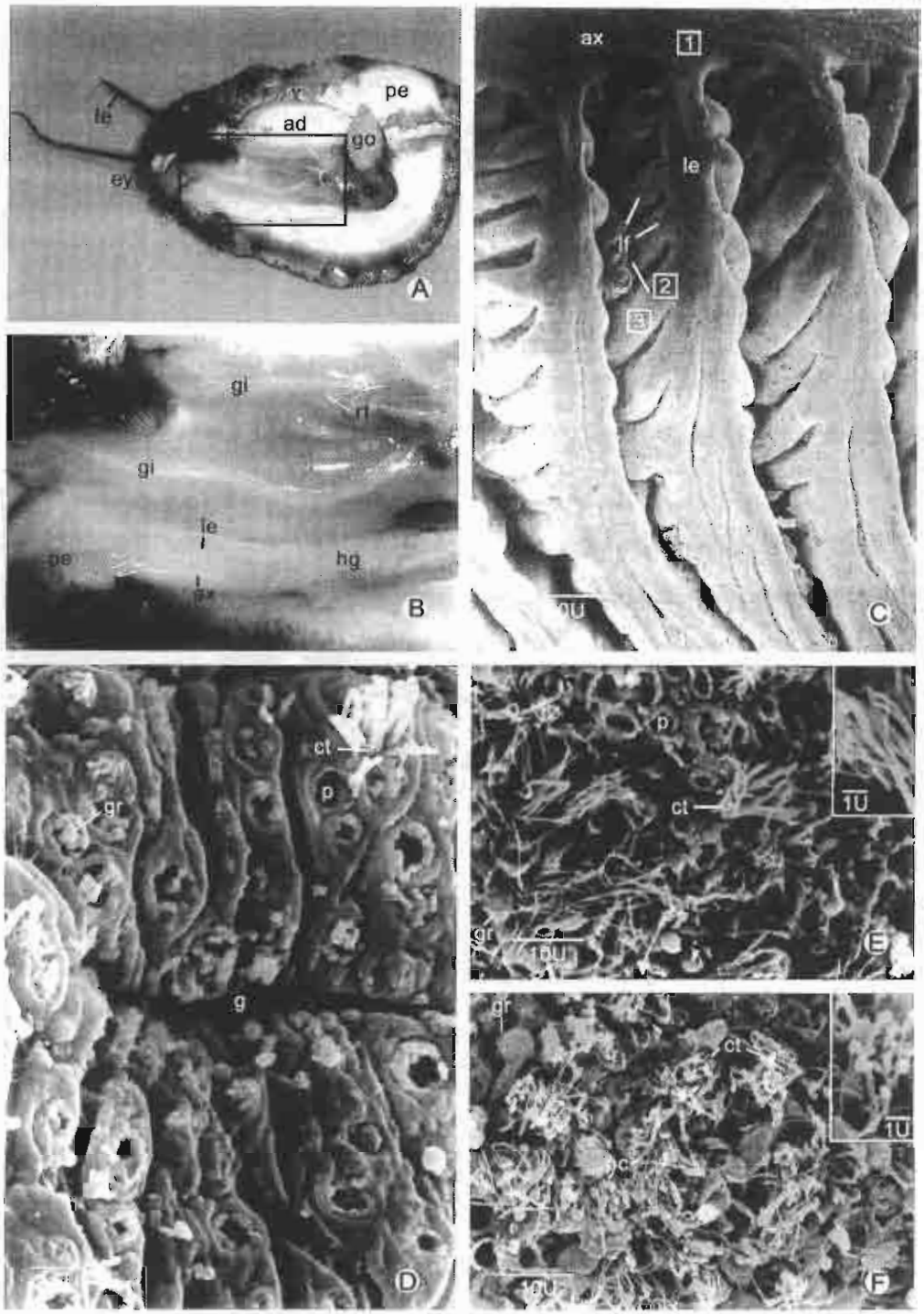


Figure 1. A & B. Photographs of the dorsal view of the mantle cavity showing the external features of adult *H. asinina* (16 mo old), after removing the shell and dissecting away mantle membrane. ad-adductor muscle, ax-axis, dig-digestive gland, ey-eye, gi-gill, go-gonad, hg-hypobranchial gland, le-leaf, pe-pedal muscle, rt-rectum, te-cephalic tentacle. C. A low-power SEM micrograph of a hypobranchial gland of *H.asinina* showing the leaf (le) which arises from the axis (ax), and leaflets (lf) which branch off from both sides of the leaf. D. Higher magnification of a part on the axis from box 1 in C showing ciliary tuft (ct), secreted granules (gr) and exocytosed pores (p) on the tegumental fold. Notice many deep groove (g) between the tegumental fold. E. A high-power micrograph of a part of the leaflet from box 2 in C, showing numerous ciliary tufts (ct) that are enlarged in the inset, secreted granules (gr) and exocytosed pore (p). F. A nearby area from box 3 in C at the same magnification, showing many paddle-like (pc) cilia that are magnified in the inset.


**Figure 2. Light micrographs of cross section of the hypobranchial gland. A. A survey photomicrograph showing the location of gill (gi) and hypobranchial gland (hg), which are connected by the mantle (mt). d-dorsal, rt-rectum, v-ventral. B and C. Micrographs showing many leaves (le) and leaflets (lf), whose basal (ba) and apical (ap) parts appear to contain mucus cells of distinct characteristics.**

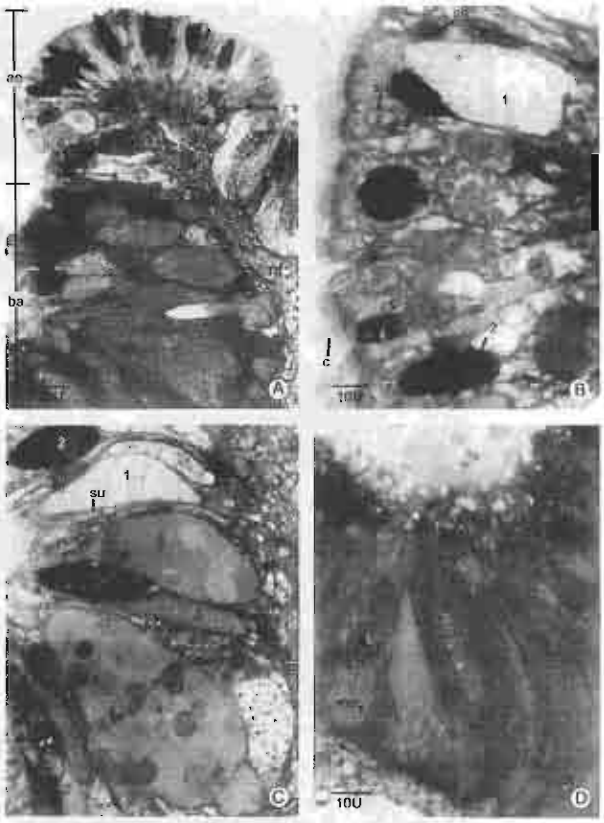


**Figure 3. Semithin cross sections of the leaf of hypobranchial gland stained with PAS-methylene blue. A. A micrograph showing apical part (ap) and basal part (ba) which contain different types of mucus cells and nerve fiber (nf) in the core of the leaflet. B and C. High-power micrographs of the apical part showing supporting cell (su), sensory cell (se) and 4 types of mucus cells: type-1 (1), type-2 (2), type-3 (3), type-4 (4). D. A high-power micrograph of the basal part, showing two cell types of mucus cells lying in alternation; the first cell-type is PAS positive mucus cell ($mc_1$), and the second cell type ($mc_2$) methylene blue positive cell.**

## DISCUSSION

### *Hypobranchial Gland*

There are some controversies on the types of cells found in the hypobranchial gland. Crofts (1929) and Bevelander (1988) reported 3 cell types in the hypobranchial gland of *Haliotis tuberculata* and *H. rufescens*, respectively. Both authors described 2 types of mucus cells that contain different secretion. Type-1 mucus cell contains rodlike or spindle-shaped secretion while type-2 mucus cell contains granular secretion (Crofts 1929, Bevelander 1988). The third cell type is the supporting cell (Bevelander 1988), which is ciliated (Crofts 1929). These two types of mucus cells correspond to those found in the basal area of hypobranchial gland of *H. asinina*. The first type of mucus cell contains large, rodlike mucin granules that gave an intense positive reaction to PAS, indicating the presence of neutral mucopolysaccharide. In *H. rufescens*, the mucus cell also contains rodlike granules that were identified to be acid mucopolysaccharide in nature (Bevelander 1988). The second type of mucus cell in the basal area of *H. asinina* hypobranchial gland appears homogenous and stains purple with PAS-methylene blue. This may be equivalent to the second type of mucus cell of *H. rufescens*, but the content appears more homogenous in *H. asinina*. Bevelander (1988) suggested that the granules in these cells were glycoprotein.

In *H. asinina*, the apical areas of hypobranchial gland leaves and leaflets represent specialized zones where at least 6 types of cells are formed, (i.e., supporting cell, ciliated sensory cell, and 4 types of mucus cells) whose classification is based on the appearance and staining characteristics of the granules. These mucus cells appear very different from those found in the basal area, both in cell shape and secretion. Judging from the staining pattern to PAS-methylene blue, type-1 and type-3 mucus cells contain neutral mucopolysaccharide granules, whereas type-2 cells contain basophilic granules suggesting acidic protein in nature (Humason 1972). Type-4 mucus cell contains both types of granules, neutral mucopolysaccharide and basophilic granules.

Because of the vast number and considerable variety of mucus cells, the principal function of hypobranchial gland should be the secretion of mucin (Hyman 1967). The surface area of the gland is increased by the folding of the glandular epithelium into large pleats to increase the mucus-secreting area. The quantity of mucus

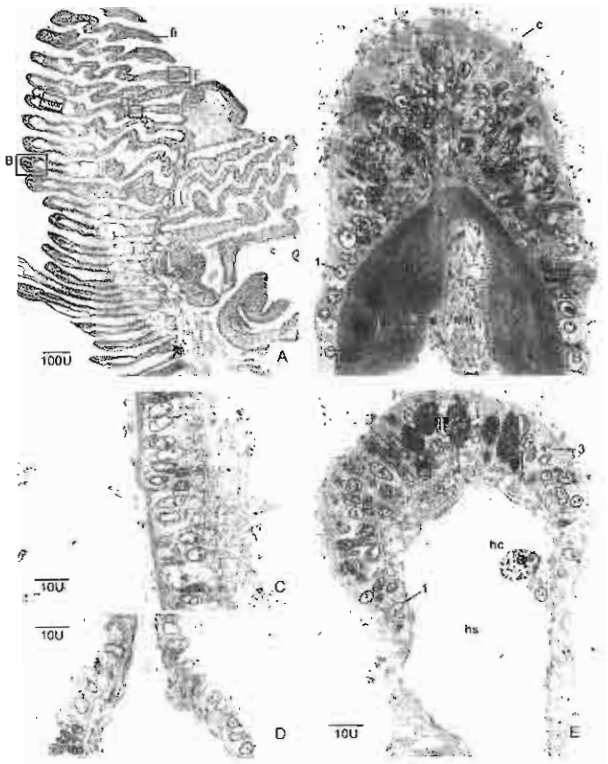


**Figure 4. Photomicrographs of the gill of *H. asinina*. A. A micrograph of the gill showing many filaments (fi) aligning parallel to each other. B. An enlargement from the efferent end of the filament from box B in Fig. A, showing four types of cells (1–4) in the terminal epithelium which possess both microvilli and short cilia. C. A bundle of muscle (mu) is attached to the V-shaped skeletal rods (ro). C and D. High-power micrographs of the epithelium of the gill taken from boxes C and D in Fig. A, showing many high columnar cells with long cilia in the epithelium near the efferent side and low columnar or cuboidal cells in the epithelium at the middle of the filament. E. An enlargement from the afferent end of the filament taken from box E in Fig. A, showing four types of cells in the epithelium (1–4). A hemocyte (hc) is seen in the hemocoelomic space (hs).**

discharging into the respiratory chamber increases suddenly if the animal is irritated. Mucus is thus produced and secreted for the protection and for clearing away debris from the anus and renal organs, to keep the gills and mantle cavity clean. Furthermore, when foreign irritating particles from turbid water are attached to the surface of the gland, the mucus cells may release mucus to bind particles that will be brushed away by the ciliary action of the epithelial cells. The mucus cells that perform this function may be type-2 mucus cells because they have similar characteristics to those observed in the gill epithelium that may perform similar function. Crofts (1929) found that irritating oils introduced into the entrance of the respiratory chamber seemed to be perceived at once by the hypobranchial gland, and the shell closed down abruptly, and at once a large amount of mucus was released from the mucus cells. In a similar experiment, Alexander (1970) introduced milk into the respiratory chamber, and obtained similar responses. Furthermore, some mucus cells may release mucin into the seawater, perhaps to clear away the offending substance, as well as to adjust pH of seawater to be suitable for respiration. The mucus cells participating in this protective action may belong to 2 types (i.e., the acidic and basic mucus cells types-1 and 3). The remaining mucus cell (type-4) may act as general mucus cells that produce mucin to lubricate the organ and protect the gills. Furthermore, the heterogeneity of the mucus cells of hypobranchial gland implies that the secretion of mucin for clearing irritants and debris may not be the only function. The complexity of the mucin released could be involved in other process, such as acting as the inducers for the larval settlement, because it has been shown that mucus trial from adult animals is one of the most important factors for settlement.

*Gill*

Light microscopic observation shows that the internal structure of the gills and the gill filaments of *H. asinina* have an internal architecture similar to those of other mollusks. The gills are bipectinate, with individual filaments showing basic similarities. All filaments are positioned parallel to each other and are linked by a common base through which the hemolymph is directed and distributed to the individual filaments (Eertman 1996). Each filament is corrugated in the middle part, which encloses the hemocoelic space, thus it may be a modification to enlarge the total gill surface area and improve respiratory gas exchange (Crofts 1929, Eertman 1996).

The epithelium of the gills in *H. asinina* is a simple columnar or cuboidal type, which presumably helps to enhance the rapid gas exchange. This feature has been found in most species of mollusks studied so far (Crofts 1929, Eertman 1996, De Villiers & Hodgson 1987). The gill filaments possess areas of ciliated cells alternating with areas of nonciliated cells. In our study, the efferent margin of the filament and both sides of the hemocoelic space in the efferent side consist of ciliated cells (Crofts 1929). Ciliary movement may take part in sweeping mucus secretions from the mucus cells that serve to capture foreign particles and remove them from the gills (Nuwayhid et al. 1978). Hence, the ciliated cells lining the gills observed in the present study may play both roles in making water current and removing irritating particles.

Nuwayhid et al. (1978) did not find any mucus cells in the gills of *Patella vulgata*, whereas in *Siphonaria capensis* there were a larger number of these cells (De Villiers & Hodgson 1987), and in *Austrocochlea constricta* there were two types of mucus goblet cells (Eertman 1996). The present study revealed two types of mucus cells on the gills of *H. asinina*. All of them are grouped at the efferent and afferent sides of the filament. It was suggested that these mucus cells function primarily in the cleaning of gills by removing dirt in coordination with muscle contraction and ciliary movement (Yonge 1952). The chitinous skeletal rods found in the efferent side may serve for attachment of muscles that bring about considerable movement of the gill filament (Crofts 1929, Haszprunar 1987). In *S. capensis*, it was found that the muscle fibers were located at intervals on the hemocoelic surface (De Villiers & Hodgson 1987). On the contrary, the present study reveals that the muscle fibers are attached to the inner surface of the rod. The function of this muscle may be the same as described earlier.

## ACKNOWLEDGMENTS

This research was supported financially by the Thailand Research Fund to Prasert Sobhon for a Senior Research Scholar Fellowship.

## LITERATURE CITED


Alexander, C. G. 1970. The osphradium of *Conus flavidus*. *Marine Biol.* 6:236–240.

Bevelander, G. 1988. Abalone gross and fine structure. Pacific Grove California: The Boxwood Press. pp. 1–80.

Crofts, D. R. 1929. Haliotis. *Liverpool Mar. Biol. Comm. Mem.* 29:1–174.

De Villiers, C. J. & A. N. Hodgson. 1987. The structure of the secondary gills of *Siphonaria capensis* (Gastropoda: Pulmonata). *J. Moll. Stud.* 53:129–138.

Eertman, R. H. M. 1996. Comparative study on gill morphology of gastropods from Moreton Bay, Queensland. *Moll. Res.* 17:3–20.

Haszprunar, G. 1987. The fine structure of the ctenidial sense organs (bursicles) of vetigastropoda (Zeugobranchia, Trochoidea) and their functional and phylogenetic significance. *J. Moll. Stud.* 53:46–51.

Hayat, M. A. 1993. Stains and cytochemical methods. New York: Plenum Press. pp. 1–455.

Humason, G. L. 1972. Animal tissue techniques. 3rd ed. USA: W.H. Freeman and Company. pp. 1–641

Hyman, L. H. 1967. The invertebrates. Mollusca I, vol. 6. New York: McGraw-Hill. pp. 1–792.

Nuwayhid, M. A., D. P. Spencer & H. Y. Elder. 1978. Gill structure in the common limpet *Patella vulgata*. *J. Mar. Biol Assoc. UK.* 58:817–823.

Schulte-Oehlmann, U., M. Tillmann, B. Markert, I. Oehlmann, B. Watermann & S. Scherf. 2000. Effects of endocrine disruptors on prosobranch snails (Mollusca: Gastropoda) in the laboratory. Part II: Triphenyltin as a xeno-androgen. *Ecotoxicology* 9:399–412.

Singhagraiwan, T. & M. Doi. 1993. Seed production and culture of a tropical abalone, *Haliotis asinina* Linne. *Bull. Tokai Reg. Fish. Res. Lab* 5:29–102.

Yonge, C. M. 1952. The mantle cavity of *Siphonaria alternata*. *Proc. Malacol. Soc. London.* 29:190–199.

*Journal of Shellfish Research*, Vol. 23, No. 4, 1031–1035, 2004.

# AMINOPEPTIDASE REACTIVITY IN THE DIGESTIVE TRACT OF ADULT ABALONE *HALIOTIS ASININA* LINNAEUS

**PORNCHARN SAITONGDEE,[1] PORNRUT RABINTOSSAPORN,[1] PRAPEE SRETARUGSA,[1] TANES POOMTONG,[2] AND PRASERT SOBHON[1]***

[1]*Anatomy Department, Faculty of Science, Mahidol University, RamaVI Road, Bangkok 10400, Thailand;* [2]*The Coastal Aquaculture Development Center, Department of Fisheries, Ministry of Agriculture and Cooperatives, Klong Wan, Prachaubkirikhun 77000, Thailand*

***ABSTRACT*** Histologically, the epithelium of the digestive tract is pseudostratified columnar type, which is composed of 3 kinds of cells (i.e., granulated cells, nongranulated cells, and mucus cells). The subsets of these three types of cells vary from region to region. By an enzyme-histochemical method, leucine aminopeptidase reactivity was localized principally within the cytoplasm of granulated cells in the buccal cavity, esophagus, esophageal pouch, hepatopancreas, and the third intestinal region, which implies that these sites are responsible for the synthesis and secretion of this peptidase for the digestion of proteinaceous nutrients.

***KEY WORDS:*** *Haliotis asinina*, abalone, digestive tract, aminopeptidase

## INTRODUCTION

The abalone *Haliotis asinina* is considered the most economically important abalone among the three species found along the coastal water of Thailand (Nateewathana & Bussawarit 1988) because of its good taste, high proportion of flesh, and the fastest growth rate. Due to increased demand, the collection of these abalone from natural habitat could not keep pace. To increase the abalone stocks and yields, the animals have been cultured and fed artificial diets for enhancing the growth rate (Serviere-Zaragoza et al. 1997). The rate of growth and nutritional composition of abalone were significantly affected by the level of proteins in the diet (Britz & Hecht 1997), which could be increased up to 30% (Fallu 1991). This high protein content could be broken down by proteolytic enzymes in the digestive tract of abalone, even though abalone are considered to be herbivorous animals that feed on mainly macroalgae, which are richer in carbohydrates. One possible protease inducible in the abalone is aminopeptidase, which is a family of zinc-dependent enzyme that catalyzes the hydrolysis of amino acid residues at the amino terminus of peptide substrates (Acosta et al. 1998). The source of this enzyme is most likely the epithelium of the digestive tract. The epithelial cells of the digestive tract of gastropods have been classified into 3 cell types and termed by different names, for example, columnar storage cell, secretory cell and mucus-producing cell (Tiebskorn & Kunast 1990), nonciliated, ciliated, and glandular cell (Leal-Zanchet 1998, Roldan & Garcia-Corrales 1988). Campbell (1965) and Chitramvong et al. (2000) have studied the abalone and also classified these epithelial cells into 3 types, which include pigmented cell, secretory cell, and mucus cell. The aim of this study is to investigate the presence of aminopeptidase in epithelial cells of some parts of the digestive tract of *H. asinina* by an enzyme–histochemical method.

## MATERIALS AND METHODS

### *Collection of Abalone Specimens*

Adult abalone *H. asinina* (age >16 mo old) of both sexes were obtained from the Coastal Aquaculture Development Center, Department of Fisheries, Prachuabkirikan province, Thailand. The animals were reared in the raceways of concrete tanks, which were well flushed with mechanically circulated seawater and air delivery system to maintain controlled environment. Abalone were fed with a diet of macroalgae (*Gracilaria spp.* and *Laminaria spp.*) supplemented with artificial food, and kept under normal daylight cycle.

### *Burstone and Folk Method for Detecting Aminopeptidase*

Abalone with body weights of 36.5 ± 2 g were anesthetized with 5% magnesium chloride for about 30 min. The shells (average size of 6.5 cm × 2.8 cm) were removed and digestive organs were dissected out and diced into small pieces before being embedded in the cryo-supporting medium. Frozen specimens were sectioned at 5-μm thick. The cryosections were fixed in two changes of chloroform for 4 min each, then hydrated in graded series of acetone, and finally in distilled water. The sections were incubated in a substrate solution containing the mixture of L-leucyl-β-naphthylamide, distilled water, tris buffer and garnet GBC for 1h at 37°C, then in tap water for 5 min and counterstained by Hematoxylin. After the final run through tap water for 10 min, the sections were mounted on glass slides in buffered glycerol (Burstone & Folk 1956).

### *Histology of the Digestive Tract*

To identify the cell types and characterize the cellular details for the enzyme localization, the histology of the abalone digestive tract was also studied from paraffin and semi thin plastic sections by preparing the specimens as follows.

For paraffin sections, various parts of the digestive tract were cut and fixed in the fixative of Bouin at 4°C overnight. Specimens were washed in 70% ethyl alcohol for removal of the fixative. Then, they were dehydrated through a graded series of ethyl alcohol (70% to 100%) for 1–2 h each, cleared with dioxane, infiltrated and embedded in paraffin wax, sectioned at 5 μm thick, and finally stained with Hematoxylin-Eosin (H&E) or Hematoxylin-PAS (H&PAS). The specimens were observed and evaluated for the characteristics of each cell type under microscope equipped with a digital camera.

For semithin plastic sections, the corresponding parts of the digestive tract were fixed in a solution of 4% glutaraldehyde and

*Corresponding author. Fax: +662-354-7168; E-mail: scpso@mahidol.ac.th

2% paraformaldehyde in 0.1 M Millonig buffer at 4°C overnight. After washing with buffer, the samples were postfixed in 1% osmium tetroxide in 0.1 M Millonig buffer at 4°C for 1 h, and then dehydrated in graded series of ethanol and pure propylene oxide. After that the specimens were infiltrated and embedded in Araldite 502 resin, and finally polymerized at 60°C for 24 h. Blocks of plastic embedded specimens were sectioned at 1 μm. These semithin sections were stained with 1% methylene blue, and then observed under microscope equipped with a digital camera.

## RESULTS

### *Histology and Aminopeptidase Reactivity*

#### The Buccal Cavity

The epithelium of buccal cavity consists of 3 cell types, the tall granulated columnar cells bearing microvilli; which appear as a "brush border" under the light microscope, the nongranulated cells, and the mucus cells having a "goblet" appearance; which are widely scattered in the epithelium (Fig. 1a). The granulated cells show red orange product in the apical cytoplasm overlapping on the granulated area (Fig. 1c), indicating the presence of aminopeptidase in this area of the cytoplasm, and at the luminal surface, whereas nongranulated and mucus cells are not stained. The control section does not show the presence of aminopeptidase (Fig. 1b).

#### The Esophagus

The epithelium of the esophagus contains 4 cell types: 2 types of granulated columnar cells, nongranulated columnar cells, and mucus cells (Fig. 1d to f). The two types of granulated columnar cells are distinguished by the presence of different size granules and color (i.e., in H&E stain type 1 contains small brownish granules whereas type 2 contains large reddish eosinophilic granules, whereas in semithin section all the granules appear bluish with different intensities (Fig. 1d to f)). The granulated cells with large reddish granules, nongranulated cells, and the mucus cells do not show aminopeptidase reactivity, whereas the granulated cells with small brownish granules show intense aminopeptidase reactivity in the granules (Fig. 1h). The control section does not show red product (Fig. 1g).

#### The Crop

The epithelium of crop appears to be pseudostratified columnar epithelium that is composed of only one cell type (i.e., the tall columnar cells, bearing a brush border). These cells also contain small clear mucin granules that are tightly packed together in both the apical and basal cytoplasm (Fig. 1i). This cell type shows only weak reactivity at its luminal surface but not in the cytoplasm (Fig. 1k), hence probably does not contain aminopeptidase enzyme.

#### The Stomach

The stomach epithelium comprises 3 cell types: mucus cell, tall granulated columnar cells with fine granules in the apical cytoplasm, and nongranulated columnar cells. The epithelium is covered by a thick layer of PAS-positive gastric shield (Fig. 1l). The intense aminopeptidase reactivity is present in the gastric shield overlying the epithelium but absent in the epithelial cells' cytoplasm (Fig. 1n). The control section shows negative reaction (Fig. 1m).

#### The Intestine

The intestinal epithelium contains four types of columnar epithelial cells. The former group comprises two types of granulated cells with different characteristics of granules (i.e., the first type of granulated cell appears to be similar to those found in the stomach whereas the second type possesses larger granules with varying density (Fig. 2a, b, c)). There is one type of nongranulated cell (Fig. 2b), and one type of mucus cell appearing similar to those in the crop (Fig. 2a). All two types of granulated cells show intense aminopeptidase reactivity in their cytoplasm (Fig. 2d, g). These four cell types occupy almost the entire epithelium except at the two prominent longitudinal folds, which contain only nongranulated cells that are devoid of aminopeptidase reactivity (Fig. 2d, e). The mucus cells, which are dispersed in the epithelium do not show any aminopeptidase reactivity either. The control section does not show any reaction product (Fig. 2f).

#### Hepatopancreas

The hepatopancreas comprises a large number of acini (Fig. 2h). The apical part of the acinar cells near the lumen exhibits intense aminopeptidase reactivity (Fig. 2j). The control section shows no reaction of aminopeptidase (Fig. 2i).

## DISCUSSION

In this study epithelial cells of the abalone digestive tract is classified into 3 types. The granulated cells (GC) are so called because they contain dense granules (serous type) with different sizes. This cell type could correspond to secretory cells as reported by Campbell (1965) and Chitramvong et al. (2000). In contrast to these earlier works we could identify at least four subtypes of these cells in various parts of the digestive tract because of their well preserved characteristics in semithin plastic sections. All GC except those in the stomach exhibit the aminopeptidase activity, which overlaps on the granulated area of the cytoplasm. There is only one type of nongranulated cell (NC), which does not exhibit aminopeptidase activity. There are at least 2 types of mucus cells (MC), in contrast to only one type of mucin producing cell reported by Campbell (1965) and Chitramvong et al. (2000). The first type of MC appears like goblet cells containing large mucin granules in the apical part, which tend to be dissolved away as shown in buccal cavity, esophagus, and stomach; whereas the second type is usually loaded with small tightly packed mucin granules as shown in the crop and intestine. Again the identification of these two subtypes of mucus cells is possible because of the use of plastic embedment. The presence and distribution of proteolytic enzyme was studied by detecting aminopeptidase (AP) reaction in different regions of the alimentary tract, from the buccal region to the anus. Almost all parts of the digestive tract show positive AP activities restricted at the brush border of the epithelial cells or in the lumen. The distinct appearance of AP reactivity was only observed in the cytoplasm of the granulated cells of buccal cavity, esophagus, esophageal pouch, as well as intestine. In addition, the intense enzyme reactivity was also detected in the acinar cells of the hepatopancreas. Hence these cells are producing zymogen granules that may contain aminopeptidase. The results agree with the work of Serviere-Zaragoza et al. (1997) who detected the pro-

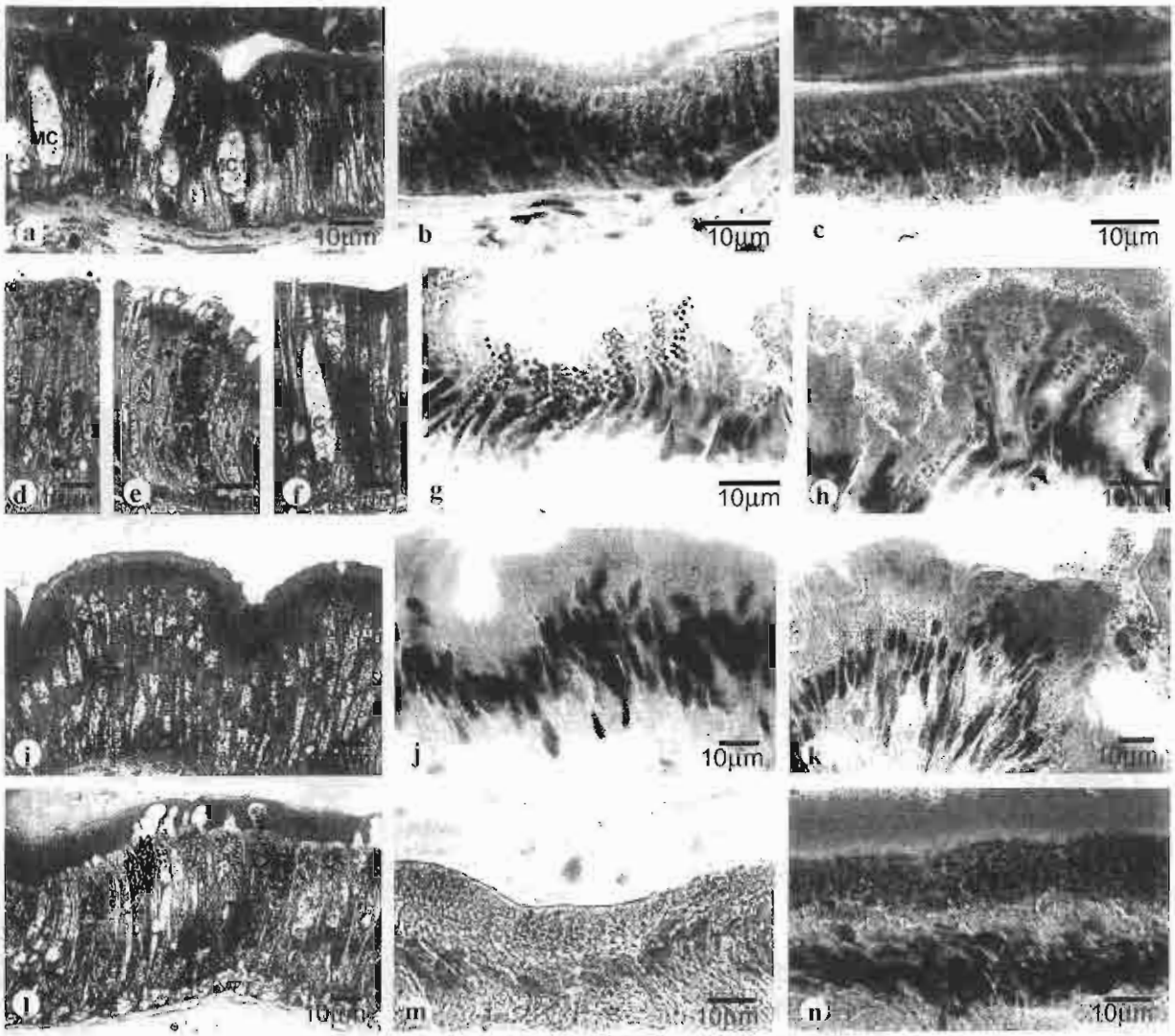


**Figure 1. The epithelium of various parts of *H. asinina* digestive tract. Left column: semithin sections stained with methylene blue. Middle column: The control sections for aminopeptidase reaction. Right column: The cryosections exhibiting the presence of aminopeptidase (AP) reactivity. (a.) A semithin section of buccal cavity stained with methylene blue showing tall granulated columnar cells (GC1) bearing microvilli, nongranulated cell (NC), and mucus cells (MC1). (b.) A control cryosection showing no AP reactivity. (c.) A cryosection showing moderate AP reactivity at the luminal surface of the granulated columnar cell. (d to f.) Semithin sections of esophagus showing 4 cell types including granulated columnar cells with small size granules (GC1) and granulated cell with large size granules (GC2), nongranulated cells (NC) and mucus cells (MC1). (g.) The absence the AP reactivity in the control cryosection. (h.) An intense AP reactivity in the granulated columnar cells. (i.) A semithin section of crop showing the tall columnar cells bearing brush border and containing small clear mucin granules (MC2) in the cytoplasm. (j.) The control section showing no AP reactivity. (k.) AP reactivity is localized on the luminal surface but not in epithelial cell cytoplasm. (l.) A semithin section of the stomach showing 3 types of epithelium cells (i.e., mucus cell [MC1], tall granulated columnar cells [GC3] containing fine granules at the apical part, and nongranulated cells [NC]). Note the presence of a thick gastric shield (gs) covering the luminal surface of the epithelium. (m.) Control cryosection showing no reactivity. (n.) Cryosection showing moderate aminopeptidase reactivity at gastric shield but not in the epithelial cells.**

teolytic activity in the hepatopancreas, crop and stomach content, and intestine and rectal fluid of the blue abalone, *H. fulgens*. The proteolytic activity observed in the intestinal and rectal fluid has optimal pH at alkaline range, whereas those from the hepatopancreas, crop, and stomach content were at acid pH. In the hepatopancreas, many proteases (three types of hydrolases and a carboxypeptidase) were detected by enzyme assays in *H. sorenseni* (Erasmus et al. 1997, Hernandez-Santoyo et al. 1998). Moreover, trypsin and chymotrypsin activities were also detected in the intestine and rectum by using specific synthetic substrates and inhibitors in kinetic and electrophoresis assays (Groppe & Morse 1993, Serviere-Zaragoza et al. 1997). The AP reactivity recognized in other parts of the digestive tract observed in the present study could possibly be the result of the released enzyme being mixed with the nutrients passing through these regions of the digestive tract rather than the enzyme being synthesized by epithelial cells of these regions. This

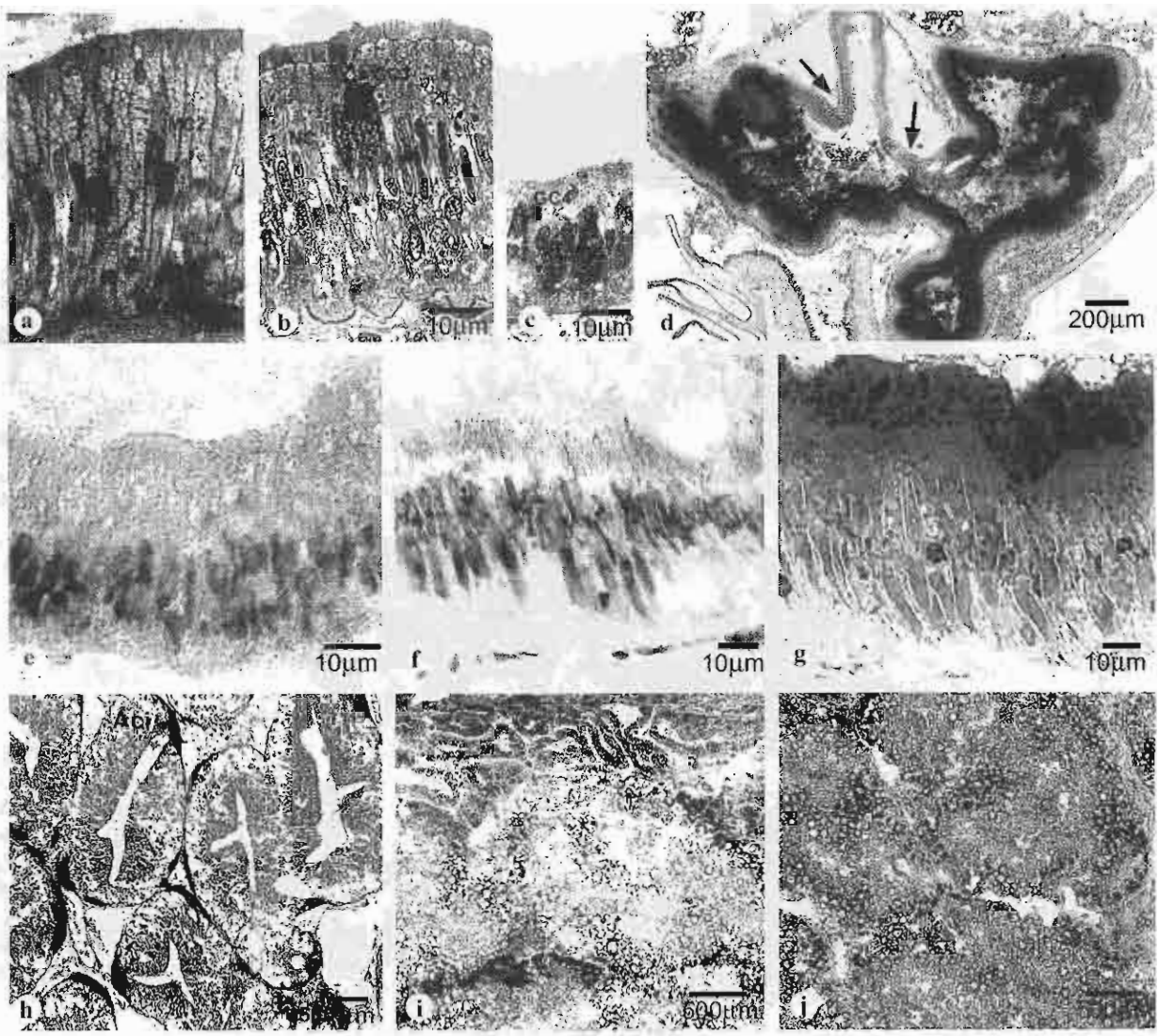


Figure 2. (a to c.) Semithin sections of the intestine showing 4 types of columnar epithelial cells (i.e., granulated cells with small granules [GC3], with large variable density granules [GC4] in the apical cytoplasm, mucus cells [MC2], and nongranulated cells [NC]). (d.) A low magnification of the intestine showing intense AP reactivity in most epithelial area except at the two prominent longitudinal folds (typhlosole) (arrows). (e.) Higher magnification of the area of typhlosole in d showing no AP reaction. (f.) The control cryosection of intestine showing the absent of AP reactivity. (g.) The higher magnification of the intestinal epithelium in d showing intense AP reactivity in their cytoplasm. (h.) Paraffin section of the hepatopancreas stained with H&E, showing many acini (Aci). (i.) The control cryosection showing no AP reactivity. (j.) The cryosection of hepatopancreas showing intensely AP reactivity near the lumen.

could explain the weak AP activity at the luminal surface of the crop, the first and second intestinal parts, and in the gastric shield of the stomach.

The absence of AP activity on the secondary foldings in the crop epithelium indicates that this organ may be the main part for food absorption rather than secreting the enzymes. Our observation is in agreement with Mclean (1970) who found, by using autoradiography with $^{14}$C-labeled algae, that in *H. rufescens* the crop is the major absorptive area. This author also demonstrated that the crop epithelium is permeable to phenylalanine and glucose. However, enzymes other than protease may be present in crop, because high lipase activity was detected in the crop (Mclean 1970). Interestingly, in the intestine there is an area called the longitudinal fold (typhlosole), which does not exhibit any AP activity as most cells are nongranulated, and this structure probably is involved mainly in the absorption, whereas the rest of intestine synthesizes and secretes the protease enzyme.

ACKNOWLEDGMENT

This research was supported financially by the Thailand Research Fund (Senior Research Scholar Fellowship to Prasert Sobhon)

## LITERATURE CITED


Acosta, D., F. Goni & C. Carmona. 1998. Characterization and partial purification of a leucine aminopeptidase from *Fasciola hepatica*. *J. Parasitol.* 84:1–7.

Britz, P. J. & T. Hecht. 1997. Effect of dietary protein and energy level on growth and body composition of South African abalone, *Haliotis midae*. *Aquaculture* 156:195–210.

Burstone, M. S. & J. E. Folk. 1956. Histochemical demonstration of aminopeptidase. *J. Histochem. & Cytochem.* 4:217–226.

Campbell, J. L. 1965. The structure and function of the alimentary canal of the black abalone, *Haliotis cracherodii* Leach. *Transactions of the American Microscopical Society* 84:376–395.

Chitramvong, Y., M. Kruatrachue, E. S. Upatham, K. Parkpoonsukanol & S. Singhakaew. 2000. Digestive system of *Haliotis asinina* Linnaeus and *Haliotis ovina* Gmelin (Gastropoda: Haliotidae) in Thailand. *J. Med. & Appl. Malacol.* 10:121–131.

Erasmus, J. H., P. A. Cook & V. E. Cuyne. 1997. The role of bacteria in the digestion of seaweed by the abalone *H. midae*. *Aquaculture* 155: 377–386.

Fallu, R. 1991. Abalone farming. Fishing News Books, Oxford: Division of Blackwell Science LTD. 195 pp.

Groppe, J. C. & D. E. Morse. 1993. Molluscan chymotrypsin-like protease: structure, localization, and substrate specificity. *Arch Biochem Biophys.* 305:159–169.

Hernandez-Santoyo, A., A. Hernandez-Arana, R. Arreguin-Espinosa & A. Rodriguez-Romero. 1998. Purification and characterization of several digestive proteases from the blue abalone. *Haliotis fulgens*. *Aquaculture* 159:203–216.

Leal-Zanchet, A. M. 1998. Comparative studies on the anatomy and histology of the alimentary canal of the Limacoidea and Milacidae (Pulmonata: Stylommatophora). *Malacologia* 39:39–57.

Mclean, N. 1970. Digestion in *Haliotis rufescens* Swainson (Gastropoda: Prosobranchia). *J. Exp. Zool.* 173:303–318.

Nateewathana, A. & S. Bussawarit. 1988. Abundance and distribution of abalone along the Andaman Sea Coast of Thailand. *Kasetsart J.* 22:8–15.

Roldan, C. & P. Garcia-Corrales. 1988. Anatomy and histology of the alimentary tract of the snail *Theba pisana* (Gastropoda: Pulmonata). *Malacologia* 28:119–130.

Serviere-Zaragoza, E., M. A. Navarrete del Toro & F. L. Garcia-Carreño. 1997. Protein hydrolysing enzymes in the digestive systems of the adult Mexican blue abalone, *Haliotis fulgens* (Gastropoda). *Aquaculture* 157:325–336.

Tiebskorn, R. & C. Kunast. 1990. Ultrastructural changes in the digestive system of *Derocerus reticulatum* (Mollusca: Gastropoda) induced by lethal and sublethal concentrations of the carbamate molluscicide cloethocarb. *Malacologia* 32:89–106.

Available online at www.sciencedirect.com
SCIENCE DIRECT
Molecular & Biochemical Parasitology 136 (2004) 1–10
MOLECULAR & BIOCHEMICAL PARASITOLOGY

# Molecular cloning and analysis of stage and tissue-specific expression of cathepsin B encoding genes from *Fasciola gigantica*☆

Krai Meemon[a], Rudi Grams[b], Suksiri Vichasri-Grams[c], Annemarie Hofmann[d], Günter Korge[d], Vithoon Viyanant[b], Edward Suchart Upatham[c], Shigehisa Habe[e], Prasert Sobhon[a,*]

[a] *Department of Anatomy, Faculty of Science, Mahidol University, Rama VI Rd., Bangkok 10400, Thailand*
[b] *Department of Medical Technology, Faculty of Allied Health Science, Thammasat University, Phahonyothin Rd., Klongluang, Pathumthani 12120, Thailand*
[c] *Department of Biology, Faculty of Science, Mahidol University, Rama VI Rd., Bangkok 10400, Thailand*
[d] *Institut für Genetik, Freie Universität Berlin, Arnimallee 7, Berlin 14195, Germany*
[e] *Department of Parasitology, School of Medicine, Fukuoka University, 45-1, 7-Chome, Nanakuma, Jonan-ku, Fukuoka 814-80, Japan*

Received 30 July 2003; received in revised form 22 February 2004; accepted 24 February 2004

**Abstract**

The transcriptional products of *Fasciola gigantica* genes encoding cathepsin B proteases were cloned from adult, newly excysted juvenile (NEJ), and metacercarial stages. The obtained cDNAs were named FG cat-B1, FG cat-B2, and FG cat-B3. The deduced amino acid sequences of the encoded proteases have identities ranging from 64 to 79%. Sequence comparison with homologous proteins showed that all functional important residues formerly described for cathepsin B are conserved. Southern analysis confirmed the presence of a family of related cathepsin B genes in the genome of *F. gigantica*. Northern analysis revealed a common transcript size of 1400 nucleotides with abundant cathepsin B transcripts detected in metacercarial and NEJ stages. Cathepsin B transcripts were located by RNA in situ hybridization in the caecal epithelial cells, in cells underlining the proximal part of the digestive tract, and in the tegumental cells underlining the surface tegument. Furthermore, transcripts were detected in the tissues of the reproductive system including cells of prostate, Mehlis, and vitelline glands, testis, and eggs. Stage-specific gene expression was investigated by RT-PCR using gene-specific primers and hybridization with a labeled cathepsin B probe. FG cat-B1 transcripts were detected in all stages, whereas FG cat-B2 and FG cat-B3 transcripts were expressed in metacercariae, NEJ, and juvenile parasites only. The switching off of the cat-B2 and cat-B3 genes during the maturation of the parasites implicates that these enzymes may be involved in digesting host tissues during penetration and migration to the liver, whereas cat-B1 present in all stages may perform general digestive function.


*Keywords.* *Fasciola gigantica*; Cathepsin B; Northern hybridization; Southern hybridization; RNA in situ hybridization; Stage-specific expression

## 1. Introduction

*Fasciola gigantica* causes tropical fascioliasis in infected water buffaloes and cattle in Thailand and countries in the tropical region. Moreover, the parasite can also cross-infect human [1], which has been considered an important public health problem in many parts of the tropics. Control of the disease is so far carried out by treatment with antihelminthics, grazing management, and the application of molluscicides [2]. All of these preventive methods have limitations and transient effect. Vaccination is considered to be the ultimate, most cost-effective, and sustainable strategy. Many antigens have been tested as vaccine candidates in *Fasciola* spp., such as fatty acid binding proteins (FABP), glutathione *S*-transferase (GST), and cathepsin L proteases (CatL) [3–8], because of their specific and important functions in the parasite's survival. However, these vaccine candidates affect mainly the adult parasites which reside in the bile duct where lower concentrations of antibodies and immune effector cells are found. In addition, the adult parasites

☆ *Note:* Nucleotide sequence data reported in this paper are available in the GenBank™, EMBL and DDBJ databases under the accession numbers AY227673- AY227675.

* Corresponding author. Tel.: +66-2201-5406; fax: +66-2247-9880.
*E-mail address:* scpso@mucc.mahidol.ac.th (P. Sobhon).

0166-6851/$ – see front matter © 2004 Published by Elsevier B.V.
doi:10.1016/j.molbiopara.2004.02.010

have already developed the full complements of immune evasion mechanisms. Therefore, the chance of damaging and killing parasites would be higher if the vaccine candidates can be directed at the newly excysted and juvenile stages.

In the parasitic life cycle, proteases have been deployed in some important tasks, which include tissue penetration, digestion of host tissue for nutrition, and evasion from the host immune responses [9–11]. Although the most characterized proteases in *Fasciola* spp. belong to the cathepsin L group of cysteine proteases [12,13], Wilson et al. [14] have reported that cathepsin B proteases are the major proteases secreted by the newly excysted juvenile (NEJ) of *F. hepatica*. In a recent publication the cloning and expression of the major secreted cathepsin B protein from juvenile *F. hepatica* has been reported [15]. This protein could be detected in early stages of infection and the investigators suggested that the protease may help the juvenile parasite in penetration and migration through the host's liver. However, cathepsin B gene fragments have also been amplified from adult *F. hepatica* RNA [16], but its function in adults has not been studied yet.

In the present study, we have cloned cDNAs of *F. gigantica* cathepsin B genes from three different stages (adult, newly excysted juveniles, and metacercariae) and analyzed the identity of their sequences. The genes have been characterized in respect to their copy number and differential expression in several developmental stages. The distribution of cathepsin B gene transcripts in *F. gigantica* tissues has been analyzed by RNA in situ hybridization using a cathepsin B antisense RNA probe.

## 2. Materials and methods

### 2.1. Parasite specimens

*F. gigantica* metacercariae were obtained from experimentally infected snails *Lymnaea ollula*. To activate the excystment, the metacercariae were incubated in a solution containing 2% pepsin and 0.5% HCl at 37 °C for 45 min and then in a solution of 0.02 M sodium dithionite, 0.2% taurocholic acid, 1% $NaHCO_3$, 0.8% NaCl, and 0.5% HCl at 37 °C for 45 min. The metacercariae were excysted in RPMI-1640 medium (Sigma Chemical Co., St. Louis, MO, USA) containing 10% normal sheep serum and 10 μg/ml gentamycin at 37 °C. After 3 h of incubation the NEJs were collected. Adult worms were obtained from the bile ducts and gall bladders of naturally infected animals killed at the local abattoirs. The juvenile parasites were obtained from Golden Syrian hamster experimentally infected with metacercariae. The specimens used for nucleic acid preparations were kept in liquid nitrogen until required.

### 2.2. Nucleic acid preparations

Genomic DNA was extracted from frozen and powdered adult *F. gigantica* as previously described [17]. Total RNA was extracted from developmental stages of *F. gigantica* by using TRIzol reagent (Life Technologies), according to the manufacturer's protocol. Poly(A)$^+$ RNA was extracted using oligo(dT) cellulose columns from the MessageMaker Reagent Kit (Life Technologies). Nucleic acids were stored at −20 °C until used.

### 2.3. Construction of the cDNA libraries

The cDNA libraries from adult, NEJ and metacercaria of *F. gigantica* were constructed using the SMART cDNA library construction kit (Clontech), according to the manufacturer's protocol. Briefly, the poly(A)$^+$ RNA from the three stages were reverse-transcribed into double-stranded (ds) cDNA with SMART IV oligonucleotide and CDSIII/3′ PCR primers. The ds cDNA were amplified by long distance (LD) PCR for construction of metacercaria and NEJ libraries, or by primer extension for the adult library construction. The PCR products were digested with proteinase K and then with *Sfi*I restriction endonuclease before being size-fractionated through CHROMA SPIN-400 columns. The ds cDNAs (>400 bp length) were inserted in the *Sfi*IA and *Sfi*IB sites of λTriplEx2, and the recombinant DNA was then packaged in vitro using Gigapack III Gold packaging extracts (Stratagene). The λTriplEx2 phages containing cDNA inserts were subsequently amplified on plate lysates. The amplified libraries were checked for their titers and kept at −80 °C in the presence of 7% DMSO.

### 2.4. Library screening for cathepsin B genes

Incomplete cDNAs of the cathepsin B genes were isolated from the cDNA libraries using primers designed from homologous sequences of *F. hepatica*. Briefly, 10 μl of cDNA libraries from each *F. gigantica* stage were used as templates to obtain amplified DNA fragments of the cathepsin B gene by a standard polymerase chain reaction (PCR) with *Taq* DNA polymerase (Life Technologies; 35 cycles at 94, 55, 72 °C, 1 min each step) using a forward primer (5′ TGGCCACAATGCTGGACG 3′) and a reverse primer (5′ TCAAAGACGTGGCATTCC 3′) deduced from the nucleotide sequences of a *F. hepatica* cathepsin B gene [14]. The obtained PCR products were labeled with radioactive $^{32}$P-dCTP using the Hexalabel DNA Labeling Kit (MBI Fermentas) and used as probes to isolate full length cDNAs.

The cDNA libraries were screened to obtain complete sequences of cathepsin B genes according to the procedure of Sambrook et al. [18]. Each library was plated out with $5 \times 10^4$ pfu per petri dish (diameter 15 cm) and grown at 37 °C for 8–10 h until the plaques just began to contact each other. After a plaque lift to nylon membranes the released and denatured DNA was fixed by baking at 80 °C for 2 h. The membranes were hybridized with cathepsin B probes constructed as mentioned above at 42–45 °C overnight in 50% formamide, 5× SSPE, 5× Denhardt's solution, 0.5%

SDS, and 100 μg/ml denatured, low molecular weight salmon sperm DNA. Autoradiographic film was exposed to the membranes overnight at −70 °C with intensifying screens. Ten cathepsin B-hybridized clones were isolated, converted to pTriplEx2, and analyzed by restriction endonuclease digestion and agarose gel electrophoresis. DNA sequencing was done at MWG AG Biotech, Germany and NSTDA Bioservice Unit, Thailand. Sequence analysis was done with MacMolly Lite (Softgenc, Germany) and BioEdit (http://www.mbio.ncsu.edu/BioEdit/bioedit.html). The cathepsin B genes obtained from the adult, NEJ, and metacercaria libraries were named FG cat-B1, cat-B2, and cat-B3, respectively.

### 2.5. Nucleic acids hybridization analysis

Southern and Northern blot analyses were done as previously described by Grams et al. [17]. For Southern blot analysis, 10 μg each of genomic DNA was digested with restriction endonucleases *Eco*RI, *Pst*I, *Eco*RI/*Pst*I and size-separated in a 0.7% agarose gel in TBE buffer. For Northern blot analysis, 5 and 25 μg of total RNA was size-separated in 1.2% agarose gels containing 2.2 M formaldehyde in 1× MOPS buffer. Nucleic acids were transferred to nylon membranes (Schleicher & Schuell). Hybridization was done at 50 °C (DNA) or 68 °C (RNA) in 50% formamide, 5× SSC, 2% blocking reagent (Roche), and 0.02% SDS for 15 h. A digoxigenin (DIG)-labeled RNA antisense probe generated from the full length cat-B1 clone was produced with the RNA DIG Labeling Kit (Roche), and used in Southern, Northern, and in situ hybridizations. A DIG-labeled RNA sense probe of the cat-B1 clone was constructed by the same method and used as control. The nucleic acids detection was done enzymatically using alkaline phosphatase and CDP-Star (Roche) chemiluminescence.

### 2.6. RNA in situ hybridization

Cathepsin B mRNA was detected in the tissues of adult and juvenile *F. gigantica* using a DIG-labeled RNA cat B1 antisense probe. The parasites were first fixed in DEPC-treated phosphate buffer saline (PBS: 140 mM NaCl; 2.7 mM KCl; 10 mM $Na_2HPO_4$; 1.8 mM $KH_2PO_4$; pH 7.4) containing 4% paraformaldehyde, pH 7.4 for 3–4 h at room temperature and then embedded in paraplast. Tissue sections were cut (10 μm), dewaxed in fresh xylene, and rehydrated in serial dilutions of ethanol, i.e., 100, 95, and 70%, and finally in DEPC-treated $H_2O$. Prehybridization and hybridization of tissue sections with a DIG-labeled cat-B1 probe were done following the protocol of the non-radioactive in situ hybridization application manual (Roche). Briefly, the tissue sections were treated twice with PBS containing 100 mM glycine for 5 min each, and then with PBS containing 0.3% Triton X-100 for 15 min. The sections were subsequently permeabilized with TE buffer containing 5–20 μg/ml RNase-free proteinase K at 37 °C for 30 min, post-fixed with PBS containing 4% paraformaldehyde for 5 min at 4 °C, and acetylated with 0.1 M triethanolamine (TEA) buffer, pH 8.0, containing 0.25% (v/v) acetic anhydride for 5 min. Prehybridization was done by incubating with 4× SSC containing 50% (v/v) deionized formamide at 37 °C for at least 10 min. The sections were incubated with hybridization buffer (40% deionized formamide, 10% dextran sulfate, 1× Denhardt's solution, 4× SSC, 10 mM dithiothreitol, 1 mg/ml yeast t-RNA, 1 mg/ml denatured and sheared salmon sperm DNA) containing 5–10 ng of DIG-labeled cat-B RNA probe at 45 °C overnight. The hybridized sections were washed in a water bath at 37 °C as follows: two times in 2× SSC, two times in 1× SSC for 15 min each, in NTE buffer (500 mM NaCl, 10 mM Tris, 1 mM EDTA, pH 8.0) containing 20 μg/ml RNase A for 30 min at 37 °C, and two times in 0.1× SSC for 30 min each. Immunological detection was done using anti-DIG-alkaline phosphatase and NBT/BCIP substrates. Control experiments were similarly done but with a DIG-labeled sense RNA probe.

### 2.7. Stage-specific expression of cathepsin B genes by PCR

The cDNA libraries were used as starting materials for PCR analysis employing three sets of gene-specific primer pairs (Table 1). The PCR was set up as described before for the isolation of the cathepsin B genes. The PCR products were transferred to a nylon membrane and hybridized with a cat-B1 antisense RNA probe. Detection was done as described before. A control experiment was done by RT-PCR with total RNA extracted from adult and juvenile parasites.

Table 1
Specific primers used for PCR analysis

| Sets | Primers | Sequences | Product sizes (bp) |
|---|---|---|---|
| I | FG cat-B1(forward) | 5′-TCGTCGTAGACTATGTTCG-3′ | 840 |
| | FG cat-B1(reverse) | 5′-GTAAATCGTACTGACAGG-3′ | |
| II | FG cat-B2(forward) | 5′-CACGGCGCCAGCCAGTGC-3′ | 506 |
| | FG cat-B2(reverse) | 5′-TGAATTTACCGGCCACG-3′ | |
| III | FG cat-B3(forward) | 5′-TCCTCATAAACAAGGCTCG-3′ | 1087 |
| | FG cat-B3(reverse) | 5′-TCAGAATGCGAACACACG-3′ | |

FG, *Fasciola gigantica*

## 3. Results

### 3.1. Cloning and sequencing of the cDNAs encoding cathepsin B of F. gigantica

Screening of the cDNA libraries, using the generated *F. gigantica* cathepsin B fragments as probes, resulted in 270 positive clones out of $5 \times 10^4$ plaques from the metacercaria cDNA library, 100 positive clones out of $5 \times 10^4$ plaques from the NEJ cDNA library, and 12 positive clones out of $5 \times 10^4$ plaques in the adult cDNA library. Five of the ten selected clones from each library contained the complete coding sequences for cathepsin B genes. The clone isolated from the adult cDNA library (named cat-B1) showed an open reading frame of 1008 nucleotides encoding a cathepsin B protease of 335 amino acid residues. The clones isolated from the NEJ and metacercaria cDNA libraries (named cat-B2 and cat-B3) contained open reading frames of 1020 and 1014 nucleotides which encoded proteases of 339 and 337 amino acid residues, respectively (Fig. 1).

Analysis of nucleic acid and deduced amino acid sequences indicated that these three clones encoded putative cathepsin B proteases. Identities between the clones ranged from 64 to 79% (Table 2). Alignment of the cathepsin B amino acid sequences showed that the thiol consensus pattern (Gln-*X*(3)-[Gly, Glu]-*X*-Cys-Trp-*X*(2)-[Ser, Thr, Ala, Gly]), where *X* is any amino acid residue, and the active site residues ($Cys^{29}$, $His^{200}$, $Asn^{220}$, human cathepsin B numbering) are highly conserved in the sequences of *F. gigantica* cathepsin B (Fig. 1) [14,16,19–21]. An occluding loop (residues 104–127, human cathepsin B numbering) and 12 cysteine residues forming disulfide bridges are also conserved in all three cathepsin B proteins. However, from the two His residues 110/111 which are responsible for exopeptidase activity as found in mammalian cathepsin B [22,23] only $His^{110}$ is conserved. The pre–pro region of the protein involved in the inhibition of the enzyme activity, correct folding, and stabilization of the enzyme, is also highly conserved (Fig. 1). By analysis with the SignalP program (http://www.cbs.dtu.dk/services/SignalP) and comparison with mammalian cathepsin B, amino acids 1–15 of all three *F. gigantica* cathepsin B proteins form the pre-region and amino acids 16–85 form the pro region. The mature protease, after cleaving off pre- and pro-regions, varies in length from 250 amino acids in cat-B1, to 254 amino acids in cat-B2, and 252 amino acids in cat-B3 (Fig. 1).

### 3.2. Gene copy number of F. gigantica cathepsin B

A Southern blot analysis was done to estimate the cathepsin B gene copy number in *F. gigantica*. Genomic DNA extracted from adult *F. gigantica* was digested with restriction endonucleases *Eco*RI and *Pst*I. The cloned cathepsin B cDNAs do not contain recognition sites for these enzymes. The digested DNA was size separated by agarose gel electrophoresis, transferred to a nylon membrane and hybridized with a FG cat-B1 antisense RNA probe using stringent hybridization conditions. Five to six DNA fragments of 4–23 kb size were detected with a single prominent hybridized band (Fig. 2). The observed hybridization pattern indicates a small family of closely related cathepsin B genes in *F. gigantica*.

### 3.3. Cathepsin B gene expression analysis

A Northern blot analysis was done with total RNA extracted from metacercaria, NEJ, 6-weeks-old juvenile, and adult *F. gigantica* using a cat-B1 antisense RNA probe. Under standard stringent hybridization conditions at 68 °C, the probe hybridized to transcripts of approximately 1.4 kb length in all developmental stages (Fig. 3A–C). Cathepsin B transcripts were found to be abundant in metacercarial and NEJ stages, less abundant in 6-weeks-old juvenile, and to exist only in small amounts in the adult stage.

Table 2
Sequence identity/similarity matrix of *Fasciola* cathepsin B amino acid sequences

| | FG cat-B1 | FG cat-B2 | FG cat-B3 | FH U58000 | FH AJ488928[a] | FH Z22768[a] | SJ X70968 | SM M21309 | HS L16510 |
|---|---|---|---|---|---|---|---|---|---|
| FG cat-B1 | 1 | *0.81* | *0.91* | *0.83* | *0.79* | *0.56* | *0.67* | *0.67* | *0.62* |
| FG cat-B2 | 0.65 | 1 | *0.81* | *0.99* | *0.80* | *0.56* | *0.70* | *0.70* | *0.67* |
| FG cat-B3 | 0.79 | 0.64 | 1 | *0.82* | *0.79* | *0.57* | *0.67* | *0.69* | *0.65* |
| FH U58000 | 0.65 | 0.99 | 0.64 | 1 | *0.80* | *0.56* | *0.70* | *0.70* | *0.67* |
| FH AJ488928[a] | 0.69 | 0.65 | 0.66 | 0.65 | 1 | *0.59* | *0.66* | *0.65* | *0.65* |
| FH Z22768[a] | 0.35 | 0.36 | 0.35 | 0.39 | 0.38 | 1 | *0.55* | *0.55* | *0.53* |
| SJ X70968 | 0.48 | 0.49 | 0.49 | 0.49 | 0.52 | 0.36 | 1 | *0.89* | *0.68* |
| SM M21309 | 0.49 | 0.49 | 0.50 | 0.49 | 0.52 | 0.37 | 0.74 | 1 | *0.65* |
| HS L16510 | 0.44 | 0.44 | 0.44 | 0.45 | 0.48 | 0.40 | 0.46 | 0.46 | 1 |

The similarity values between the different sequences analyzed using the GONNET matrix are shown in italic, while their identity values are shown in plain text formatting.

[a] Only the available partial sequences were used for calculation. FH: *Fasciola hepatica*; SJ: *Schistosoma japonicum*; SM: *Schistosoma mansoni*; HS: *Homo sapiens*. U58000 ([14], complete sequence reported in [15]), AJ488928 [unpublished], Z22768 [16], X70968 [19], M21309 [20], L16510 [21] are accession numbers of cathepsin B sequences available from GenBank™.

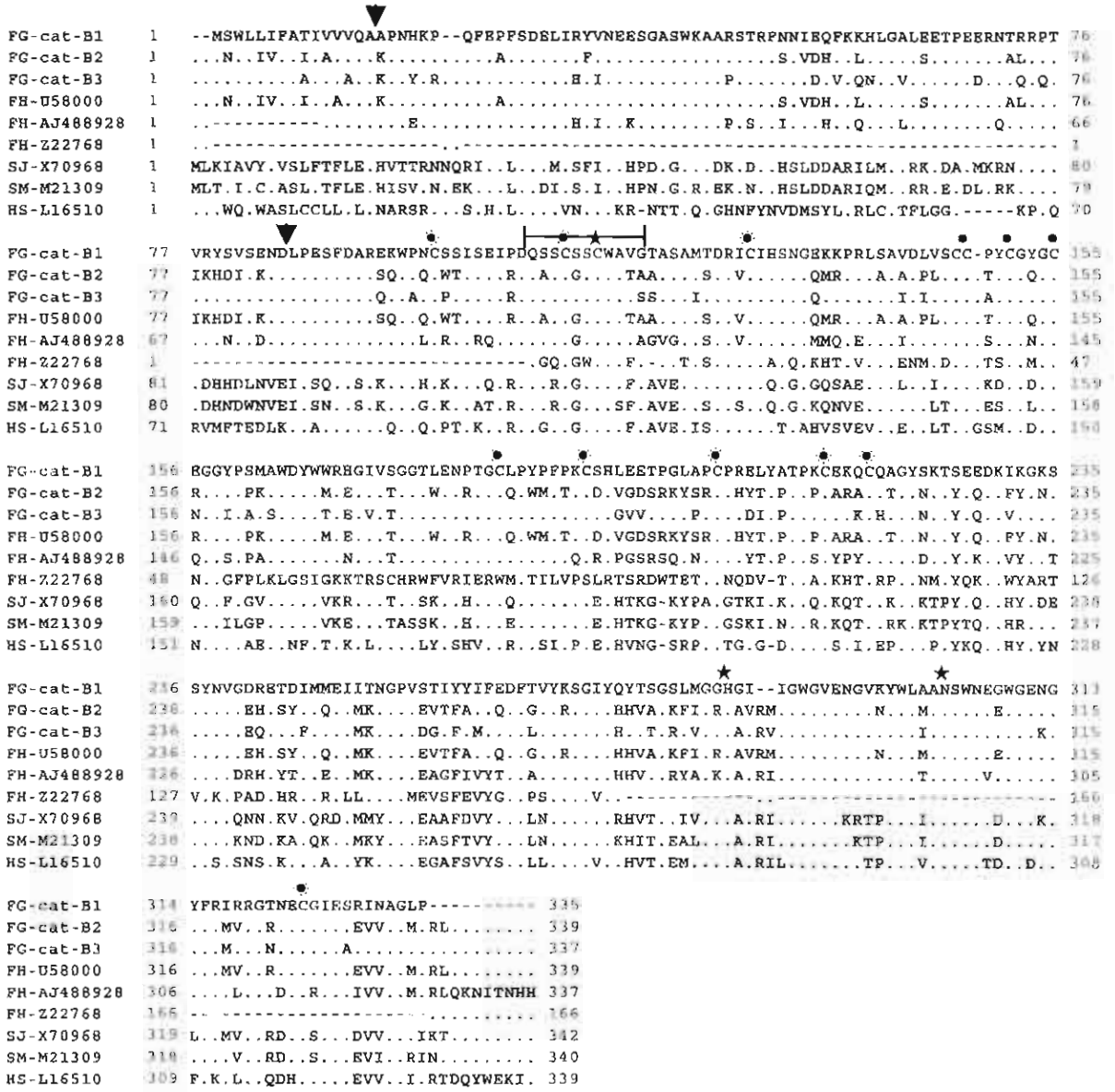

Fig. 1. Alignment of the deduced *F. gigantica* cathepsin B sequences (FG cat-B1, FG cat-B2, and FG cat-B3) with related cathepsin proteases. Full sequence is given for FG cat-B1. Dots indicate sequences identical to that in FG cat-B1. (▼) indicates the first amino acid of the pro region and the mature protein in *F. gigantica* cathepsin B, respectively. The thiol consensus pattern represented as (I——I); active site residues, (★); cysteine residues involved in disulfide bonding, (●). FG: *Fasciola gigantica*; FH: *Fasciola hepatica*; SJ: *Schistosoma japonicum*; SM: *Schistosoma mansoni*; HS: *Homo sapiens*. U58000 ([14], complete sequence is reported in [15]), AJ488928 [unpublished]; Z22768 [16]; X7968 [19]; M21309 [20]; L16510 [21] are accession numbers of cathepsin B sequences available from GenBank™.

### 3.4. Distribution of cathepsin B gene transcripts

The localization of cathepsin B RNA in parasite tissues was done by in situ hybridization on sections of adult and 4-weeks-old juvenile *F. gigantica*, using a cat-B1 antisense RNA probe. In both stages, the cathepsin B mRNA was localized in the caecal epithelial cells and cells underlining the proximal part of the digestive tract which included the pharynx, oral, and ventral suckers (Fig. 4A–C). Moreover, cathepsin B mRNA was detected in the tegumental cells underlining the surface tegument (Fig. 4A, B and D). Interestingly, in the adult parasites cathepsin B mRNA was also detected in the tissues of the reproductive system, such as cells of prostate gland, Mehlis gland, vitelline gland, testis, eggs, and cells underlining the uterine epithelium (Figs. 4D and 5A–E).

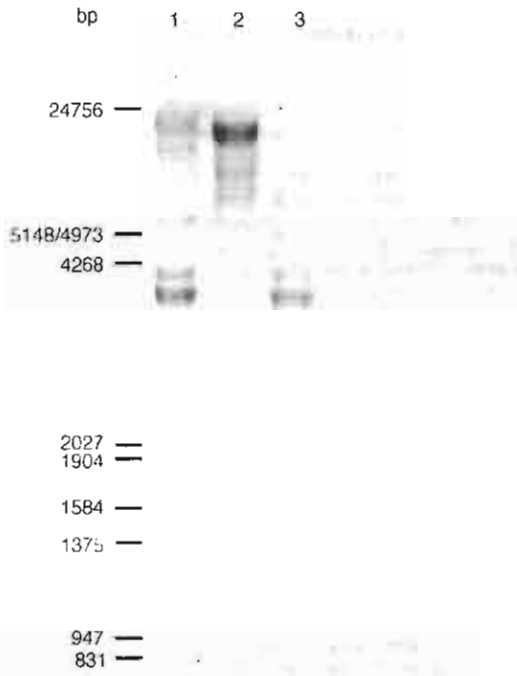


Fig. 2. Southern hybridization analysis of *F. gigantica* genomic DNA with a cathepsin B probe. Five microgram each of genomic DNA were digested with *Eco*RI (lane 1), *Pst*I (lane 2), *Eco*RI/*Pst*I (lane 3), size separated in a 0.7% agarose gel and hybridized with a FG cat-B1 antisense RNA probe. Lambda DNA digested with *Eco*RI/*Hin*dIII was used as a marker represented on the left hand side.

### 3.5. Stage-specific expression of *F. gigantica* cathepsin B genes

PCR products were obtained from the three cDNA libraries using gene-specific primers for each cathepsin B gene (Table 1). The PCR products were transferred to nylon membranes and hybridized with a cat-B1 antisense RNA probe. The cat-B1 fragment was detected in all three cDNA libraries, while the cat-B2 and cat-B3 fragments were detected only in metacercaria and NEJ cDNA libraries (Fig. 6). This result indicated that the cat-B1 gene was expressed in all stages of the parasite, whereas the cat-B2 and cat-B3 genes were expressed only in metacercarial and NEJ stages. The same result was obtained by RT-PCR with total RNA extracted from developmental stages as used for cDNA library construction.

## 4. Discussion

In this study we have cloned three cDNAs encoding cathepsin B proteases from stage-specific libraries (adult, NEJ, and metacercaria) of *F. gigantica* and analyzed their stage- and tissue-specific expression by Northern hybridization, PCR techniques and RNA in situ hybridization. The three cathepsin B clones showed differences in length and nucleotide/amino acid sequences which imply that they are distinct members of the same gene family. Interestingly, FG cat-B2 showed 99% identity to *F. hepatica* NEJ

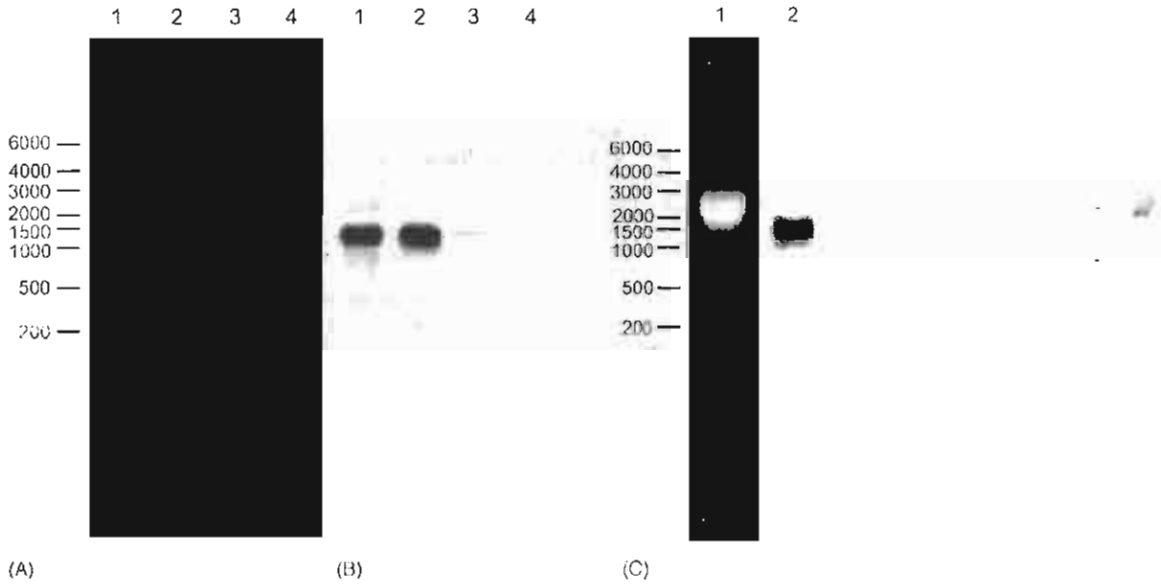


Fig. 3. Northern hybridization analysis of *F. gigantica* total RNA with a FG cat-B1 antisense RNA probe. Panel A: total RNA (5 μg) extracted from metacercariae (lane 1), NEJ (lane 2), 6-weeks-old juveniles (lane 3), and adult parasites (lane 4) separated in a 1.2% formaldehyde-agarose gel before blotting. Panel B: cathepsin B gene transcripts detected after hybridization. Panel C: total RNA (25 μg) extracted from adult parasites before (lane 1) and after hybridization (lane 2) with a cathepsin B probe. Transcript sizes (nucleotides) are shown on the left hand side (high range markers, RNA ladder, MBI Fermentas).

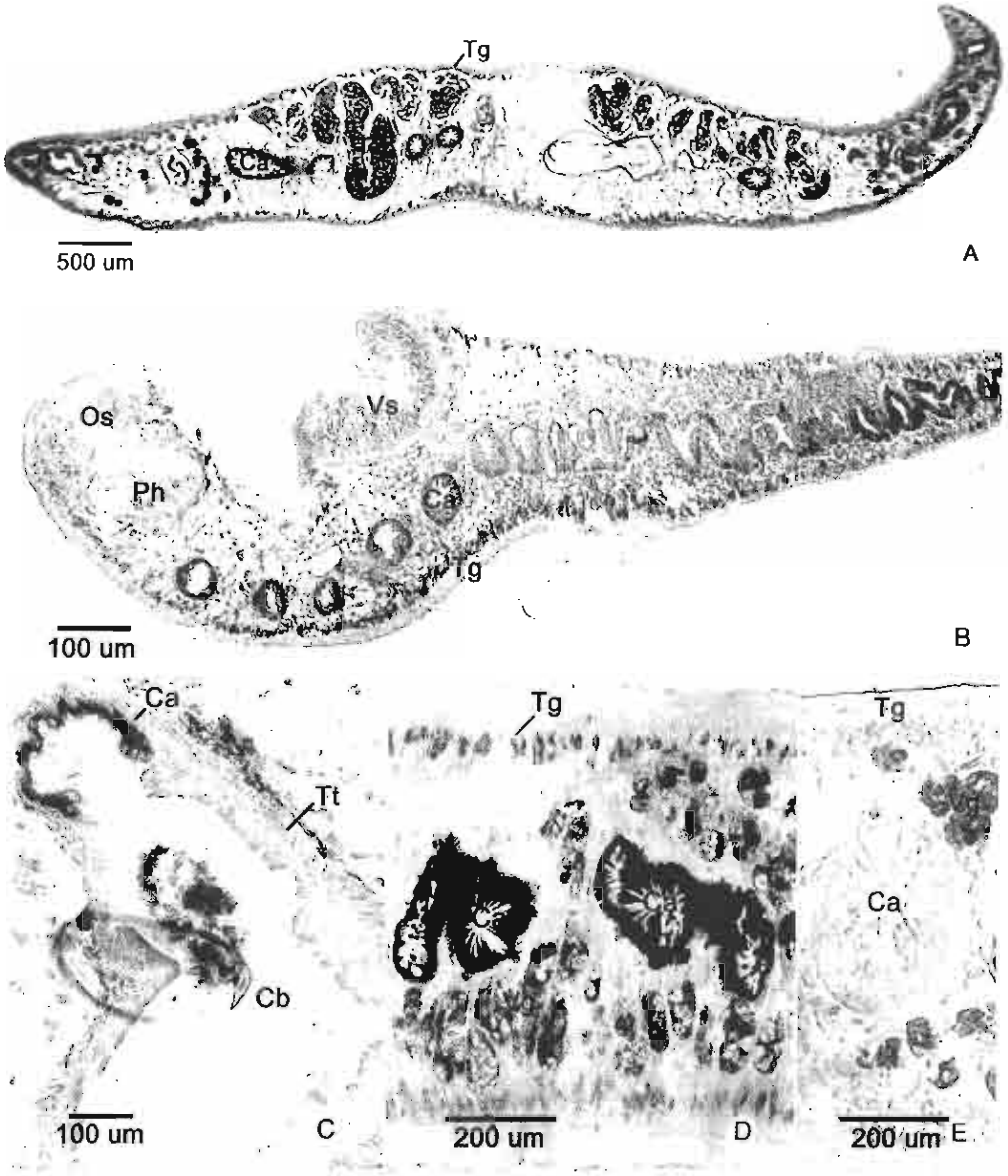


Fig. 4. Localization of cathepsin B mRNA in *F. gigantica* by in situ hybridization using a FG cat-B1 antisense RNA probe. (A) Cross section of an adult fluke, showing positive staining in caecal epithelium (Ca), tegumental cells (Tg), testis (Te), and vitelline gland (Vg). (B) Sagital section of a 4-weeks juvenile fluke, showing positive staining at the same organs as found in adult fluke, except in the reproductive tissues which are not yet developed. (C) At caecal bifurcation (Cb), the staining was present both in the caecal-type epithelium (Ca) of the distal digestive tract and in tegumental-type epithelium (Tt) of the proximal digestive tract. (D) Higher magnification of a cross section of an adult fluke, showing the positive staining in the caecal epithelium (Ca), tegumental cells (Tg), and vitelline gland (Vg). (E) Control section stained with a FG cat-B1 sense RNA probe.

cathepsin B [15] with only three amino acids different in the pre/pro-region. The DNA sequences coding for the mature form of the enzyme are completely identical which indicates a very close relationship between the two species. The deduced amino acid sequences of all cloned *F. gigantica* cathepsin B genes contain the residues generally conserved in the cathepsin B family (Fig. 1), except for the absence of the $His^{111}$ residue, which is present in mammalian cathepsin B as substrate binding site for the exopeptidase activity [23]. This residue is replaced by Leu, Val, and Gly in cat-B1, cat-B2, and cat-B3, respectively. However, the exopeptidase activity of cathepsin B in *F. gigantica* is not affected because $His^{111}$ is not critical for the enzymic activity. In human cathepsin B the mutation of $His^{111}$ to Ala showed only a small decrease of exopeptidase activity when compared with the mutation of cross bridge $His^{110}$ and

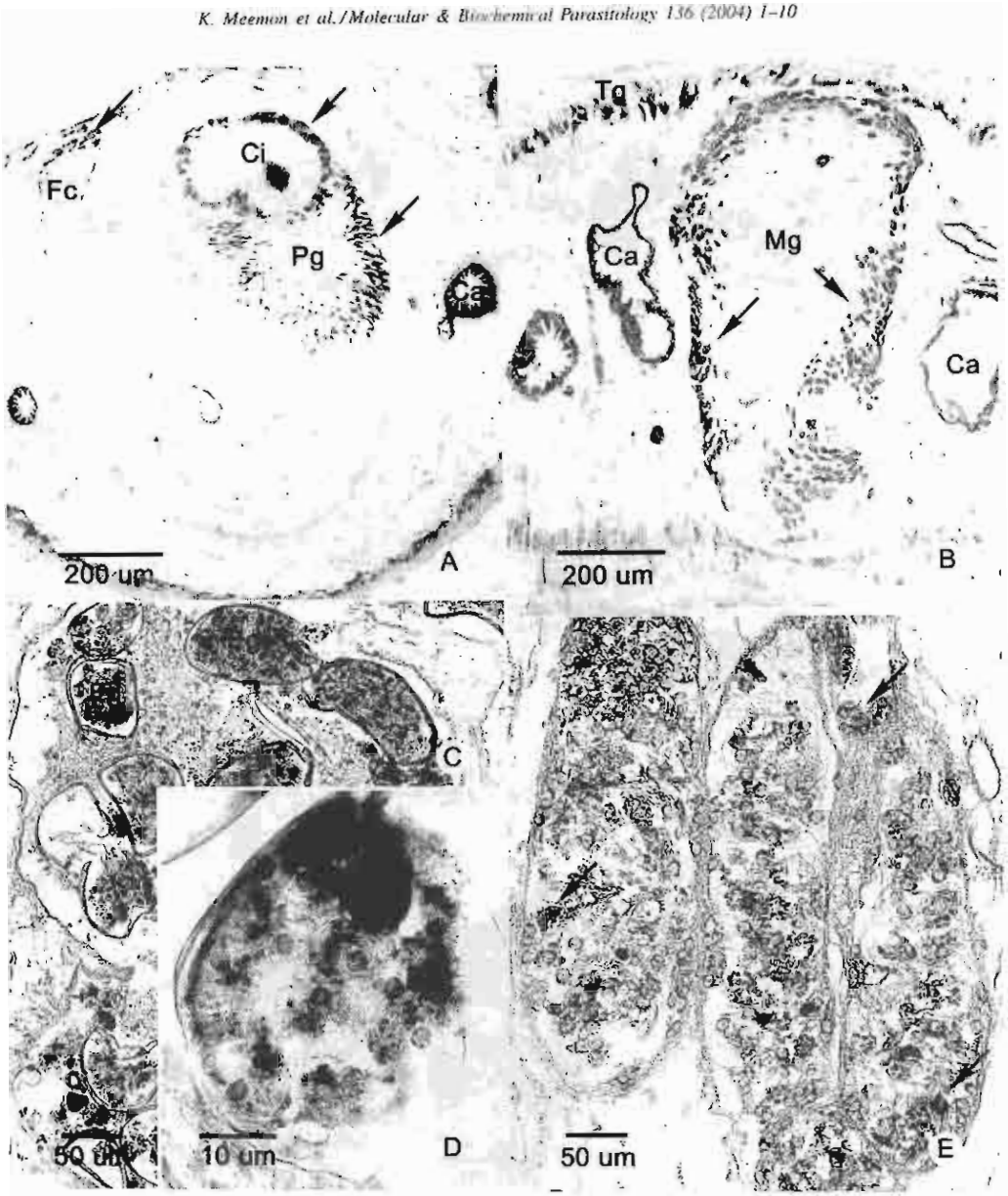


Fig. 5. Localization of cathepsin B mRNA in the reproductive tissues of adult *F. gigantica* by in situ hybridization using FG cat-B1 antisense RNA probe. (A) Positive staining in the prostate gland' cells (Pg, arrow), cells underlining the cirrus epithelium (Ci, arrow), and female genital canal (Fc, arrow). (B) Positive staining in cells in the Mehlis gland (Mg, arrow). (C, D) The positive staining in vitelline cells within the eggs (Eg) present in the uterine lumen. (E) Positive staining in cells of various spermatogenesis stages (arrows) within the testicular tubule.

$Asp^{22}$, which showed a dramatic loss of the activity [23]. The exopeptidase activity of the cathepsin B in *Fasciola* spp. need to be further analyzed biochemically.

The cathepsin B proteases of *F. gigantica* are encoded by a gene family comparable to the cathepsin L proteases of *Fasciola* spp. [16,17] or *Schistosoma mansoni* [24]. The stringent hybridization conditions used in this study limited the detection sensitivity to only closely related genes. This subgroup of cathepsin B genes may not contain more than three members assuming only a single recognition site for one of the used restriction endonucleases in intron sequences. Variations in the strength of the hybridization signal are due to differences in the DNA sequences and probe overlap.

The processed transcripts of the cathepsin B genes are of approximately 1.4 kb size. An average of 1000 nucleotides are contained in the coding region and 300 nucleotides, not including the poly(A)$^+$ tail, make up the 3′-untranslated region. This indicates a short length of the 5′-untranslated region of the mRNA. The combination of Northern and PCR analyses showed that the three studied cathepsin B genes

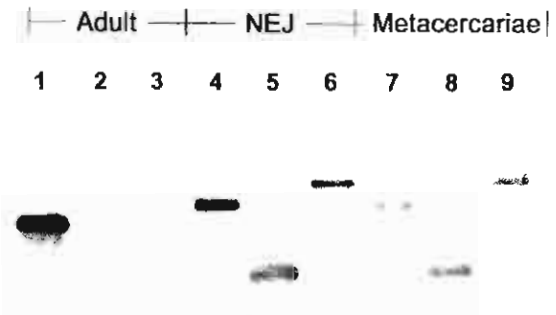


Fig. 6. Southern hybridization of PCR products generated from cDNA library samples with gene-specific primers (Table 1). A FG cat-B1 antisense RNA probe was used for hybridization. Lanes 1–3 = adult cDNA; lanes 4–6 = NEJ cDNA; lanes 7–9 = metacercariae cDNA. Lanes 1–7 = PCR product using set I primers; lanes 2, 5, and 8 = PCR product using set II primers; lanes 3, 6, and 9 = PCR product using set III primers. Twenty-five microliters of the PCR products were loaded in each lane.

are differentially expressed. Metacercarial and NEJ stages contain abundant cathepsin B transcripts, whereas less transcripts were found in 6-weeks-old juvenile and adults; and the latter of which contained the lowest amount of RNA. This corresponds to the results observed during screening of the cDNA libraries in which the metacercaria and NEJ libraries showed higher numbers of positive plaques than the adult library. The presence of these transcripts in early developmental stages is also matching a previous study in which cathepsin B proteins were detected in early *F. hepatica* stages [15]. The abundance of cathepsin B transcripts in metacercariae and early juveniles suggests that the proteases are important in the stage of penetration and in the excystment of metacercariae. In the present study we have also demonstrated the stage-specific expression of cat-B1, cat-B2, and cat-B3. Cat-B1 mRNA could be detected in all analyzed stages, whereas cat-B2 and cat-B3 could be detected only in NEJ and metacercariae. This may indicate the switching off of the cat-B2 and cat-B3 genes as the parasites become mature. The reason could be that cat-B1 may be a general protease that the parasites, especially the adult stage, use in the routine digestive function. Since the intestine of the juvenile fluke has only a secretory function, and not yet the absorptive function as in adult fluke [25], cat-B2 and cat-B3 may not possess the general digestive function for acquiring nutrition but may be involved more specifically in the parasite invasion and migration, thus they are present only in metacercariae, NEJ and possibly very early juvenile stages.

In adult and 4-weeks-old juvenile parasites, the cathepsin B transcripts were found by RNA in situ hybridization in the caecal epithelial cells, cells underlining the proximal part of the digestive tract including oral and ventral suckers, the tegumental cells underlining the surface tegument. Furthermore, in the adult stage the transcripts were detected in cells of the prostate, Mehlis, and vitelline glands, testis, eggs and cells underlining the uterine epithelium. In a previous study of *F. hepatica*, cathepsin B was detected in electron-dense granules within the caecal epithelium of NEJ and within the parenchyma of the adult parasite [26]. Our study correlates with this finding in detecting cathepsin B genes in the caecal epithelial cells of the adult *F. gigantica*, suggesting its possible function as a general digestive enzyme. Moreover, we have shown that cathepsin B is specifically expressed in the cells underlining the proximal part of the digestive tract (anterior to caecal bifurcation) whose epithelium is the tegumental type rather than the caecal type [27]. This pattern of expression is similar to the tegumental cells underneath the surface tegument. It is conceivable that cathepsin B from the tegumental cells may also be secreted outside to perform immune evasion functions, possibly by preventing the attachments of immune effector molecules [10] and cells to the surface of adult parasites, and to aid in the sloughing of the tegumental glycocalyx [28]. Direct evidence for cathepsin B secretion across the tegument syncytium is, however, still lacking. Up to now there is no report on cathepsin B expression in cells of the parasites' reproductive system. The presence of cathepsin B mRNA in adult reproductive glands associated with the production of eggs and sperm is quite surprising. The synthesis of egg shell requires the participation of secretions from Mehlis gland [29], and vitelline gland [29–31]. It is possible that cathepsin B present in the cells of these glands may be involved in the processing of the precursors for the egg shell proteins into proper sizes before they could be assembled into the mature egg shell proteins. Cathepsin B found within the vitelline cells of developing eggs [32] may also perform in a similar process of egg shell production. Moreover, cathepsin B protease may be involved in the degradation of vitellogenin, a yolk protein precursor, during embryogenesis as previously investigated in a variety of animals [33–35]. In the male reproductive system this enzyme may be a part of the acrosomal enzymes as found in some species of vertebrate animals, for example, in Xenopus sperm, cathepsin B is an acrosomal enzyme which participates in the egg activation during fertilization [36]. However, the localization of this enzyme in the sperm head of *F. gigantica* still remains to be demonstrated.

## Acknowledgements

This research was supported by the Thailand Research Fund (Senior Research Fellowship to Prasert Sobhon, and Royal Golden Jubilee Ph.D. Scholarship to Krai Meemon).

## References

[1] Anon. Control of foodborne trematode infections. WHO technical series, vol. 849. Geneva: WHO, 1995. p. 157.
[2] Spithill TW, Smooker PM, Copeman DB. *Fasciola gigantica*: epidemiology, control, immunology and molecular biology. In: Dalton JP, editor. Fasciolosis. UK: Cambridge University Press; 1999. p. 465–525.

[3] Estuningsih SE, Smooker PM, Wiedosari E, Widjajanti S, Vaiano S, Partoutomo S, et al. Evaluation of antigens of *Fasciola gigantica* as vaccines against tropical fasciolosis in cattle. Int J Parasitol 1997;27:1419–28.

[4] Morrison CA, Colin T, Sexton JL, Bowen F, Wicker J, Friedel T, et al. Protection of cattle against *Fasciola hepatica* infection by vaccination with glutathione *S*-transferase. Vaccine 1996;14:1603–12.

[5] Piacenza L, Acosta D, Basmadjian I, Dalton JP, Carmona C. Vaccination with cathepsin L proteinases and with leucine aminopeptidase induces high levels of protection against fasciolosis in sheep. Infect Immunol 1999;67:1954–61.

[6] Smooker PM, Kennedy NJ, Steeper KR, Christopoulos H, Spithill TW. *Fasciola*: kinetics and quality of humoral responses to fatty acid binding protein and cathepsin L following delivery as DNA vaccines in mice. Exp Parasitol 2001;97:154–60.

[7] Smooker PM, Steeper KR, Drew DR, Strugnell RA, Spithill TW. Humoral responses in mice following vaccination with DNA encoding glutathione *S*-transferase of *Fasciola hepatica*: effects of mode of vaccination and the cellular compartment of antigen expression. Parasite Immunol 1999;21:357–64.

[8] Wijffels GL, Salvatore L, Dosen M, Waddington J, Wilson L, Thompson C, et al. Vaccination of sheep with purified cysteine proteinases of *Fasciola hepatica* decreases worm fecundity. Exp Parasitol 1994;78:132–48.

[9] Berasain P, Goni F, McGonigle S, Dowd A, Dalton JP, Frangione B, et al. Proteinases secreted by *Fasciola hepatica* degrade extracellular matrix and basement membrane components. J Parasitol 1997;83:1–5.

[10] Carmona C, Dowd AJ, Smith AM, Dalton JP. Cathepsin L proteinase secreted by *Fasciola hepatica* in vitro prevents antibody-mediated eosinophil attachment to newly excysted juveniles. Mol Biochem Parasitol 1993;62:9–18.

[11] Halton DW. Nutritional adaptations to parasitism within the platyhelminthes. Int J Parasitol 1997;27:693–704.

[12] Dalton JP, Heffernan M. Thiol proteases released in vitro by *Fasciola hepatica*. Mol Biochem Parasitol 1989;35:161–6.

[13] Smith AM, Dowd AJ, McGonigle S, Keegan PS, Brennan G, Trudgett A, et al. Purification of a cathepsin L-like proteinase secreted by adult *Fasciola hepatica*. Mol Biochem Parasitol 1993;62:1–8.

[14] Wilson LR, Good RT, Panaccio M, Wijffels GL, Sanderman RM, Spithill TW. *Fasciola hepatica*: characterization and cloning of the major cathepsin B protease secreted by newly excysted juvenile liver fluke. Exp Parasitol 1998;88:85–94.

[15] Law RHP, Smooker PM, Irving JA, Piedrafita D, Ponting R, Kennedy NJ, et al. Cloning and expression of the major secreted cathepsin B-like protein from juvenile *Fasciola hepatica* and analysis of immunogenicity following liver fluke infection. Infect Immunol 2003;6921–32.

[16] Heussler VT, Dobbelaere DAE. Cloning of a protease gene family of *Fasciola hepatica* by the polymerase chain reaction. Mol Biochem Parasitol 1994;64:11–23.

[17] Grams R, Vichasri-Grams S, Sobhon P, Upatham ES, Viyanant V. Molecular cloning and characterization of cathepsin L encoding genes from *Fasciola gigantica*. Parasitol Int 2001;50:105–14.

[18] Sambrook T, Fritsch EF, Maniatis T. Molecular cloning: a laboratory manual, 2nd ed. Cold Spring Harbor: Cold Spring Harbor Laboratory Press; 1989.

[19] Merckelbach A, Hasse S, Dell R, Eschibeck A, Ruppel A. cDNA sequences of *Schistosoma japonicum* coding for two cathepsin B-like proteins and Sj32. Trop Med Parasitol 1994;45:193–8.

[20] Klinkert MQ, Felleisen R, Link G, Ruppel A, Beck E. Primary structures of Sm31/32 diagnostic proteins of *Schistosoma mansoni* and their identification as proteases. Mol Biochem Parasitol 1989;33:113–22.

[21] Cao L, Taggart RT, Berquin IM, Moin K, Fong D, Sloane BF. Human gastric adenocarcinoma cathepsin B: isolation and sequencing of full-length cDNAs and polymorphisms of the gene. Gene 1994;139:163–9.

[22] Musil D, Zucic D, Turk D, Eng RA, Mayr I, Huber R, et al. The refined 2.15 Å X-ray crystal structure of human liver cathepsin B: the structural basis for its specificity. EMBO J 1991;10:2321–30.

[23] Krupa JC, Hasnain S, Naplet DK, Menard R, Mort JS. $S_2'$ substrate specificity and the role of $His^{110}$ and $His^{111}$ in the exopeptidase activity of human cathepsin B. Biochem J 2002;361:613–9.

[24] Dalton JP, Clough KA, Jones MK, Brindley PJ. Characterization of the cathepsin-like cysteine proteinases of *Schistosoma mansoni*. Infect Immunol 1996;1328–34.

[25] Bennett CE, Threadgold LT. Electron microscope studies of *Fasciola hepatica* XIII. Fine structure of newly excysted juvenile. Exp Parasitol 1973;34:85–99.

[26] Creaney J, Wilson L, Dosen M, Sanderman RM, Spithill TW, Parsons JC. *Fasciola hepatica*: irradiation-induced alterations in carbohydrate and cathepsin-B protease expression in newly excysted juvenile liver fluke. Exp Parasitol 1996;83:202–15.

[27] Sriburee S. Characterization of epithelial cells and the expression of cathepsin L gene in the digestive tract of *Fasciola gigantica*. MSc thesis 2000. Bangkok, Thailand: Mahidol University.

[28] Lammas DA, Duffus WP. The shedding of the outer glycocalyx of juvenile *Fasciola hepatica*. Vet Parasitol 1983;12:165–78.

[29] Smyth JD, Halton DW. The physiology of trematodes. Cambridge: Cambridge University Press; 1983.

[30] Colhoun LM, Fairweather I, Brennan GP. Observations on the mechanism of eggshell formation in the liver fluke. *Fasciola hepatica*. Parasitology 1998;116:555–67.

[31] Wells KE, Cordingley JS. *Schistosoma mansoni*: eggshell formation is regulated by pH and calcium. Exp Parasitol 1991;73:295–310.

[32] Irwin SWB, Threadgold LT. Electron microscope studies of *Fasciola hepatica* X. Egg formation. Exp Parasitol 1972;31:321–31.

[33] Cho WL, Tsao SM, Hays AR, Walter R, Chen JS, Snigirevskaya ES, et al. Mosquito cathepsin B-like protease involved in embryonic degradation of vitellin is produced as a latent extraovarian precursor. J Biol Chem 1999;274:13311–21.

[34] Medina M, Leon P, Vallejo CG. *Drosophila* cathepsin B-like proteinase: a suggested role in yolk degradation. Arch Biochem Biophys 1988;263:355–63.

[35] Zhao XF, Wang JX, Xu XL, Schmid R, Wieczorek H. Molecular cloning and characterization of the cathepsin B-like proteinase from the cotton boll worm, *Helicoverpa armigera*. Insect Mol Biol 2002;11:567–75.

[36] Mizote A, Okamoto S, Iwao Y. Activation of *Xenopus* eggs by proteases: possible involvement of a sperm protease in fertilization. Dev Biol 1999;208:79–92.

ASIAN PACIFIC JOURNAL OF ALLERGY AND IMMUNOLOGY (2004) 22: 219-228

# Molecular Cloning and Characterization of a Glutathione S-Transferase Encoding Gene from *Opisthorchis viverrini*

Veerachai Eursitthichai[1], Vithoon Viyanant[1,3], Suksiri Vichasri-Grams[1], Prasert Sobhon[2], Smarn Tesana[4], Suchart Edward Upatham[5], Annemarie Hofmann[6], Günter Korge[6] and Rudi Grams[3]

**SUMMARY** An adult stage *Opisthorchis viverrini* cDNA library was constructed and screened for abundant transcripts. One of the isolated cDNAs was found by sequence comparison to encode a glutathione S-transferase (GST) and was further analyzed for RNA expression, encoded protein function, tissue distribution and cross-reactivity of the encoded protein with other trematode protein counterparts. The cDNA has a size of 893 bp and encodes a GST of 213 amino acids length (OV28GST). The most closely-related GST of OV28GST among those published for trematodes is a 28 kDa GST of *Clonorchis sinensis* as shown by multiple sequence alignment and phylogenetic analysis. Northern analysis of total RNA with a gene-specific probe revealed a 900 nucleotide OV28GST transcriptional product in the adult parasite. Through RNA *in situ* hybridization OV28GST RNA was detected in the parenchymal cells of adult parasites. This result was confirmed by immunolocalization of OV28GST with an antiserum generated in a mouse against bacterially-produced recombinant OV28GST. Both, purified recombinant and purified native OV28GST were resolved as 28 kDa proteins by SDS-PAGE. Using the anti-recOV28GST antiserum, no or only weak cross-reactivity was observed in an immunoblot of crude worm extracts against the GSTs of *Schistosoma mansoni*, *S. japonicum*, *S. mekongi*, *Eurytrema spp.* and *Fasciola gigantica*. The enzyme activity of the purified recombinant OV28GST was verified by a standard 1-chloro-2, 4-dinitrobenzene (CDNB) based activity assay. The present results of our molecular analysis of OV28GST should be helpful in the ongoing development of diagnostic applications for opisthorchiasis viverrini.

*Opisthorchis viverrini* is the agent of opisthorchiasis and causes serious health problems among human populations in North and Northeast Thailand. The prevalence of opisthorchiasis in Northeastern Thailand is estimated to be 18.57% which means about 6 million people are infected.[1,2] Infection of humans takes place through consumption of raw or undercooked cyprinoid fish harboring infective metacercariae. The parasites remain in the bile ducts for many years causing hepatobiliary diseases such as obstructive jaundice, hepatomegaly, cholangitis, cholelithiasis and cholangiocarcinoma.[3-6] Infected persons develop strong humoral and cell mediated immune responses probably due to the contact of parasite products with the host immune system through the inflamed epithelial lining of the bile ducts.

At present, knowledge about the host/parasite relationship and molecular biology of *O. viverrini* is limited. Several protein antigens have been characterized and used for immunodiagnosis and attempts have also been made to develop a method to detect parasite DNA in feces.[10-12] Both techniques have been found to be effective but have still not replaced microscopic examination. In order to develop an immunodiagnosis with high sensitivity and specificity, a good candidate

From the [1]Department of Biology and [2]Department of Anatomy, Faculty of Science, Mahidol University, Bangkok, Thailand, [3]Graduate Program in Biomedical Sciences, Faculty of Allied Health Sciences, Thammasat University, Pathumthani, Thailand, [4]Department of Parasitology, Faculty of Medicine, Khon Kaen University, Khon Kaen, Thailand, [5]Faculty of Science, Burapha University, Chonburi Thailand, [6]Institut für Biologie-Genetik, Freie Universität Berlin, Berlin, Germany.
Correspondence: Rudi Grams

antigenic protein must be studied. Moreover, this protein should be readily available with high quality and purity. Glutathione S-transferase (GST) is a catalytic enzyme which is active in the parasite's defense mechanism by detoxifying bioactive chemicals. Two isozymes of GST have been reported, a 26 kDa cytosolic enzyme and a 28 kDa tegumental enzyme.[13] GST is an antigenic protein of trematodes that induces a strong host immune response. Recombinant GST has been used for detecting IgG and IgE antibodies in clonorchiasis.[14] In the present study, the gene that codes for *O. viverrini* GST was cloned and the recombinant 28 kDa GST was characterized and compared with GSTs of other species.

## MATERIALS AND METHODS

### Construction of cDNA library

Adult *O. viverrini* (1 mg wet weight) obtained from infected hamsters (*Mesocricetus, auratus*) were homogenized in TRIzol reagent (Invitrogen-Life Technologies, Carlsbad, USA) by use of an Ultra-Turrax T25 homogenizer (IKA, Staufen, Germany) and the total RNA was extracted. The RNA (1 µg) was used to construct a directional cDNA library in Lambda TriplEx2 (SMART cDNA synthesis kit, BD Biosciences-Clontech, Palo Alto, USA). The recombinant Lambda DNA was packaged in Gigapack III Gold packaging extracts (Stratagene, La Jolla, USA). The primary library ($4 \times 10^6$ pfu/ml) was amplified to a titer of $1 \times 10^9$ pfu/ml and stored at -80°C in 7% DMSO.

### Screening of cDNA library

The cDNA library was screened for abundant transcripts with a $^{32}$P-dCTP labeled mixed cDNA probe (Hexalabel DNA labeling, Fermentas Life Sciences, Vilnius, Lithuania). Briefly, a plaque lift of 50,000 plaques was done to a nitrocellulose membrane (BA85, Schleicher & Schuell, Dassel, Germany) and the DNA of the transferred phage particles was released and denatured under alkaline conditions. The air-dried membrane was baked at 80°C for 1 hour, prehybridized and hybridized in 5x SSPE, 5x Denhardt's solution, 50% Formamide, 0.5% SDS, 1 mg/ml herring sperm DNA, and 20 ng/ml of the $^{32}$P-dCTP labeled cDNA probe. The hybridization reaction was done at 55°C for 16 hours. Posthybridization washes of the membrane were done in 1x SSC, 0.1% SDS at room temperature for 10 minutes and in 0.1x SSC, 0.1% SDS at 50°C for 30 minutes to remove nonspecifically bound probe. An autoradiograph of the air-dried membrane was produced on Kodak XAR-5 film at -80°C for 16 hours. Positive plaques were recovered from the original plate and rescreened at low density (100-200 pfu/90 mm plate) to obtain single clones. Cre-recombinase-mediated recombination was used to release the pTriplEx2 phagemid carrying the cDNA from the viral DNA. Several single clones were obtained but only the analysis of clone C1A2 is reported in this publication.

### Sequencing and sequence analysis of cDNA

Plasmid DNA was prepared using the Jet Star Plasmid Midi Kit (Genomed, Lohne, Germany). Sequencing of the cDNAs was done by MWG AG Biotech, Ebersberg, Germany. Sequence analysis was done using MacMolly Lite (SoftGene GmbH, Berlin, Germany). The BLAST program[15] was used to search the GenBank database for related sequences. Multiple sequence alignments were done using the CLUSTAL W program[16] through the emboss emma program.[17] A prediction of the secondary structure of the encoded protein was done by the PHD program.[18] A phylogenetic tree was constructed to examine relationships among selected homologous proteins using the program PAUP 4.0[19] and based on 1,000 replicates.

### Northern hybridization

Twenty micrograms of total RNA was size separated in a 1.5% denaturing agarose gel (2.2 M formaldehyde) in 1x MOPS buffer (0.2 M MOPS [3-(N-morpholino) propanesulfonic acid], 50 mM sodium acetate, 10 mM EDTA adjusted to pH 7.0) and transferred to a nylon membrane (Nytran N, Schleicher & Schuell). The air-dried membrane was baked at 80°C for 1 hour, prehybridized and hybridized in hybridization buffer II (5x SSC, 2% blocking solution, 50% formamide and 0.02% (w/v) SDS) at 65°C for 16 hours. A DIG-labeled antisense RNA of OV28GST (DIG-RNA labeling and detection kit, Roche Diagnostics AG, Rotkreuz, Switzerland) was used as a hybridization probe at a concentration of 100 ng/ml. The hybridized probe was detected by an anti-DIG/alkaline phosphatase conjugate on the membrane using NBT/BCIP as substrates.

### RNA *in situ* hybridization

RNA *in situ* hybridization was done as described before.[20] Adult parasites were fixed over-

night in 4% paraformaldehyde, 0.1 M PBS, pH 7.4, dehydrated through a series of ethanol steps and embedded in paraplast. Sections were cut at 6 µm (Leica RM2145, Wetzlar, Germany) mounted on coated slides (Histogrip, Zymed, San Francisco, USA) and dried at 42°C overnight. The sections were dewaxed in xylene, rehydrated and post-fixed in 4% paraformaldehyde, 0.1 M PBS. Afterwards the sections were treated two times in 0.1% DEPC, 0.1 M PBS for 15 minutes each and equilibrated in 5x SSC (0.75 M NaCl, 75 mM sodium citrate). The sections were hybridized at 60°C with 60 µl of 400 ng/ml DIG-labeled antisense OV28GST RNA probe (DIG-RNA labeling kit, Roche Diagnostics AG) in hybridization buffer II for 16 hours. After the hybridization reaction the sections were washed in 2x SSC for 30 minutes at 25°C, 1 hour at 65°C and finally in 0.1x SSC for 1 hour at 65°C. Enzymatic detection of the hybridized probe was done as described before.

**Expression and purification of recombinant and native OV28GST**

A subfragment of C1A2, beginning at the start codon in position 23 of AY057838 was subcloned into the pET21a expression vector (Novagen, Madison, USA) as follows: DNA of pTriplEx2-C1A2 was used as a template in a standard PCR (30 cycles at 94°C, 55°C, 72°C, 1 minute each step) using the forward primer 5'-CAT ATG AGT GGT GAA AAA TAC AA-3' and reverse primer 5'-GAC TCA CTA TAG GGC GAA TTG G-3' (pTriplEx2 bases 653 to 674, BD Biosciences-Clontech). The PCR product was subcloned into pGEM T-easy (Promega, Madison, USA) and the sequence verified (Bioservice Unit, Bangkok, Thailand). Afterwards it was cut with restriction endonucleases *Nde* I (introduced by the forward primer) and *Xho* I (contained in the multiple cloning site of pTriplEx2) and inserted into the *Nde* I/ *Xho* I recognition sites of pET21a.

The expression of recombinant OV28GST protein in the transformed *E. coli* strain BL21 was induced at an $OD_{600}$ of 0.6 by adding IPTG to a final concentration of 1 mM into the medium. After 4-hour growth the bacterial cells were pelleted at 2,600 x *g* and 4°C for 10 minutes, resuspended in PBS (1.37 M NaCl, 27 mM KCl, 101.4 mM $Na_2HPO_4$, 17.6 $KH_2PO_4$ [pH 7.3]) and sonicated on ice in short bursts (Microson ultrasonic cell disruptor, Heat Systems, New York, USA). The soluble product of the lysate was separated by centrifugation for 5 minutes at 12,000 x *g* at 4°C from the insoluble cellular debris and used for purification of the recombinant OV28GST protein by the Bulk-GST Purification Module Kit (Amersham Biosciences, Piscataway, USA). Purification was done according to the manual supplied in the kit. In addition, the native OV28GST was also purified by the Bulk-GST Purification Module kit. Freshly obtained adult parasites were suspended in lysis buffer (10 mM Tris-HCl, pH 7.2, 150 mM NaCl, 0.5% Triton-X 100, 1 mM EDTA, pH 7.2, 1 mM phenyl-methyl-sulphonyl-fluoride) and homogenized on ice. The homogenate was rotated at 4°C for 1 hour, the insoluble material pelleted for 15 minutes at 12,000 x *g* and the native OV28GST purified from the supernatant.

The extraction of crude worm preparations from *O. viverrini*, *S. mansoni*, *S. japonicum*, *S. mekongi*, *F. gigantica* and *Eurytrema spp.* was done as described above for the native OV28GST protein. Fresh worms were suspended and homogenized in lysis buffer. The homogenate was rotated at 4°C for 1 hour and insoluble material pelleted for 15 minutes at 12,000 x *g*. The supernatant was used as crude worm protein extract.

**Production of anti-recOV28GST polyclonal antiserum**

A polyclonal antiserum against recombinant OV28GST protein (recOV28GST) was raised in a female BALB/c mouse. Three subcutaneous injections with doses of 50 µg recombinant OV28GST cut from gels after SDS-PAGE were done in weeks 0, 3, and 6. In the priming step, recombinant OV28GST was injected with complete Freund's adjuvant; the second and third immunization steps were done with incomplete Freund's adjuvant (http://dicty.com.nwu.edu/Chris_lab/Lab%20Manual/Immunological_techniques.htm). Blood was collected and the serum obtained in weeks 0 (preimmune), 2, 5, and 8 by centrifugation at 2,600 x *g* for 15 minutes. The sera were tested for their antibody titer by ELISA and were kept at -20°C before being used for EITB and immunolocalization.

**Glutathione S-transferase activity assay**

The enzyme activity of 1 µg recombinant OV28GST was measured in 1 ml reaction buffer (0.01 M potassium phosphate, pH 7.0, 10 mM 1-chloro-2, 4-dinitrobenzene, 10 mM reduced glutathione) at room temperature for 5 minutes. The photometric

absorption values at a wavelength of 340 nm were recorded in one-minute steps.[21]

**Enzyme-linked electroimmunotransfer blot (EITB)**

EITB was performed as previously described.[22] Crude worm extracts of 10 µg each of *O. viverrini*, *S. mansoni*, *S. japonicum*, *S. mekongi*, *F. gigantica* and *Eurytrema* spp., 0.5 µg each of purified native and recombinant OV28GST proteins were size separated by SDS-PAGE (12.5%) and transferred to a nitrocellulose membrane (Hybond-C extra, Amersham Biosciences). The immunogenicity of the transferred proteins was determined by EITB using the raised polyclonal mouse anti-recOV28GST serum and an alkaline phosphatase-rabbit anti-mouse immunoglobulin conjugate. Enzymatic detection was done with the substrates NBT (0.3 mg/ml) and BCIP (0.15 mg/ml) in 100 mM Tris-HCl, pH 9.5, 100 mM NaCl, and 50 mM $MgCl_2$.

**Immunolocalization of OV28GST**

Native OV28GST protein was localized in paraffin sections (5 µm) prepared from adult specimens as described above. The dewaxed and rehydrated sections were covered with 1 mM EDTA pH 8.0 and heated in a microwave oven at 700 watts for 5 minutes. Unspecific binding sites were blocked by incubation with 0.1% glycine in TBS (20 mM Tris-HCl pH 7.5, 150 mM NaCl) for 30 minutes at room temperature and in 4% bovine serum albumin in TBS for 30 minutes. The sections were incubated in a 1:200 dilution of polyclonal mouse anti-recOV28GST antiserum in TBS for 16 hours and washed in TBST (0.1% Tween-20 in TBS) three times for 5 minutes each. The sections were then incubated in a 1:50 dilution of biotinylated rabbit anti-mouse immunoglobulin in TBS for 30 minutes and avidin:biotinylated horseradish peroxidase complex (ABC complex-HRP, DAKO) for 30 minutes. Enzymatic detection was done using 3, 3' diaminobenzidine (Sigma-Aldrich, St. Louis, USA) as a substrate.

**Species names, database entry names, and accession numbers of the GSTs used for comparisons in this publication**

These included 28 kDa GST of *O. viverrini* (OV28GST AAL-23713), 28 kDa GST of *Clonorchis sinensis* (CS28GST AAD17488), mu class GST of *C. sinensis* (CsMuGST AAB46369), 28 kDa GST of *S. haematobium* (SH28GST AAA29892), 28 kDa GST of *S. bovis* (SB28GST AAA29893), 28 kDa GST of *Paragonimus westermani* (PW28GST AAB63382), alpha class GST of *Fasciola hepatica* (FhGST-alpha AAB28746), GST of *F. gigantica* (FgGST AAD23997), mu class GST of *F. hepatica* (FhMu-GST AAA29140), S-crystallin of *Loligo opalescens* (SQCRYS AAB-01054), GST of *Ommastrephes sloanei pacificus* (SQGST 1GSQ), GST of *Caenorhabditis elegans* (CEGST AAB65417), mu class GST of *Rattus norvegicus* (RatMuGST AAD00603), 28 kDa GST of *S. mansoni* (SM28GST P09792), 28 kDa GST of *S. japonicum* (SJ28-GST P26624), 26 kDa GST1 of *S. mansoni* (Sm26GST1 P15964), 26 kDa GST2 of *S. mansoni* (Sm26-GST2 P35661), GST of *Ascaris suum* (ASGST P46436), GST of *Onchocerca volvulus* (ONCVGST P46434), pi class GST of *Onchocerca volvulus* (OncvGSTP2 P-46427), GST of *Dirofilaria immitis* (DimmitisGST P4642), GST of *Blattella germanica* (BlageGST O18598), sigma class GST of *Musca domestica* (HouseFlyS1 P46437), pi class GST of *Macaca mulatta* (MonkeyGSTPi Q28514), pi class GST of *Mus musculus* (MouseP1 P19157), alpha class GST of *Rattus norvegicus* (RatGSTA8 P14942), GST-Yc1 of *Rattus norvegicus* (RatGSTYc P04904), pi class GST of *Rattus norvegicus* (Rat-GSTP7 P04906), Prostaglandin-D-synthase of *Rattus norvegicus* (Rat-PGDS P22057), alpha class GST of *Gallus gallus* (ChickGSTalpha Q08392), mu class GST of *Gallus gallus* (ChickMuGST P20136), Prostaglandin-D-synthase of *Gallus gallus* (ChickPGDS CAA07005), GST of *Brugia malayi* (BmalayiGST CAA73325), mu-5 class GST of *Mus musculus* (MouseM5 NP_034490), mu-2 class GST of *Mus musculus* (MouseM2 NP_032209), and pi class GST of *Sus scrofa domestica* (pigpiGST S13780).

## RESULTS

**Screening of cDNA library and sequence analysis of isolated cDNA**

An adult stage cDNA library of *O. viverrini* was constructed in Lambda TriplEx2 (ClonTech) and screened for abundant transcripts with a mixed cDNA probe prepared from *O. viverrini* RNA. One of the positive clones detected in the primary screen (C1A2) was selected for further analysis. The cDNA insert of C1A2 is 893 bp in length. It contains a 22 bp 5' UTR, an open reading frame of 639 bp length and a 198 bp 3' UTR followed by the poly(A) tail. A putative polyadenylation signal (TATAAA) is located 23

bp upstream of the poly(A) tail. The encoded protein of 213 amino acid residues size has a computational predicted molecular weight of 24 kDa and is rich in leucine and glutamic acid residues (a total of 20.66%). A search of the GenBank database through the BLAST program[15] showed that the encoded protein is homologous to the 28 kDa glutathione S-transferases of other helminths and to the related S-crystallin of cephalopods. The percentages of identical residues shared between the newly found OV28GST and homologous proteins of trematodes, nematodes and cephalopods are shown in Fig. 1A. It varies between 57% for the 28 kDa GST of the liver fluke *C. sinensis* (GenBank AAD17488) and 29% for *Onchocerca volvulus* GST-1 (SWISS-PROT P46434). An alignment of GST amino acid sequences obtained through the CLUSTAL W program[16] shows eleven residues to be identical among the compared proteins. These are Tyr10*, Phe11*, Glu18, Arg21, Asp33, Trp41*, Pro54*, Asp88, Gly155, Asp162, and Arg208 (Fig. 1C). Individual amino acids forming part of the GSH-binding site are indicated by a star. In the GST-related squid lens protein S-crystallin, an additional stretch of 15 amino acids (KNGRFFFENGKE-SEMN) exists. The prediction of the secondary structure of OV28GST by the PHD program[18] revealed a conserved structure of the active site of the protein responsible for glutathione binding. A phylogenetic analysis through the PAUP program[19] (Neighbor-Joining with 1,000 replicates) showed that OV28GST is in one cluster with the 28 kDa sized, sigma class GSTs (Fig. 1B). The next neighbor of OV28GST in the phylogenetic tree is the GST of

| | OV28GST | CS28GST | SB28GST | SH28GST | SM28GST | SJ28GST | PW28GST | SQGST | ASGST | SQCRYS | CEGST |
|---|---|---|---|---|---|---|---|---|---|---|---|
| CS28GST | 57.1 | | | | | | | | | | |
| SB28GST | 44.6 | 42.7 | | | | | | | | | |
| SH28GST | 45.5 | 44.1 | 97.2 | | | | | | | | |
| SM28GST | 46.0 | 43.1 | 91.9 | 90.0 | | | | | | | |
| SJ28GST | 45.4 | 41.9 | 78.2 | 76.7 | 77.2 | | | | | | |
| PW28GST | 37.7 | 37.6 | 38.6 | 38.6 | 38.6 | 42.6 | | | | | |
| SQGST | 34.1 | 31.4 | 36.0 | 27.5 | 27.9 | 30.1 | 28.2 | | | | |
| ASGST | 31.9 | 31.0 | 31.1 | 31.1 | 32.5 | 31.6 | 32.8 | 29.6 | | | |
| SQCRYS | 30.9 | 38.7 | 36.0 | 35.3 | 36.0 | 34.3 | 28.8 | 39.9 | 33.6 | | |
| CEGST | 30.8 | 26.1 | 29.1 | 29.1 | 30.1 | 30.9 | 37.6 | 38.5 | 47.0 | 35.8 | |
| ONCVGST | 29.4 | 28.8 | 29.6 | 29.1 | 29.2 | 28.8 | 30.8 | 25.8 | 36.8 | 36.9 | 34.2 |

**Fig. 1A** Cross-species identity values (%) for amino acid sequences of OV28GST and homologous GST proteins. Details of species names and accession numbers of the compared glutathione S-transferases are given in the Materials and Methods section.

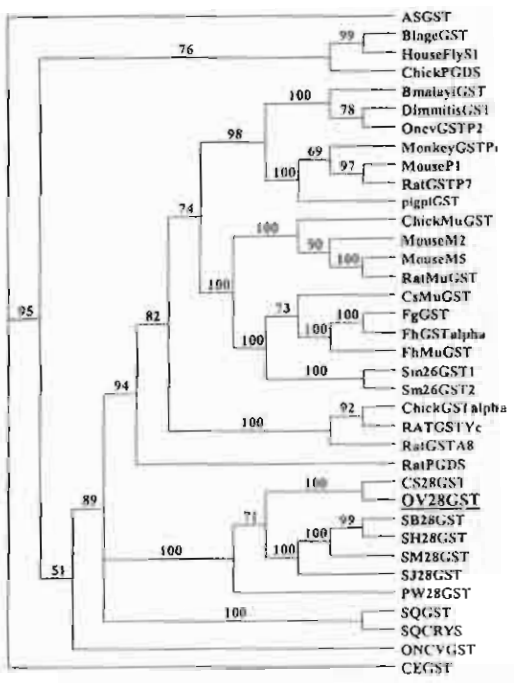


**Fig. 1B** A phylogenetic tree showing the relationship of *O. viverrini* OV28GST to glutathione S-transferases of other species. Details of species names and accession numbers of the compared glutathione S-transferases are given in the Materials and Methods section.

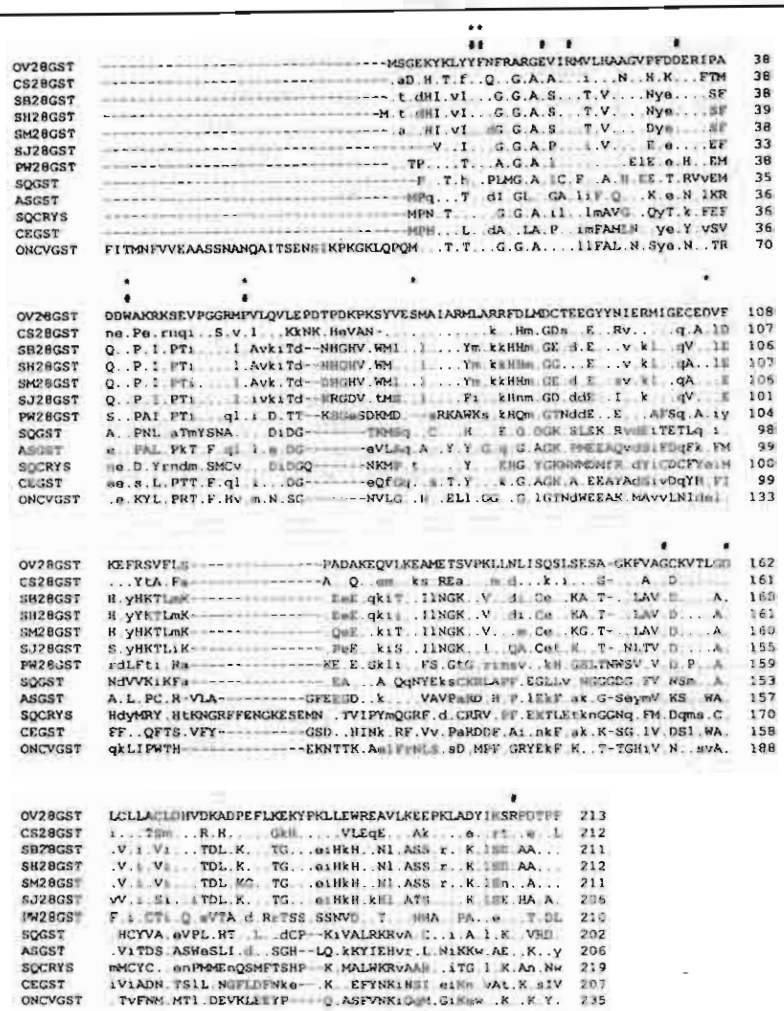

Fig. 1C Amino acid sequence alignment of OV28GST and homologous proteins. Identical residues are indicated by dots (.), similar residues by lower case letters and different residues by upper case letters. Gaps are indicated by a dash (-) and residues forming the GSH binding site are indicated by asterisks (*). Residues identical for all of the aligned sequences are indicated by hatch signs (#). Details of species names and accession numbers of the compared glutathione S-transferases are given in the Materials and Methods section.

*C. sinensis* (CS28GST)[13] confirming the sequence alignment.

### Northern hybridization

Northern hybridization of *O. viverrini* total RNA with an antisense OV28GST RNA probe resulted in a single prominent hybridization signal at a transcript size of 900 nucleotides (Fig. 2). The transcript size indicates that the full length of the mRNA sequence is contained in the cloned OV28GST cDNA. The size is identical to the 28 kDa GST of *Paragonimus westermani*[23] whereas *C. sinensis* GST is encoded by a mRNA of 1 kb size.[13]

### RNA *in situ* hybridization

Paraffin cross sections of adult *O. viverrini* were hybridized with an antisense OV28GST RNA probe. Positive hybridization signals were detected in the parenchymal cells (Fig. 3A). Hybridization signals were not observed in vitelline cells, tegument and caecum. A sense strand OV28GST RNA probe did not result in positive hybridization signals (Fig. 3B) as was true for a control with only the enzyme substrates to reveal endogenous phosphatase activity (data not shown).

### Enzyme-linked electroimmunotransfer blot (EITB)

The crude worm protein extracts of *O. viverrini*, *S. mansoni*, *S. japonicum*, *S. mekongi*, *F. gigantica*,